



Safety assessment of a guided research missile

Sicherheitsanalyse einer Forschungsrakete

Semesterarbeit

Author: Florian Wachter

Matriculation Number: 3628475

Supervisor: Philippe Petit

June 2016

Statutory Declaration

I, Florian Wachter, declare on oath towards the Institute of Flight System Dynamics of Technische Universität München, that I have prepared the present Semester thesis independently and with the aid of nothing but the resources listed in the bibliography. This thesis has neither as-is nor similarly been submitted to any other university.

Garching, June 13, 2016

Florian Wachter

Kurzfassung

Für die Betriebserlaubnis zum Testen der neu entwickelten Guided Research Missile (GRM) auf dem Schießplatz Meppen der Wehrtechnischen Dienststelle 91 (WTD 91) werden sicherheitskritische Berechnungen und Simulationen verlangt. In dieser Arbeit werden die Anforderungen bezüglich stabiler Flug, Windeinfluss und Reichweitenberechnungen und Sicherheitszonenbestimmung beantwortet. Dazu wird ein Simulationsmodell der GRM in Matlab/Simulink erstellt und mit aerodynamischen Daten aus Missile DAT-COM versehen. Einflussparameter, welche den sicheren Betrieb gefährden, beziehungsweise die Flugbahn der Rakete beeinflussen, werden mit Hilfe der Fault Tree Analysis erarbeitet. Durch Einsatz einer Monte Carlo Simulation (MCS) kann somit die Aufschlagswahrscheinlichkeit der Rakete geschätzt werden. Ein genetischer Algorithmus (GA) bestimmt die maximale Reichweite in jede Richtung unter Einfluss aller betrachteten Einflussgrößen. Der Vorteil dieser Methode ist, dass die dabei benötigte Rechenzeit um ungefähr Faktor 10 niedriger ist als mit Monte Carlo Simulation bei besserer Qualität der Ergebnisse. Die somit erlangten Informationen ergeben den Sicherheitsbereich, in dem ein Aufschlag der Rakete stattfinden kann. Dieser und die Aufprallwahrscheinlichkeit ergeben den Hauptkern der Sicherheitsnachweise. Eine zusätzliche Berechnung stellt sicher, dass auch von einer Explosion der Rakete vor Start keine Gefährdung durch ausreichend Sicherheitsabstand ausgeht. Schlussendlich werden die Ergebnisse zusammengefasst und die nächste Vorgehensweise erläutert.

Abstract

To obtain an operating license for the newly developed Guided Research Missile (GRM) at the shooting range Meppen of Wehrtechnische Dienststelle 91 (WTD 91) some safety critical calculations and simulations are required. In this thesis compliance with these requirements, i.e. stable flight condition, wind influence, range and safety area calculations, is proven. For this purpose a simulation model of the GRM is build within Matlab/Simulink and aerodynamic data delivered by Missile DATCOM. Parameters that influence the safe operation or the projected flight path of the missile are identified by applying an Fault Tree Analysis. Subsequent Monte Carlo simulation (MCS) approximates the impact probability distribution. A genetic algorithm (GA) calculates the maximum range in every possible direction at once, incorporating every influential parameter. This method reduces the required computation time by factor 10 while delivering a better quality of results. These results finally lead to the danger zone, the area within the missile might go down and harm humans and equipment. The impact probability distribution and danger zone estimation are the core of safety assessment. An additional calculation ensures that an explosion of the GRM prior start poses no safety threat by providing safety clearances. Last but not least the results are discussed and further steps to do are described.

Table of Contents

1	Introduction.....	- 1 -
1.1	Purpose of this Thesis	- 1 -
1.2	Structure of this Thesis	- 1 -
1.3	WTD 91	- 1 -
2	Guided Research Missile	- 3 -
2.1	Basic Description	- 3 -
2.2	Mechanical and Aerodynamic Design.....	- 3 -
2.3	Electronic Design.....	- 5 -
2.4	Propulsion	- 5 -
3	Requirements	- 7 -
3.1	Stable Flight under various Conditions.....	- 7 -
3.2	Wind Influenced Range.....	- 8 -
3.3	Range and Behavior in the Case of Rudder Failure	- 8 -
3.4	Danger Zone Estimation.....	- 8 -
4	Fault Tree Analysis	- 9 -
4.1	Fault Tree for the Danger Zone Estimation	- 10 -
4.1.1	Event Descriptions.....	- 11 -
4.2	Event Probabilities - Value Distributions	- 15 -
4.2.1	Events with Varying Parameters.....	- 15 -
4.2.2	Events without Parameters.....	- 16 -
4.2.3	Events with no Safety Thread or Not Considered	- 16 -
5	Missile Model	- 17 -
5.1	Missile Flight Dynamics.....	- 17 -
5.1.1	Missile DATCOM	- 18 -
5.1.2	Modeling Framework and Programs Used.....	- 19 -
5.2	Simulink Missile Model	- 19 -
5.3	Submodels.....	- 20 -
5.3.1	Propulsion.....	- 20 -
5.3.2	Mass and Gravity	- 21 -
5.3.3	Aerodynamic Coefficients	- 21 -
5.3.4	Forces and Moments	- 22 -
5.3.5	Environmental Models	- 22 -
5.3.6	Alpha, Beta, Mach	- 24 -
5.4	Model Validation	- 25 -
5.4.1	Comparison to Real Flight Recordings	- 25 -
5.4.2	Comparison to OpenRocket.....	- 26 -

6	Sensitivity Analysis.....	- 27 -
6.1	Nominal Flight.....	- 28 -
6.2	Azimuth Deviations.....	- 29 -
6.3	CoG Deviation.....	- 30 -
6.4	Mass and Inertia Deviation.....	- 33 -
6.5	Trust Deviation	- 37 -
6.6	Control Surface Deflections.....	- 40 -
6.7	Shape Deviations.....	- 41 -
6.8	Model Uncertainty Deviation.....	- 44 -
6.9	Temperature and QNH Deviation	- 45 -
6.10	Wind.....	- 47 -
7	Safety Assessment.....	- 49 -
7.1	Monte Carlo Simulation.....	- 49 -
7.2	Genetic Algorithms and Pareto Optimization.....	- 49 -
7.2.1	Multi Objective Optimization.....	- 49 -
7.2.2	Genetic Algorithms	- 51 -
7.3	MCS and GA Results	- 53 -
7.3.1	1050 Simulation Runs.....	- 53 -
7.3.2	2100 Simulation Runs.....	- 53 -
7.3.3	6300 Simulation Runs.....	- 53 -
7.3.4	MCS with 70000 Simulation Runs.....	- 53 -
7.4	Explosion on Ground.....	- 58 -
8	Results and Conclusion	- 59 -
8.1	Stable Flight under Various Conditions	- 59 -
8.2	Wind Influenced Range.....	- 59 -
8.3	Range and Behavior in the Case of Rudder Failure	- 59 -
8.4	Danger Zone Estimation.....	- 59 -
8.5	Next Steps and Suggestions.....	- 59 -
A	1	- III -

List of Figures

Figure 2-1:	GRM first draft	- 3 -
Figure 2-2:	Guided Research Missile	- 4 -
Figure 2-3:	Initial condition of stable flight	- 4 -
Figure 2-4:	Moments and forces after small deflect.....	- 4 -
Figure 3-1:	Allowed impact zone	- 8 -
Figure 4-1:	Example fault tree	- 9 -
Figure 4-2:	Types of events	- 10 -
Figure 4-3:	Altitude and azimuth	- 12 -
Figure 4-4:	NED coordinate frame.....	- 14 -
Figure 5-1:	Position in the NED system.....	- 17 -
Figure 5-2:	Forces and moments acting on the missile	- 18 -
Figure 5-3:	Angular speeds	- 18 -
Figure 5-4:	Reference dimensions and airflow.....	- 19 -
Figure 5-5:	Program interaction	- 19 -
Figure 5-6:	Propulsion subsystem	- 20 -
Figure 5-7:	Trust deviation.....	- 20 -
Figure 5-8:	Mass over time, after the engine burn out it remains constant.....	- 21 -
Figure 5-9:	The CoG shifts forwards during the engine burn phase.....	- 21 -
Figure 5-10:	Mass and gravity subsystem.....	- 22 -
Figure 5-11:	Aerodynamic coefficients subsystem.....	- 23 -
Figure 5-12:	Forces and moments subsystem	- 23 -
Figure 5-13:	Environment subsystem	- 24 -
Figure 5-14:	Alpha, Beta, Mach subsystem	- 24 -
Figure 5-15:	Height simulation comparison	- 25 -
Figure 5-16:	Velocity simulation comparison	- 25 -
Figure 5-17:	Height simulation comparison	- 26 -
Figure 5-18:	Velocity simulation comparison	- 26 -
Figure 6-1:	Nominal case trajectories and flight data	- 28 -
Figure 6-2:	Start pitch angle sensitivity trajectories and flight data.....	- 29 -
Figure 6-3:	CoG in x-direction sensitivity trajectories and flight data.....	- 30 -
Figure 6-4:	CoG in y-direction sensitivity trajectories and flight data.....	- 31 -
Figure 6-5:	CoG in z-direction sensitivity trajectories and flight data.....	- 32 -
Figure 6-6:	ZFW sensitivity trajectories and flight data	- 33 -
Figure 6-7:	Mol Ixx gain sensitivity trajectories and flight data	- 34 -
Figure 6-8:	Mol Iyy gain sensitivity trajectories and flight data	- 35 -
Figure 6-9:	Mol Izz gain sensitivity trajectories and flight data	- 36 -
Figure 6-10:	Trust gain sensitivity trajectories and flight data	- 37 -
Figure 6-11:	Trust direction sideways sensitivity trajectories and flight data	- 38 -
Figure 6-12:	Trust direction pitch sensitivity trajectories and flight data	- 39 -
Figure 6-13:	Fin deflection sensitivity impact positions	- 40 -
Figure 6-14:	Maximum fin deflection impact positions	- 40 -
Figure 6-15:	Missile diameter sensitivity trajectories and flight data	- 41 -
Figure 6-16:	Fin shape chord sensitivity trajectories and flight data	- 42 -
Figure 6-17:	Fin shape span sensitivity trajectories and flight data	- 43 -
Figure 6-18:	Aerodynamic coefficient gain sensitivity trajectories and flight data	- 44 -

Figure 6-19:	Temperature sensitivity trajectories and flight data	- 45 -
Figure 6-20:	QNH sensitivity trajectories and flight data	- 46 -
Figure 6-21:	Wind speed influence	- 47 -
Figure 6-22:	Wind speed and direction influence.....	- 47 -
Figure 7-1:	Multiobjective optimization	- 50 -
Figure 7-2:	Pareto front example	- 51 -
Figure 7-3:	Dominance and Pareto front.....	- 52 -
Figure 7-4:	Pareto front after 20 generations and a population Size of 50	- 54 -
Figure 7-5:	MC Simulation with 1050 simulations, same amount as with GA	- 54 -
Figure 7-6:	Pareto front histogram after 20 generations and a population size of 50.....	- 54 -
Figure 7-7:	MC Simulation histogram with 1050 simulations, same amount as with GA.....	- 54 -
Figure 7-8:	Convex hull obtained with small effort.....	- 54 -
Figure 7-9:	Pareto front after 20 generations and a population size of 100	- 55 -
Figure 7-10:	MC Simulation with 2100 simulations, same amount as with GA	- 55 -
Figure 7-11:	Pareto front histogram after 20 generations and a population size of 100.....	- 55 -
Figure 7-12:	MC Simulation with 2100 simulations, same amount as with GA	- 55 -
Figure 7-13:	Convex hull obtained with medium effort.....	- 55 -
Figure 7-14:	Pareto front after 20 generations and a population size of 300	- 56 -
Figure 7-15:	MC Simulation with 6300 simulations, same amount as with GA	- 56 -
Figure 7-16:	Pareto front histogram after 20 generations and a population size of 300.....	- 56 -
Figure 7-17:	MC Simulation with 6300 simulations, same amount as with GA	- 56 -
Figure 7-18:	Convex hull obtained with large effort	- 56 -
Figure 7-19:	Impact probability histogram with 70000 simulations	- 57 -
Figure 7-20:	Convex hull obtained with both approaches	- 57 -
Figure 7-21:	Danger zones explosion on ground	- 58 -
Figure 8-1:	Final danger zone	- 60 -
Figure 8-2:	Danger zone in comparison to area WTD 91	- 60 -
Figure A-1:	The final Fault Tree	- IV -
Figure A-2:	Electronic Architecture	- V -
Figure A-3:	WTD 91 Test Area	- VI -
Figure A-4:	Types of links	- VII -
Figure A-5:	Thrust over Time	- VII -
Figure A-6:	Start Device	- VII -
Figure A-7:	Euler Rotation	- VIII -
Figure A-8:	GRM Simulink Model	- IX -

List of Tables

Table 4-1: Parameters ranges for MCS and GA optimization.....	- 16 -
Table 5-1: Degrees of Freedom	- 17 -
Table 5-2: Deviation between model and OpenRocket	- 26 -
Table A-1: GRM technical data overview	- III -
Table A-2: Pro54 1635K445-17A data	- III -
Table A-3: Aerodynamic Coefficients.....	- VIII -

Table of Acronyms

Acronym	Description
AC	Aerodynamic Center
AoA	Angle of Attack
CoG	Center of Gravity
DCM	Direction Cosine Matrix
DoF	Degrees of Freedom
FCC	Flight Control Computer
GA	Genetic Algorithm
GRM	Guided Research Missile
MCS	Monte Carlo Simulation
MoI	Moment of Inertia
PDF	Probability Density Function
WTD 91	Wehrtechnische Dienststelle 91
ZFW	Zero Fuel Weight

Table of Symbols

Latin Letters

Symbol	Unit	Description
g	m/s^2	Gravitational acceleration
p	rad/s	Roll rate
q	rad/s	Pitch rate
r	rad/s	Yaw rate
S	m^2	Reference area
d	m	Reference length
DCM	—	Rotation matrix from NED to body system
V_∞	m/s	Free airflow speed

Greek Letters

Symbol	Unit	Description
α	rad	Angle of Attack
β	rad	Sideslip Angle
Ψ	rad	Heading
Θ	rad	Elevation
Φ	rad	Bank

Indices

Symbol	Description
x	Variable related to axial force
y	Variable related to side force
z	Variable related to normal force
l	Variable related to roll moment
m	Variable related to pitch moment
n	Variable related to yaw moment
b	Variable given in the body frame

1 Introduction

1.1 Purpose of this Thesis

In the academic field it is crucial to foster new insights and encourage young scientists. For this reason the GRM is currently developed at the Institute for Flight System Dynamics at the Technical University of Munich. Additionally new control theory algorithms and electronics can be tested with this low-cost testbed. Since the missiles size is in a class which requires airspace clearance, the institute cooperates with the WTD 91, a division of the German Army. They operate a test area for ammunition, drones and missiles that is equipped with cutting edge ground based measurement instruments. For safety reasons missile operators have to bring forward evidence that the missile to be tested is no harm for personnel or equipment. This means that a safety assessment with great diligence has to be done which proves that the required safety regulations are complied with. This study is the purpose of this thesis.

1.2 Structure of this Thesis

The first chapter deals with the requirement that dictate the work to be done. Next the missile in focus, GRM, is described for the interested reader and its technical aspects and data are reviewed. After that the faults and failures to be considered are analyzed in a qualitative and quantitative fashion. For both the fault tree analysis helps to keep an overview and to simplify the upcoming processes. After that the missile simulation model is created as a six degree of freedom model within Matlab/Simulink and Missile DATCOM. This model is then employed in a flight simulation which calculates the flight path for the various changing parameters and influences. The simulation coupled with a Monte Carlo simulation and genetic algorithm within a worst case scenario study reveal the safety implications and the requested evidence for the WTD 91. Finally the generated data and results are discussed and condensed in a short and clear chapter.

1.3 WTD 91

The WTD 91 or Wehrtechnische Dienststelle für Waffen und Munition (defense office for weapons and ammunition) belongs to the German Bundeswehr. It is located in Meppen, Northern Germany, and its history reaches back to the year 1876. It can be seen as the technology center for weapons and ammunition in Germany. The test area is 200 square kilometers large and thus the biggest shooting range in Western Europe. A map of the area can be found in the appendix, see Figure A-3. The airspace above the area is closed for civil aircraft and thus no special flight approval has to be requested from an air control authority. The three different stages of this clearance reach up to 60 000 ft with the lowest restricted area reaching 7000 ft. For the GRM this is more than sufficient. Additional various measurement equipment like Doppler radar and electro-optical tracking devices are available for test and research purposes.

2 Guided Research Missile

2.1 Basic Description

As stated in the introduction the GRM is mainly developed for research and promotion of young students and Ph.Ds. Fields of research are control system theory, thus mainly new algorithms and innovative types of flight control electronics. Compared to its predecessor, the xM, it is a lightweight missile with a start mass of 5 kg, a total length of 1000 mm and a caliber¹ of 90 mm. Other technical details are tabulated in Table A-1. At the time of writing only virtual models and specifications of the GRM exist, therefore parameters like mass and physical dimensions may vary in the final design but can be easily replaced in the developed model later on.

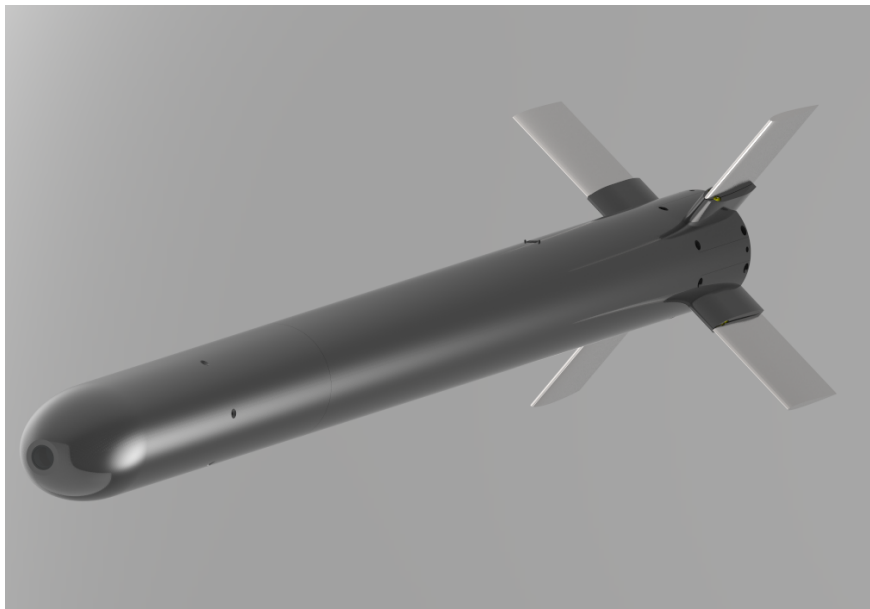


Figure 2-1: The first draft of the GRM. The aerodynamic probe is not included.

2.2 Mechanical and Aerodynamic Design

Mechanical Desing The missile is divided into 2 main parts, the front and aft tubes. In the front part an aerodynamic 5-hole probe is build in. It provides the airspeed, angle of attack (AoA) and sideslip angle β . Additionally this compartment holds the flight control computer (FCC). Sensors and telemetry modules are connected to this FCC. After this compartment a CO₂ cartridge with corresponding electronics is installed that pushes the landing parachute out the tube. Thus the next component is the parachute itself which ensures a safe landing. In the aft section the rocket engine provides the thrust. At the after circumference 4 fins are equally distributed. The actuators with fin position sensors are placed in the same section. The connection between the FCC in the front and the actuators is done via signal cables in the outer part of the two main tubes.

Aerodynamic Design The aerodynamic properties are governed mostly by the fins position at the missiles end. Aerodynamic forces of a wing can be thought to act in the so called Aerodynamic Center (AC). This point is characterized by the property that the aerodynamic moment does not change with the AoA, hence $\partial C_m^{AC} / \partial \alpha = 0$.

¹The caliber of a missile is the diameter of its body section

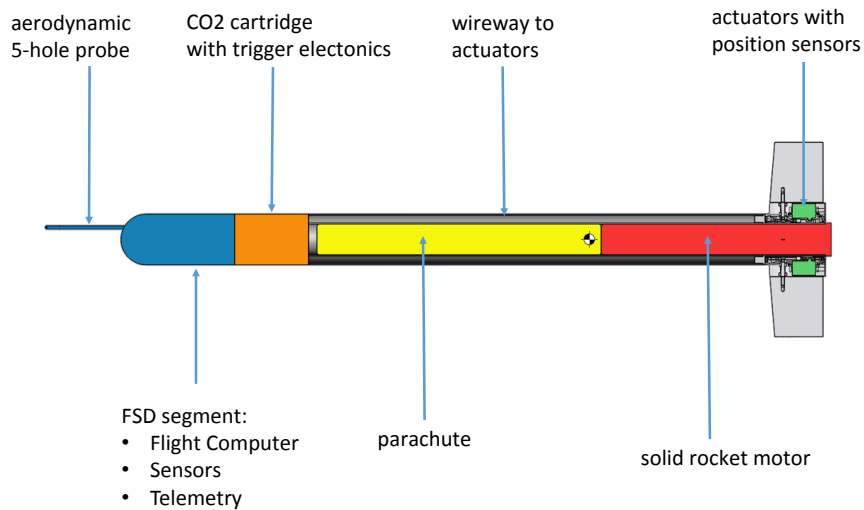


Figure 2-2: Guided Research Missile and its components
(Source: intern FSD presentation [2])

If the AC is aft the Center of Gravity (CoG) the missile is aerodynamic stable [1, pp. 33-67]. This should be explained in the next few lines. An equivalent aerodynamic missile model is shown in Figure 2-3 and Figure 2-4. The moment M_0 is generated by the body and is constant for every α because its reference is the AC. The Lift generated by the body and the control surfaces change with α . For every AoA the fins moments can be neglected since they are magnitudes smaller than the bodies moment. In the initial condition M_0 , the moment due to body lift and the moment due to fin lift are in equilibrium like shown in Figure 2-3. Now assume that a vertical gust changes α by the amount $\delta\alpha$. This disturbance tries to pitch up the missile. The lift generated by the body increases as the lift at the control surface does. The body moment does not change since its reference is still the AC. In total, due to the different distances x_{ACB} and x_{ACT} , the induced moment is pitch down, thus counteracting the disturbance. That behavior is called static stability. One problem might arise as the CoG changes during flight as a result of burned fuel. This might lead to increased stability and is discussed in the model and simulation chapter.

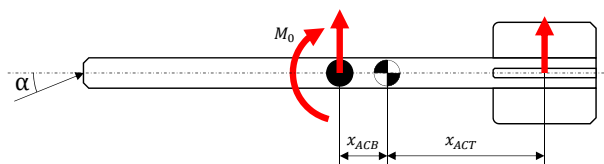


Figure 2-3: In the initial condition the moments and forces are in equilibrium.

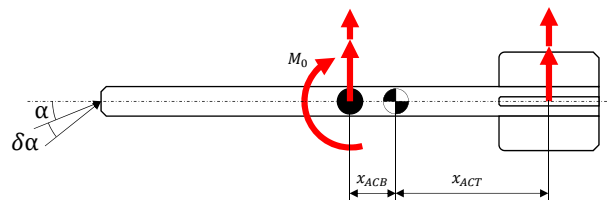


Figure 2-4: The moments and forces due to a small disturbance change but result in a stabilizing additional moment

2.3 Electronic Design

The electronic architecture is shown in Figure A-2. Centerpiece and flight control computer is the Beagle Bone Black with a custom build shield that holds various level converter and connectors. For navigation purposes a Vectornav VN-200 rugged module delivers position, velocity and orientation data. It combines accelerometer, gyroscope, magnetometer and barometric pressure sensors with a GPS receiver module and embedded Kalman filtering. A self developed power management unit supplies power to every component via a 5 V rail and a special 6 V rail for the actuators. The actuators positions are encoded contact free with RM08S rotary encoders each. The 5-hole probe in combination with a separate micro controller calculates aerodynamic information for the Beagle Bone. A telemetry module of type Amber 8350 ensures a stable data downlink to a base station. Further information is tabulated in Table A-1.

2.4 Propulsion

A commercial rocket engine type Cesaroni Pro54 1635K445-17A propels the missile and is sufficient to accelerate it to a maximum airspeed of approximately 290 m s^{-1} and an apogee of more than 2200 m. The engine can be refilled by trained personnel and is reusable. The propellant mixture is solid, other detailed technical information is tabulated in Table A-2.

3 Requirements

The WTD 91 requested various evidence that the missile operation is safe. A requirement document supplemented by them lists every point to consider in a completing form. To be precise four points regarding the GRM require safety considerations and calculations. In the following these four points are described more detailed even if they overlap some of the times. All together these points are sufficient to evaluate possible safety concerns in qualitative and quantitative means. With this the corresponding operation restrictions can be deduced to guarantee a safe research and test environment.

3.1 Stable Flight under various Conditions

It must be proven that the missile is in a stable flight condition under any of the following errors and circumstances, even if they all appear simultaneously.

Alignment Errors The missile is launched with the help of a start ramp/device. The alignment of this ramp underlies deviations since it is positioned manually. Thus the azimuth and elevation (figure 4-3) may vary but no matter what, the missile must stay in a stable flight condition after the launch. A positioning error of the start ramp can be neglected because it can be determined more precise than the alignment and cannot result in an unstable flight condition.

Surface Wind With increasing height above ground wind usually increases. Surface wind appears near earth's ground surface and the lower part of the atmosphere. It is evident that a flying object is influenced by any kind of aerodynamic disturbance like that and implies a safety threat.

Thrust Vector Deviations The missiles thrust vector is ideally congruent with the body axis such that no additional moment around the center of gravity emerges. If the thrust vector direction deviates from this desired direction the missiles flight system dynamics change and result in an additional flight path curvature thus resulting in a potential harm for individuals or equipment.

Manufacturing Deviations The missile model generated with the help of CAD programs is perfect in a physical dimensions point of view. Even if the missile is build with greatest diligence and high-end cutting tools the CAD model and real missile differentiate. The total length and diameter can vary as like the angular dimensions, e.g. the rudder and control surfaces may not be aligned with the body axes. Such influences change the aerodynamics a small amount but additional they shift the center of gravity position and the total mass of the missile. Latter two are crucial for various flight performance and stability considerations and this is the reason why they can't be neglected in a safety assessment.

Sensor Errors Inertial measurement units, gyros and other electronics may fail or produce faulty values. Both events can lead to wrong control surface deflections resulting in an unwanted flight path. A similar aspect is considered with the follow-up item *Control Surface Faults*.

Control Surface Faults They are similar to the before mentioned sensor and alignment errors. First of all the control surfaces can fail to deflect, that means they get stuck in a random position. This leads to the missile being partially or totally uncontrollable, relying only on its inherent stability. Second the opposite event, unwanted deflections of the control surfaces, no matter why, deteriorate the wanted deterministic behavior of the control augmented flight system.

3.2 Wind Influenced Range

The range of a missile or aircraft is the longest distance it can fly referenced from its starting point. Some parameters increase the range like more fuel or engines with a higher amount of total impulse. But also environmental influences like air density, temperature and wind may in- or decrease the range. In this study anything that shortens the range is basically less dangerous but tailwind can significantly increase safety hazard. It should be evident that a missile with short range is less dangerous than the same missile with a bigger reach. Cross wind lets the missile drift aside and thus possibly exit the wanted flight corridor. So in total the three scenarios tail, cross and upwind are influential parameters in this aspect of safety assessment.

3.3 Range and Behavior in the Case of Rudder Failure

The GRM is controlled by four fins (fins are control surfaces in the aft section of the missile) that are driven by one high precision servo each. This requirement item deals with the range and behavior of the missile if one or two out of these 4 servos fail. While two fins may be sufficient to still control the missile in an alternate FCC mode, the performance decreases drastically depending on the actual failed fin positions. The worst case for this scenario occurs if the control surfaces deflect such that the missile flies back to the point of start, towards equipment or alive entities.

3.4 Danger Zone Estimation

This item subsumes the first 3 in a more general manner. The danger zone can be seen as the zone where the missile can potentially hit the ground. More general it is unsafe for individuals to stay in this zone during operations. As a consequence equipment and individuals within this area can be negatively affected. Furthermore every failure and fault mentioned before influences this zone, thus the items *wind influenced range* and *range and behavior in the case of rudder failure* are partially discussed in this particular item. Also the probability of impact is not equally distributed among the danger zone. Areas further away from the point of start may be less prone to impacts and thus less dangerous. With the help of Monte Carlo simulation not only the high danger zone can be computed but the probability of impact too. In total the missile must not under any circumstances exit a given corridor and hit the ground outside a predefined area that is defined in Figure 3-1.

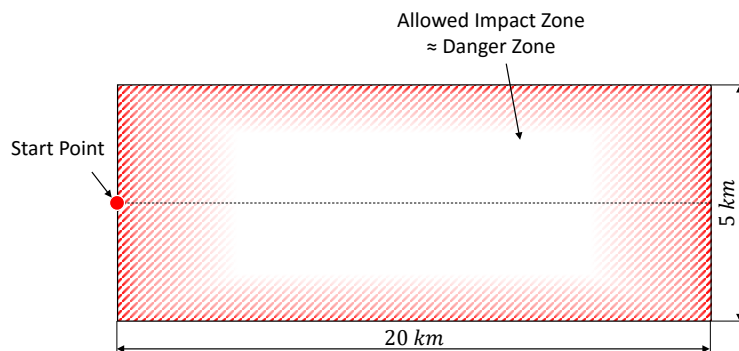


**Figure 3-1: The allowed impact zone in which the missile must go down.
The missile must not exit this defined area.**

4 Fault Tree Analysis

One of the most used graphical techniques in safety assessment is the fault tree analysis. It was developed in the 1960s to cope with the complexity of intercontinental ballistic missile systems and nuclear power plants. From then on it was steadily improved and enhanced. NASA published an FTA handbook which is an excellent start for FTA beginners [3]¹. This thesis uses similar symbols and styles as suggested by this handbook.

The FTA fulfills two main purposes, to conduct a qualitative and quantitative safety assessment. For both purposes the basic principle is the same and straight forward. For the qualitative analysis the FTA has to be conducted as followed: The goal is to identify which events drive the occurrence of an undesired top event. For instance this might be the total loss of an aircraft engine. This top event is the baseline for subsequent steps. Next the engine system is analyzed step by step and events which can cause the top event are identified. Those events may lead to the top event if more of them occur at the same time or they may independently lead to failure. For this reasons events can be linked with AND, OR or other types of gates.

The quantitative method additionally calculates the probability for top events based on the probabilities of the basic events. Every basic event is described by a probability density function. The probabilities are then calculated for every parent event until the top event is reached.

A simple fault tree is shown in Figure 4-1, this example is one of the many in [3]. The event at the top is an undesired event, in this case *D fails*. Underneath is an AND gate which links the two events *A fails* and *B OR C fail*, thus *D fails iff A fails and B or C fail*. The Gate G2 is an OR gate linking the both basic events *B fails* and *C fails*. The circles underneath the event id blocks indicate that those events are basic events. Basic events are not developed any further. Now that every event is a basic event the fault tree is complete. With that it is clear to see what causes the top event D and this supports decision making in an easy to understand manner.

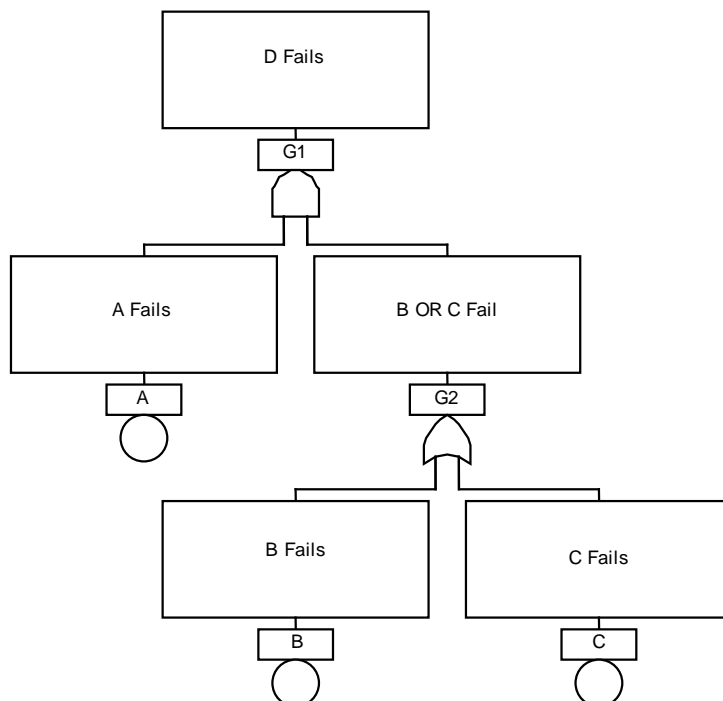


Figure 4-1: An example of a fault tree, taken from [3]

¹ It is freely available at <http://www.hq.nasa.gov/office/codeq/doctree/fthb.pdf>

Besides the basic events other types exists. Figure 4-2 gives an overview of the most often used ones and Figure A-4 states the types of links.

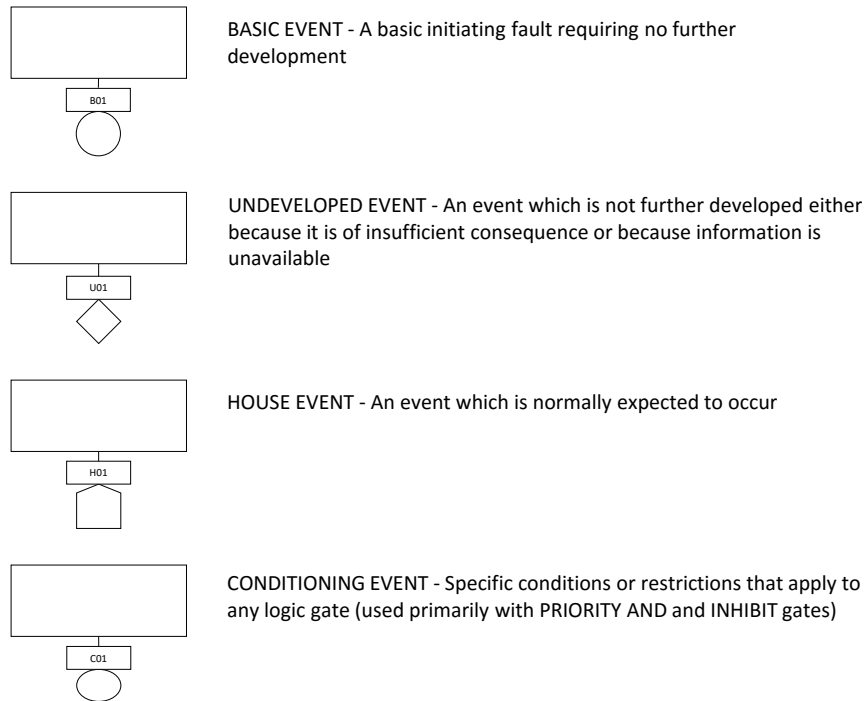


Figure 4-2: Different types of events are possible, taken from [3]

4.1 Fault Tree for the Danger Zone Estimation

The following pages deal with the top event, thus the undesired event and the underlying reasons for that. In regard of computational complexity the following circumstance has to be kept in mind. The later used kind of Monte Carlo simulation calculates thousands of flights. The complexity of this problem is of order $\mathcal{O}(D^E)$ where D denotes the fidelity and E the number of influencing elements. A simple example to visualize this dilemma is the volume calculation of an n-dimensional sphere. For 2 dimensions the sphere is a circle. Lets assume that the radius is 1. A simple approach to estimate the volume, in this case the area is as follows. Two parameters x and y are chosen randomly with values between -1 and 1 $\rightarrow x, y \in [-1, 1]$. The probability distribution is uniform, that means the probability of choosing a value for variable $x \in [0.2, 0.4]$ is the same as $x \in [0.5, 0.7]$, hence the probability for every value within the range is the same. The next step is to check if $x^2 + y^2 \leq 1$ thus the point is inside the circle. If so the variable *inside* is incremented by one. After some repetitions the quotient *inside/tries* is a good approximation for the area of the circle. If a third dimension is added, the number of tries has to increase exponentially to yield a similar magnitude of error.

In our case assume that one flight path simulation takes 0.1 seconds to compute. If the number of basic events is 10 and every basic event takes 10 different values the total computation time is $0.1 \text{ s} * 10^{10}$ which equals 31.6 years.

To calculate the danger zone some simplifications can be used to cope with this highly complex problem. Some events change the danger zone but only the biggest is of interest to us. So only the worst case scenarios are used whenever possible and events that reduce endangerment are left out. As example flight in rain increases the drag and thus reduces the danger zone. So in every simulation no rain is assumed. For other events this is not possible. The start device deviations like azimuth angle can't be cut down to one worst case. So whenever possible events are left out or assumed to be worst case if it does not corrupt the results.

4.1.1 Event Descriptions

Top Event - Missile misses Target Area In our case the undesired top event is a missile impact outside the designated target area. In a perfect world the trajectory can be computed beforehand and the target area, in this special case a point on the ground, is always hit. A second assumption states that no failures or faults occur. In such a world it would be safe for anybody to stand near the computed target area. But in reality the missile may not follow the predicted trajectory. Environmental influences, model uncertainties, assembly tolerances and further variations let the missile drift aside. Thus the area where the GRMs impact probability is nonzero needs to be computed. This area is called *Danger Zone* and is prohibited for individuals. An impact inside this danger zone poses no threat to anything or anybody while individuals or equipment may become damaged if the GRM leaves this danger zone due to false predictions and assumptions. This safety assessment deals primarily with the probability calculation of this top event, thus the possibility that the missile does not go down in the designated target area. Events that may lead to this event are subsequently listed below and discussed. Other events that at first glance also influence the probability but on a closer point of view do not need to be considered are listed as undeveloped events. And last but not least *house events*, thus events always considered in the analysis are listed in the last section of this chapter.

U##: Undeveloped Events are enlisted in the fault tree but are not considered any further. The reason for that is they influence the flight path but in every case the safety does not decrease or it has insufficient consequence. The identification of undeveloped events begins with *U*.

H##: House Events The house event is the opposite of the undeveloped event. It is normally expected to occur and thus always considered in the subsequent calculations. In this thesis it represents a worst case. The identification of house events begins with *H*.

B##: Basic Events Events like B02 - Start/Start Device Deviations - Azimuth Deviation are always considered but differ from house events. Latter are binary, they occur or they don't. In contrast base events are also described by a range of parameters. In B02 - Start/Start Device Deviations - Azimuth Deviation the azimuth angle can take a range of different values and each has to be considered. The identification of basic events begins with *B*.

B01 - Start/Start Device Deviations - Elevation Deviation The missile is launched with the help of a ramp and a sled-like apparatus. The position of this ramp can be determined precisely via GPS or other reference points. The direction in which it points, represented by the elevation and azimuth, can not be controlled that exact. The first angle, the elevation, is the angle between surface and the start direction, see Figure 4-3. The missile flight is ballistic so for a particular elevation a maximum range is achieved. As computed later in the chapter 6 it highly influences the range.

B02 - Start/Start Device Deviations - Azimuth Deviation The second angle determining the start direction is the azimuth. It is the cardinal direction of the GRM on the start device, for flight devices the term heading can be used synonymously. Figure 4-3 shows these 2 angles and Figure A-6 the real start device. Only half of the possible values have to be checked because of symmetry. That means only deviations in one direction are considered and the results are mirrored to obtain the impact positions for the other range of deviation values.

B03 - Start/Start Device Deviations - Engine Exploses The used engine propellant is made out of 792 g explosive material. It should be evident that this amount of explosives yields a very high risk and safety hazard. Thus only personnel with a proper license are allowed to handle and operate the engine. Yet the possibility of a manufacturing fault etc. are existent which can lead to the bespoken explosion of the engine while the missile is still on the start device. This event is not simulated but considered in a calculation on its own.

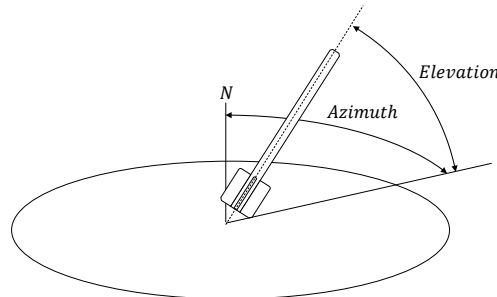


Figure 4-3: Altitude and azimuth of the start device

U01 - Start/Start Device Deviations - Missile Jammed For the first 3m the missile is connected to a sled on the start device. In the case of jamming, thus the GRM is not released from the sled or the sled is jammed, the missile can not take off. In this case the danger zone is more concentrated around the start zone and not the desired impact zone. Nevertheless the potential endangerment is none to less.

U02 - Start/Start Device Deviations - No Ignition The engine is started with an electric match which ignites the propellant. The electric match is connected with wires to the remote start console. If one element in this chain fails the missile is not launched. The situation is nonetheless dangerous as explosives are involved. But on its own electric matches are considered reliable.

U03 - Start/Start Device Deviations - Position Deviation The start device position can be precisely determined with GPS and accurately measured reference points. A position shift of a few meters, which is unlikely, shifts the danger zone at the same amount [4]. Later introduced safety margins and model uncertainties overshadow such small deviations.

B04 - Mass Deviations - Inertia Deviation A big influence on the aircraft dynamics is the mass distribution and other related properties like the Moment of Inertia (MoI). While the total mass and the center of gravity can stay the same, the MoI tensor can change. One reason for such deviations from the reference moment of inertia are manufacturing imperfections. The dimensions of machined parts may vary, the amount of composite resin is not homogeneous or parts may be placed not exactly at the designated place. All together these factors influence the moment of inertia. Finally the dynamics of the missile heavily depend on this, since the angular acceleration is higher the smaller the MoI is, given the same moment. And non-symmetrical MoI tensors might lead to unwanted precession movement of the missile.

B05 - Mass Deviations - CoG Deviation The center of gravity plays an outstanding role in flight dynamics since it influences the majority of characteristics. It is of most importance for the static stability of a missile. If the CoG is too much in the front, the maneuverability deteriorates. This is due to the high stability coherent with this state. On the opposite if the CoG is in the aft section, the missile is less stable or even unstable. This event regards mainly the influence of CoGs longitudinal position. But also lateral deviations impose problems, since the CoG is the reference point for forces and moments acting on the missile.

B06 - Mass Deviations - Mass Deviation Basically the same as before mentioned but in this case the MoI and CoG stay the same but the total mass changes. The reasons for a deviation are the same but the effect on dynamics is a different one. With increasing mass but constant forces like thrust and aerodynamic lift/drag the missiles ability to accelerate declines.

B07 - Thrust Deviations - More/Less Thrust The engine of the rocket is a complex chemical component. Thus impurities and manufacturing process tolerances may lead to more or less thrust than specified in the data sheet or another thrust profile over time. It should be evident that this leads to a changed flight system performance, that can lead to increased range or higher apogee.

B08 - Thrust Deviations - Thrust Direction not Axial If the thrust vector generated by the engine intersects the CoG no additional moment due to thrust is created. The other case in which this vector does not intersect the CoG is characterized by an additional moment that can reach very high magnitudes. Without a flight control system counteracting this additional moment, the flight trajectory changes dramatically [5, p. 96]. Dependent on the thrust direction, the trajectory drifts aside or the range increases. Reasons for a non-design specified thrust vector are again assembly or part tolerances and deviations of the engine itself.

U04 - Thrust Deviations - Vibrations The propellant burning is a rough non-steady chemical process. This results in a vibration of the engine and attached parts. The thrust and its direction is not altered by this phenomenon. A structural or electronic failure due to this vibrations may be an outcome. Thus this basic event can be subsumed under other basic events.

U05 - Thrust Deviations - Explosion Similar to an explosion on the start device the engine can explode mid-air. Dependent on the current height this is more or less dangerous. Like *U12 - Structural Failure* the danger of debris going down is less than the intact missile.

B09 - Aerodynamic Deviations - Control Surface Deflections The GRM has 4 fins in the aft section for control. Each fin is actuated by its own servo. Even though those servos are labeled high precision, high torque etc. the commanded fin angle is not always reached. This non-guaranteed repeatability is considered by this basic event. As an example the commanded fin angle is 0 deg but the true angle is somewhat around 0.2 deg. Now that the missile is controlled with those fins any undesired position deviation changes the aerodynamic forces acting on them. This results in a changed trajectory as every other basic event does.

B10 - Aerodynamic Deviations - Shape Deviations - Control Surface Shape Deviations The Equation 4-1 discloses other factors which influence the aerodynamic forces. The term S is the reference area of the corresponding part. In case of the fin this is the greatest projected fin area . The second term is the non-dimensional coefficient, in our example the drag coefficient C_D . Both variables change with changing geometry as it is easy to realize in the case of the projected fin area. Shape deviations of the fin can be the nose radius, the thickness and length.

$$D = \frac{1}{2} \rho V^2 S C_D \quad (4-1)$$

B11 - Aerodynamic Deviations - Shape Deviations - Body Shape Deviations The same consideration holds for the body shape, the shape of the missile without the fins. A thicker and longer missile has different aerodynamics as a thin and short missile with ceteris paribus.

B12 - Aerodynamic Deviations - Model Uncertainties Every model is a simplification of real entities. Not everything can be modeled yet like non-steady aerodynamic flow or wind turbulences. In this cases only simplifications and less detailed models are used in the subsequent simulation. Of course this leads to less exact results. But a guideline dealing with this states *keep it as simple as possible and as complex as necessary*. To cope with the final uncertainties a margin of safety can be used.

U06 - Aerodynamic Deviations - Flutter Aeroelastic effects like flutter can destroy big airline planes. Parts can be destroyed due to mechanical failure and control surface flutter negatively influences controllability. There is nothing like *the* flutter effect but different phenomenons [6]. In every case energy from the airflow encourages structural motion that deteriorates flight performance. As consequence the range is decreased or the missile might become destroyed, for that event see paragraph 4.1.1.

B13 - Aerodynamic Deviations - Air Density Deviations - Temperature Deviations One variable in the aerodynamic calculations (see equation 4-1 again) is the air density, the higher the bigger are the aerodynamic forces and vice versa. With the ideal gas law $p = \rho R T$ two easier-to-grasp variables can be

used to cope with this fluctuation. The first part is the temperature influence, the density increases with decreasing temperature. On the other hand on hot days the density decreases and so do lift and drag forces. The result is an increased range.

B14 - Aerodynamic Deviations - Air Density Deviations - QNH Deviations The second term in the ideal gas law is the air pressure. In avionics the air pressure at the local airfield is abbreviated with QNH. Like the temperature, a changing QNH influences the aerodynamic forces and thus range.

B15 - Environmental Influences - Cross Wind One major distortion on the flight path is the wind. Every aircraft respectively pilot has to compensate it in order to stay on track. In the uncontrolled case like it is assumed in this thesis nothing compensates for this and the missile drifts away from the desired path. The wind vector is divided into 3 components that match the NED coordinate frame axes at the start position.

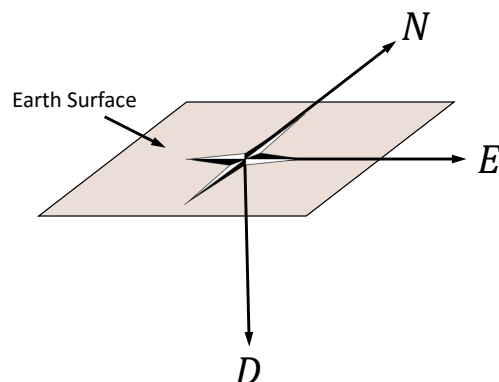


Figure 4-4: The Nord-East-Down coordinate frame

Cross wind is the horizontal component perpendicular the missiles longitudinal axis.

B16 - Environmental Influences - Back/Front Wind Wind from behind the missile or from the front changes the range dramatically. To be precise it is the wind component in the North-East plane perpendicular the cross wind component. It should be evident that for normal aircrafts back wind increases and front wind decreases the range. For missiles however this assumption might not hold as shown in the chapter 6. In the worst case, the back wind is so strong that the missile impacts on the start point or even behind it. Even front wind can lead to this scenario.

U07 - Environmental Influences - Vertical Wind The vertical component of atmospheric wind is in line with the Down axis. It only influences the range but does not shift the Danger Zone horizontally. In general the magnitude of vertical wind is much less than in the horizontal plane [7].

U08 - Environmental Influences - Rain Rainfall increases the drag of an aircraft in a magnitude that can not be neglected [8]. The missile range is thus decreased and the expected impact is closer to the start point. Finally a flight without rain results in the bigger danger zone.

B18 - Control System Fault - Stationary Control Surface Deviation During standard operation the missile is augmented by a flight control system. A handful of sensors gather data like attitude, airspeed and position and this data is then processed by the flight control computer. Depending on the difference between the desired flight trajectory and the actual trajectory the controller sends actuating commands to the fin servos. If the flight control computer, sensors or servos fail the fins stay in an arbitrary position. This of course changes the flight path.

U09 - Control System Fault - Unwanted Movement of Control Surfaces The unwanted movement of control surfaces in this case is a fluctuating movement, hence rapid random changes of the fin positions. In total the flight path trajectory changes but due to the movements energy is dissipated. The missiles range is thus decreased which poses no safety concern.

U10 - Rescue System Fault - Premature Parachute Deployment After the apogee a rescue parachute is deployed to slow down the rate of decent for a safe landing. The situations in which the rescue system fails or faults are the following. In the first case the parachute is deployed premature, that means before the top of ascent during the acceleration phase. In this case the stress is too high and destroys the parachute. A deceleration of the missile associated with a decreased range is the result which yields no increased safety thread. The second failure is described in H01 - Rescue System Fault - No Parachute Deployment.

H01 - Rescue System Fault - No Parachute Deployment The parachute is not deployed during the entire flight phase. Without the deceleration the range takes a maximum. This event represents a worst case scenario which is always considered, thus in our case the standard for the simulation and no parachute is modeled.

U11 - Rescue System Fault - Incomplete Deployment The parachute is not fully deployed and with that the generated drag is less than desired. This event is midway H01 - Rescue System Fault - No Parachute Deployment and a fully deployed parachute. Thus it can be neglected in the simulation.

U12 - Structural Failure Mechanical failures can result in the destruction of the missile in-flight. The debris has a bigger aerodynamic drag and less total impulse and mass. As a result the harm is less than the complete missile and structural failure is not considered any further.

U13 - Foreign Object Damage Bird strike or other objects colliding with the missile in-air may cause a structural failure as discussed in U12 - Structural Failure. Additionally the impact reduces the impulse of the missile even further. The same thoughts as in U12 - Structural Failure apply, the event has no safety impact.

4.2 Event Probabilities - Value Distributions

For the computational complexity to be feasible while receiving viable results the number of events with varying parameters must not exceed a certain number. All other events are always taken into account with the same parameters or left out. For instance U08 - Environmental Influences - Rain is always false because rain reduces the danger zone. In Table 4-1 value distributions for every event are listed. These probability density functions (PDF) are used for both MCS and GA.

4.2.1 Events with Varying Parameters

- B01 - Start/Start Device Deviations - Elevation Deviation
- B02 - Start/Start Device Deviations - Azimuth Deviation
- B04 - Mass Deviations - Inertia Deviation
- B05 - Mass Deviations - CoG Deviation
- B06 - Mass Deviations - Mass Deviation
- B07 - Thrust Deviations - More/Less Thrust
- B08 - Thrust Deviations - Thrust Direction not Axial
- B09 - Aerodynamic Deviations - Control Surface Deflections
- B10 - Aerodynamic Deviations - Shape Deviations - Control Surface Shape Deviations
- B11 - Aerodynamic Deviations - Shape Deviations - Body Shape Deviations
- B15 - Environmental Influences - Cross Wind
- B16 - Environmental Influences - Back/Front Wind

4.2.2 Events without Parameters

- B03 - Start/Start Device Deviations - Engine Explodes
- B12 - Aerodynamic Deviations - Model Uncertainties
- B13 - Aerodynamic Deviations - Air Density Deviations - Temperature Deviations
- B14 - Aerodynamic Deviations - Air Density Deviations - QNH Deviations
- H01 - Rescue System Fault - No Parachute Deployment

4.2.3 Events with no Safety Thread or Not Considered

- U01 - Start/Start Device Deviations - Missile Jammed
- U02 - Start/Start Device Deviations - No Ignition
- U03 - Start/Start Device Deviations - Position Deviation
- U04 - Thrust Deviations - Vibrations
- U05 - Thrust Deviations - Explosion
- U06 - Aerodynamic Deviations - Flutter
- U07 - Environmental Influences - Vertical Wind
- U08 - Environmental Influences - Rain
- U09 - Control System Fault - Unwanted Movement of Control Surfaces
- U10 - Rescue System Fault - Premature Parachute Deployment
- U11 - Rescue System Fault - Incomplete Deployment
- U12 - Structural Failure
- U13 - Foreign Object Damage

Parameter	Diameter	Fin Span	Fin Chord	ZFW	CoG x	CoG y	CoG z	Wind Speed	Wind Direction
Lower Bound	89.8 mm	139.5 mm	69 mm	3.592 kg	-522 mm	-2 mm	-2 mm	0 m s ⁻¹	0 deg
Upper Bound	90.2 mm	141.5 mm	71 mm	3.612 kg	-518 mm	2 mm	2 mm	13.9 m s ⁻¹	180 deg
Parameter	Trust Gain	Gain I_{xx}	Gain I_{yy}	Gain I_{zz}	Trust Pitch	Trust Yaw	Elevation	Azimuth	Fin Deflection
Lower Bound	0.95	0.95	0.95	0.95	-0.1 deg	-0.1 deg	77 deg	-2 deg	-0.25 deg
Upper Bound	1.05	1.05	1.05	1.05	0.1 deg	0.1 deg	83 deg	2 deg	0.25 deg

Table 4-1: Parameters and their probability distributions, every PDF is uniformly distributed

5 Missile Model

5.1 Missile Flight Dynamics

To simulate the flight with all influential parameters a six Degrees of Freedom (DoF) model has to be build. The six DoF are three translational and three rotational which is sufficient for a rigid missile model. While x , y and z are easy to grasp, see figure 5-1, the angular position is not that simple. The Euler convention rotates the missile subsequently around each axis. The first rotation is Ψ , the corresponding axis is z_b . Θ , the second rotation, is around y_b and last comes Φ , this time around x_b . An example is shown in A-7.

Translational Position	x	y	z
Translational Velocities	\dot{x}	\dot{y}	\dot{z}
Rotational Position	Ψ	Θ	Φ
Angular Velocities	p	q	r
Angular Accelerations	\dot{p}	\dot{q}	\dot{r}

Table 5-1: three translational and three rotational DoF are sufficient to describe the missiles state. Additional vectors provide accelerations [1, pp. 13-30]

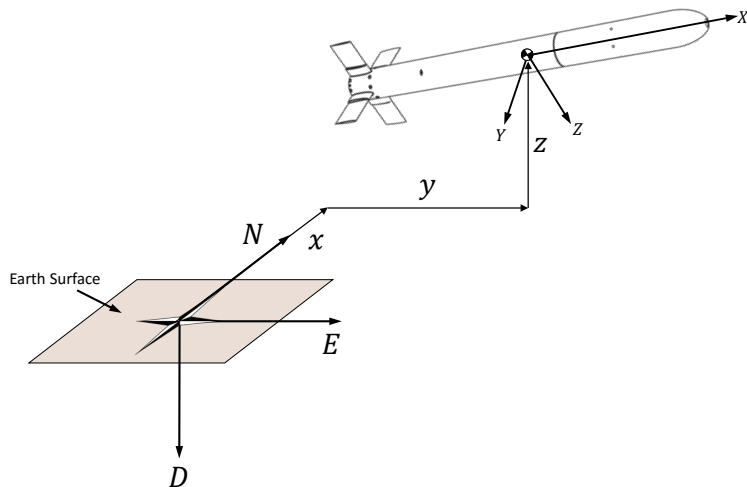


Figure 5-1: The missiles position is described with the 3 coordinates x , y and z . The origin is the earth reference coordinate system at the start point location. The reference point of the missile is its CoG, itself the origin of the body fixed coordinate system

Forces and moments acting on the missile are in reference to the body-fixed coordinate system which origin is the missiles CoG. The convention to name forces and moments is as following [1, pp. 13-30]. Forces given in the body frame are named X , Y and Z and moments L , M and N . Figure 5-2 displays this. Applying Newtonian mechanics yields the following equations for a rigid missiles accelerations [1, p. 78].

$$m(\dot{U} - rV + qW) = X \quad (5-1)$$

$$m(\dot{V} - pW + rU) = Y \quad (5-2)$$

$$m(\dot{W} - qU + pV) = Z \quad (5-3)$$

$$I_x\dot{p} - (I_y - I_z)qr - I_{xz}(pq + r) = L \quad (5-4)$$

$$I_y\dot{q} + (I_x - I_z)pr + I_{xz}(p^2 - r^2) = M \quad (5-5)$$

$$I_z\dot{r} - (I_x - I_y)pq + I_{xz}(qr + \dot{p}) = N \quad (5-6)$$

U , V and W are the speeds regarding the reference coordinate system at the start point in body axis components. Their derivatives in relation to the reference coordinate system, the accelerations, given in the body axis system can be obtained with Equation 5-1-Equation 5-3. Similar angular accelerations can be computed with the moments L , M and N , see Equation 5-4-Equation 5-6. A simple propulsion model provides the thrust forces and moments around the CoG. Gravitation can be easily computed too, referring to section 5.3. The most difficult loads to compute are aerodynamic loads. This data is generated with the help of Missile DATCOM.

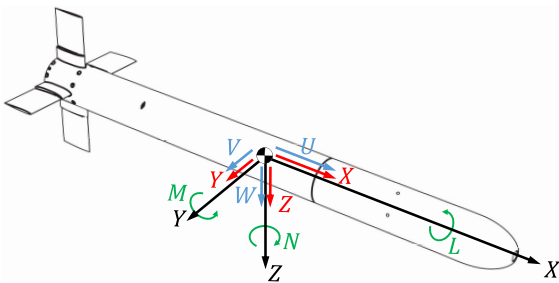


Figure 5-2: Forces (red) and moments (green) are described in the body-fixed coordinate system

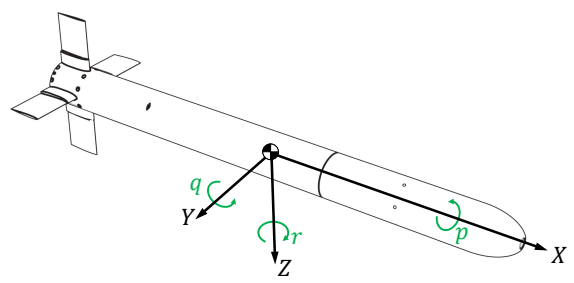


Figure 5-3: Angular speeds follow a similar notation style, they are named p, q and r .

5.1.1 Missile DATCOM

Aerodynamic loads are computed with the equations in 5-7 - 5-12. Most of the terms are easy to gather, the density ρ is one formula respectively provided by an environment submodel and the aerodynamic velocity V_∞ is provided by the model itself as a state. On the other side aerodynamic coefficients (C_X, C_Y, \dots) are hard to compute and approximated at best by empirical and standard methods, they are listed in [9]. Missile DATCOM is a batch program developed by the USAF. Its main purpose is to provide aerodynamic data for preliminary missile design. The user has to provide a file with the missiles geometry and other parameters like CoG position or surface roughness. Missile DATCOM then computes the aerodynamic coefficients for that given geometry and fin deflections. The data is tabulated for various Mach numbers and AoA as a comma-separated values file that can be imported and processed by Matlab. The coefficients e.g. C_X are not directly provided by Missile DATCOM but their derivatives as they are needed for the simulation, see equation 5-13. Hence the coefficient is a sum of the respective derivatives multiplied by the different states.

$$X = 1/2\rho V_\infty^2 S C_X \quad (5-7)$$

$$Y = 1/2\rho V_\infty^2 S C_Y \quad (5-8)$$

$$Z = 1/2\rho V_\infty^2 S C_Z \quad (5-9)$$

$$L = 1/2\rho V_\infty^2 S dC_L \quad (5-10)$$

$$M = 1/2\rho V_\infty^2 S dC_M \quad (5-11)$$

$$N = 1/2\rho V_\infty^2 S dC_N \quad (5-12)$$

$$C_{(*)} = \sum_i \frac{\partial C_{(*)}}{\partial i} i \xrightarrow{e.g.} C_M = C_{M0} + \frac{\partial C_M}{\partial \alpha} \alpha + \frac{\partial C_M}{\partial \beta} \beta + \frac{\partial C_M}{\partial q} q + \frac{\partial C_M}{\partial p} p + \dots \quad (5-13)$$

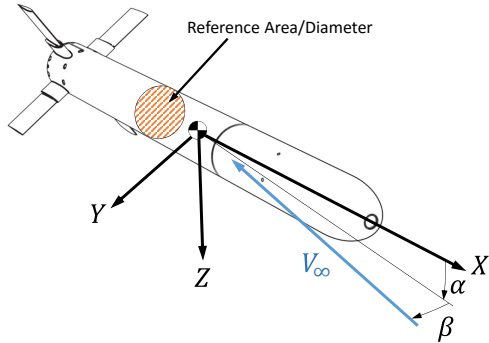


Figure 5-4: Reference area S and diameter d are needed for the force and moment equations. AoA and sideslip angle are the angles between the free airflow and the body axes

5.1.2 Modeling Framework and Programs Used

The main program used in this thesis is Matlab and Simulink in version R2015b. Within Matlab the simulation parameters are changed and afterwards Simulink is called to simulate the flight. The results are then returned to Matlab and further processed and saved. Simulation parameters are all before mentioned base events that influence the range and impact position and are listed in Table 4-1. Aerodynamic data needed for the simulation is generated with Missile DATCOM prior every Simulink call. The order of program calls and dependencies are described in Figure 5-5.

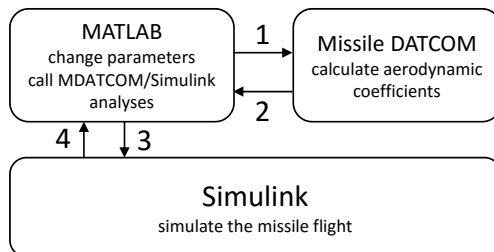


Figure 5-5: The three programs are subsequently called in this shown order

5.2 Simulink Missile Model

Before the start of modeling the missile the fundamental software and model architecture has to be worked out and fixed. Fortunately the need to build up a six DoF model by scratch was not necessary, since the Matlab/Simulink help and documentation already feature a fully working model. Despite its intentionally use for a lifting body aircraft, the HL-20, a few changes, simplifications and enhancements made it possible to reuse the core of it for the GRM model. Another plus point is that the model itself was already used and proven in an sophisticated way. Before mentioned changes include the atmosphere model, the existing submodel was replaced by a less complicated model with constant wind speed over height. Since the HL-20 has a constant mass in the scope of the featured model, the mass and CoG submodels had to be expanded or created as well. Similar the propulsion system and aerodynamic coefficients were created by scratch respectively enhanced with body rate damping coefficients. For further information on the so called HL-20 model see the Matlab/Simulink help or [10].

5.3 Submodels

For the sake of a better understanding and overview the model is divided into different submodels and atomic blocks. Later are blocks that can not be divided any further, e.g. the sum or multiplication block are atomic. A model overview is given in A-8 and the submodel details are shown in the corresponding subsections. For a clearer representation, inputs are green, outputs are magenta, atomic blocks have the color orange and look-up tables and constants imported from Matlab workspace are yellow. The state integrator (atomic) is the core of the model, it computes the states and their derivatives given the input forces, moments and mass properties. Thus it solves the Equation 5-1-Equation 5-6. A few submodels provide these inputs and are described next.

5.3.1 Propulsion

The rocket engine Cesaroni Pro54 1635K445-17A is of solid fuel type, its total impulse is 1636.3 N s. Other technical information can be found in A-2 and the trust over time behavior in A-5. Since these important characteristics are already known the only crucial step is the mass over time model. The mass flow rate can be approximated to be proportional to trust [5, p. 47-75]. Hence the mass flow rate is a maximum at the beginning and declines sharply after 3 s. Other rocket models and programs handle this the same way, see 5.4.2. The second part embedded in this submodel is the trust direction (deviation) and therefore induced additional forces in y- and z-axis direction, Figure 5-7. Moments due to that are computed in the submodel Forces and Moments. The consideration of non-axial trust is needed for the safety related simulation part as stated in chapter 4.

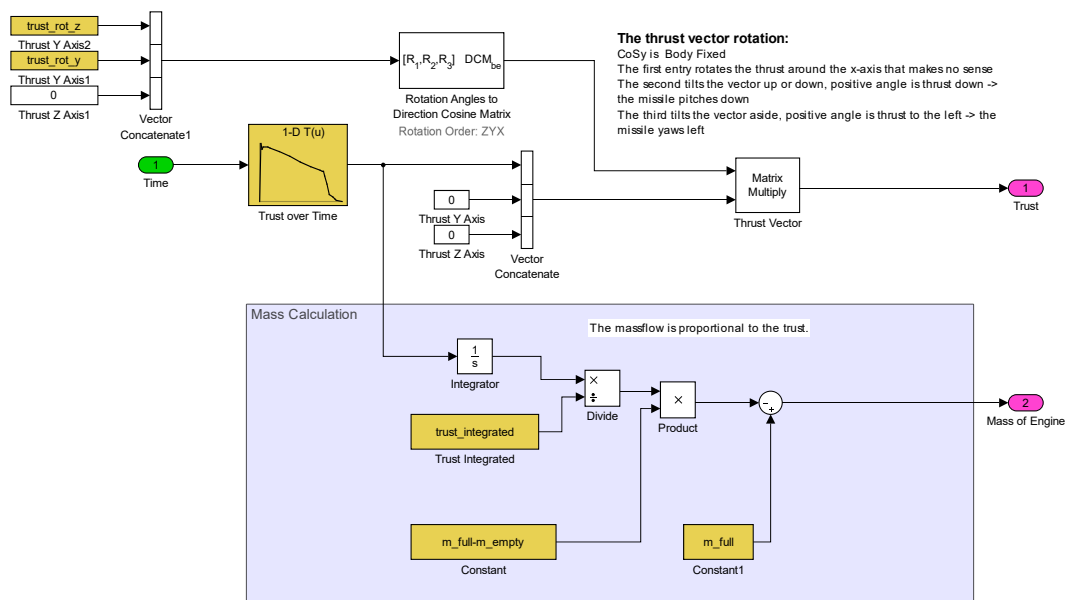


Figure 5-6: Propulsion subsystem

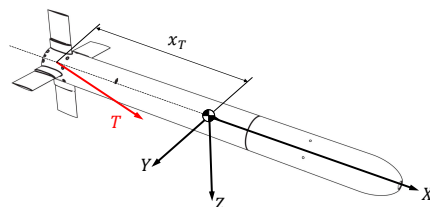


Figure 5-7: The trust force T does not have to be parallel to the x body axis

5.3.2 Mass and Gravity

One force always acting on the GRM is gravitation, in this context the approach is a constant gravitational acceleration pointing towards the ground. The total mass of the missile is made up of the engine mass m_E and the missile mass without the engine m_{GRM} . Later does not change during flight, the computation is therefor straight forward, see 5-14 for how the gravitational force is computed in the body axis system. DCM stands for direction cosine matrix, a rotation matrix from NED to body system. More difficult and important is the CoG and Mol computation, they govern the dynamic behavior and stability properties. For the model the missile is regarded as two points of mass as before and simple formulas can be used. As a result the CoG is between the GRM CoG and Engine CoG in the beginning and moves towards the GRM CoG during flight. The Mol tensor is symmetrical by nature. I_{xx} , the Mol about the body x-axis is treated as fixed and approximated as a tube where the missile mass is concentrated within 50% and 100% of the radius thus $I_{xx} = m \frac{r_1^2 + r_2^2}{2}$. Other entries of the Mol tensor like I_{xy} are derived by 5-15 assuming the two point mass model. The derivative of Mol is computed by Simulink with the derivative atomic block. For later points in time when the missile development is finished and the design is fixed CoG and Mol information is provided by CAD programs.

$$\left(F_G \right)_B = (m_E + m_{GRM}) DCM \begin{bmatrix} 0 \\ 0 \\ g \end{bmatrix} \quad (5-14)$$

$$MoI = \sum m \begin{bmatrix} 0 & -xy & -xz \\ -xy & x^2 + z^2 & -yz \\ -xz & -yz & x^2 + y^2 \end{bmatrix} + I_{xx} \quad (5-15)$$

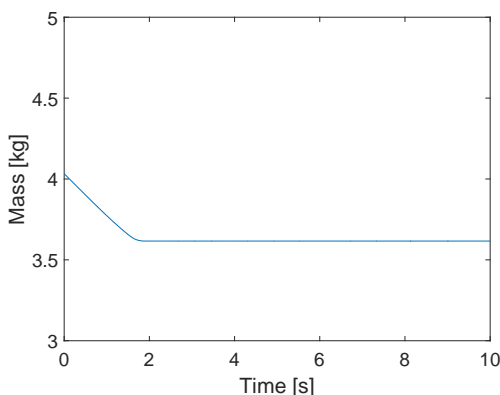


Figure 5-8: Mass over time, after the engine burn out it remains constant

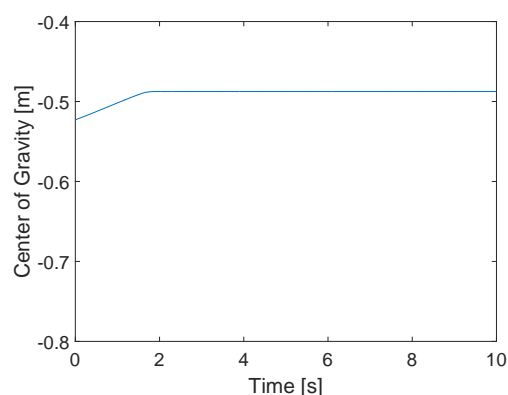


Figure 5-9: The CoG shifts forwards during the engine burn phase

5.3.3 Aerodynamic Coefficients

MDATCOM generates the aerodynamic coefficients for a set of given Mach numbers and AoA. Stored in a look-up-table the access to the right number is simple and efficient with pre-look-ups. The two parameters AoA and Mach with the addition of airspeed, body rotation rates and geometric reference lengths provide the right coefficients at the outputs. As MDATCOM divides coefficients into datum and body rate damping coefficients it is done the same way in the model. Datum values correspond to forces and moments for the non-rotating missile while body rate damping values only consider the rotating missile. For an overview a table of calculated coefficients is given in A-3. At the end both are summed up and provide the 6x1 coefficient vector, corresponding to 3 forces and 3 moments in body axis system as described in 5-7 - 5-12.

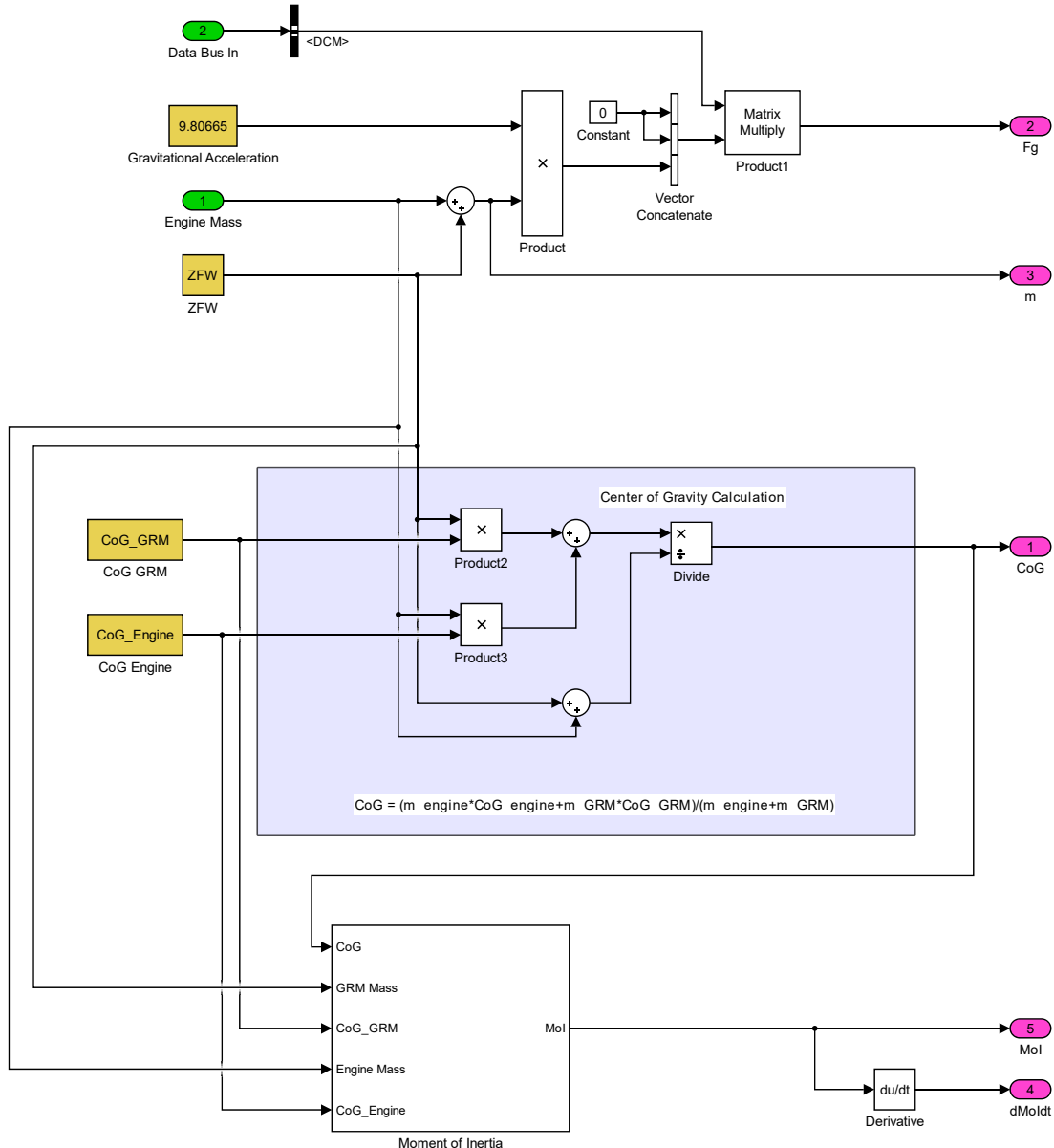


Figure 5-10: Mass and gravity subsystem

5.3.4 Forces and Moments

With the aerodynamic coefficients the equations 5-7 - 5-12 provide the aerodynamic forces and moments in body axis system. In the Forces and Moments submodel these equations are evaluated and the additional forces and moments due to thrust are added. No other loads act on the missile during flight and are considered in the model. These inputs fed into the state integrator block result in a transversal and rotational acceleration, that integrated lead to the kinematic velocity and integrated a last time provide the position in global NED coordinates.

5.3.5 Environmental Models

As the air density and wind influence the aerodynamic forces they have to be considered as well. The ISA atmosphere model is a simple but sufficient model for this case, the input parameters are the height, QNH, temperature and air density at mean sea level. To calculate the environmental characteristics for a start

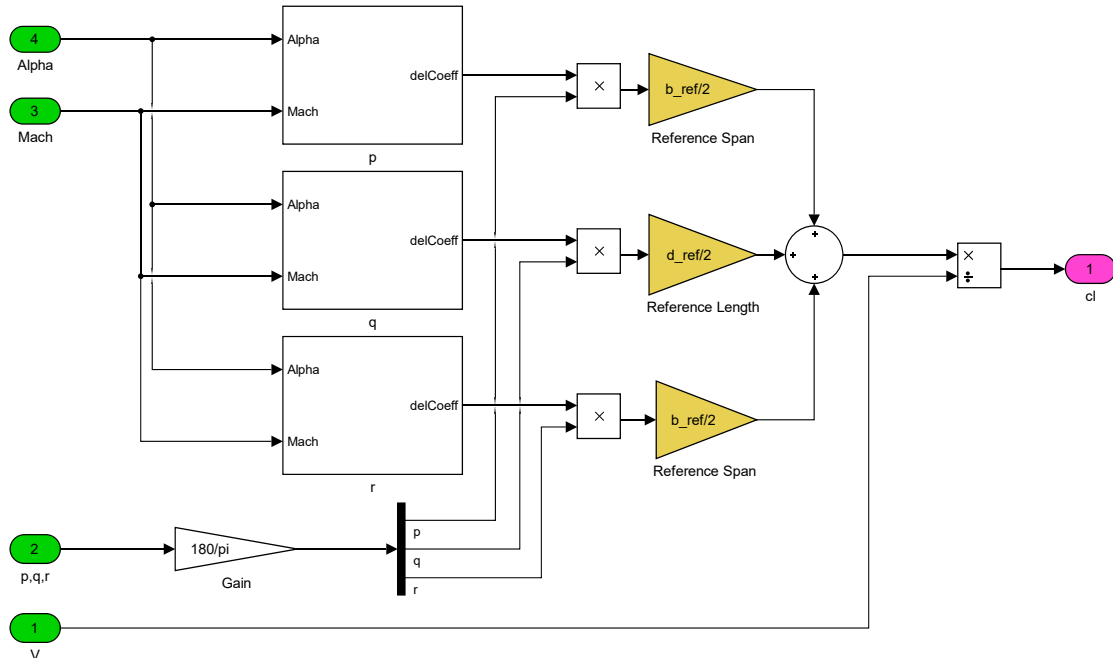


Figure 5-11: Aerodynamic coefficients subsystem

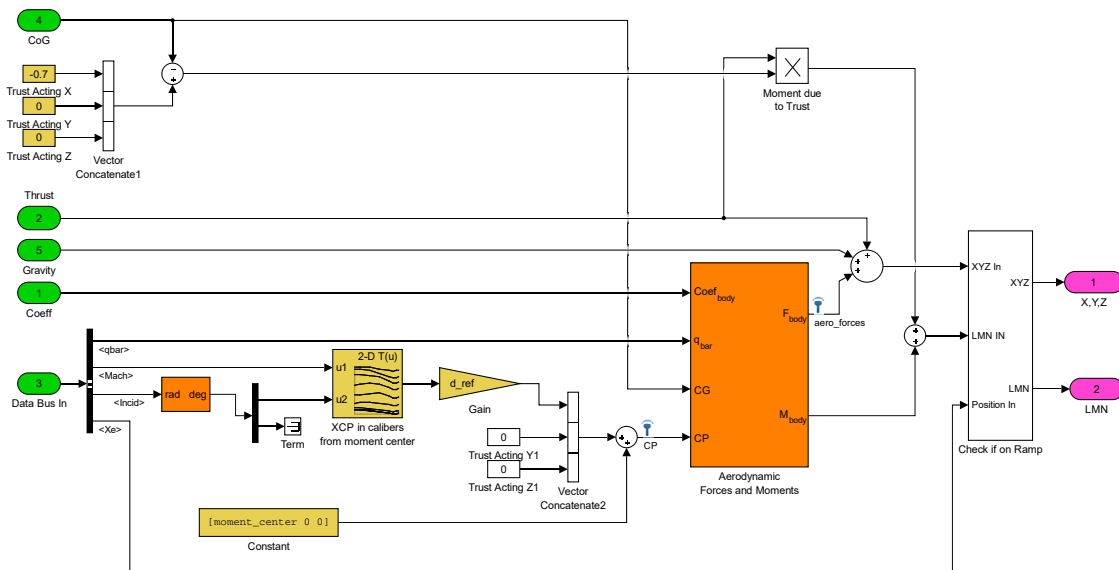


Figure 5-12: Forces and moments subsystem

point not elevated at mean sea level the QNH and temperature have to be provided to the simulation. The second possibility is to enter the standard atmosphere data (QNH = 1013.25 mbar, air density = 1.225 kg m^{-3} and temperature = 288.15 K) with the start points height above mean sea level. For a flight within a windy environment different aspects of wind speed models are considered, the steady wind speed and wind shear distributions. In this case the wind is build up of a steady wind speed distribution over height and a discrete wind gust model, but for the following ongoing simulation only constant wind is assumed. Wind gusts and turbulence may be considered at later design and development stages and were not removed respectively implemented. Both input parameters, the wind speed and wind direction do not change during the simulation time. Thus the wind speed and direction is constant over height and time. Outputs of this

submodel are the speed of sound, that is needed for the Mach computation, the wind velocity vector, the air density at the current height and wind angular rates if considered.

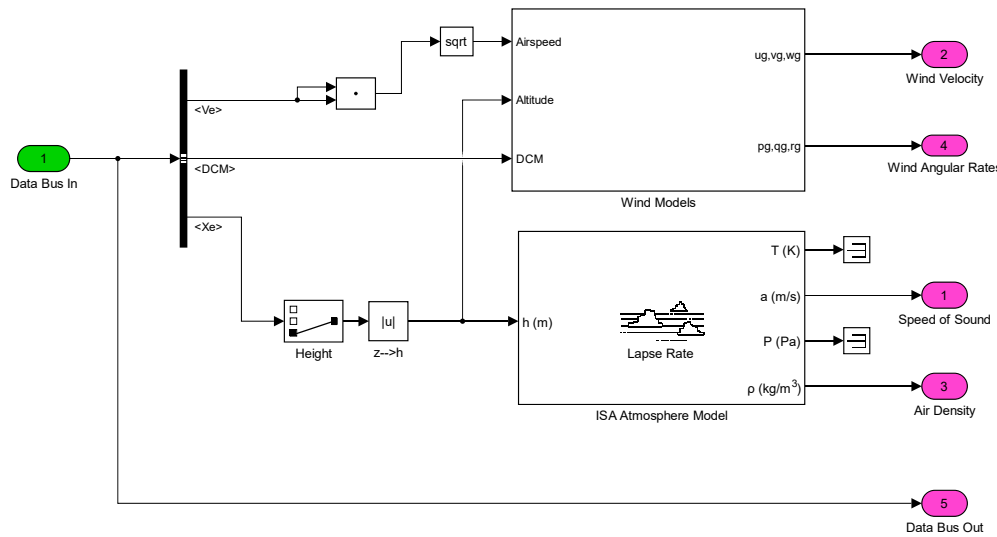


Figure 5-13: Environment subsystem

5.3.6 Alpha, Beta, Mach

With the environmental properties and wind vectors the three main parameters alpha, beta and Mach can be determined, they are needed for the coefficient look-up-tables. Extra variables aerodynamic p,q,r and the dynamic pressure $q = 1/2\rho V^2$ are outputs too for coefficient and force calculations.

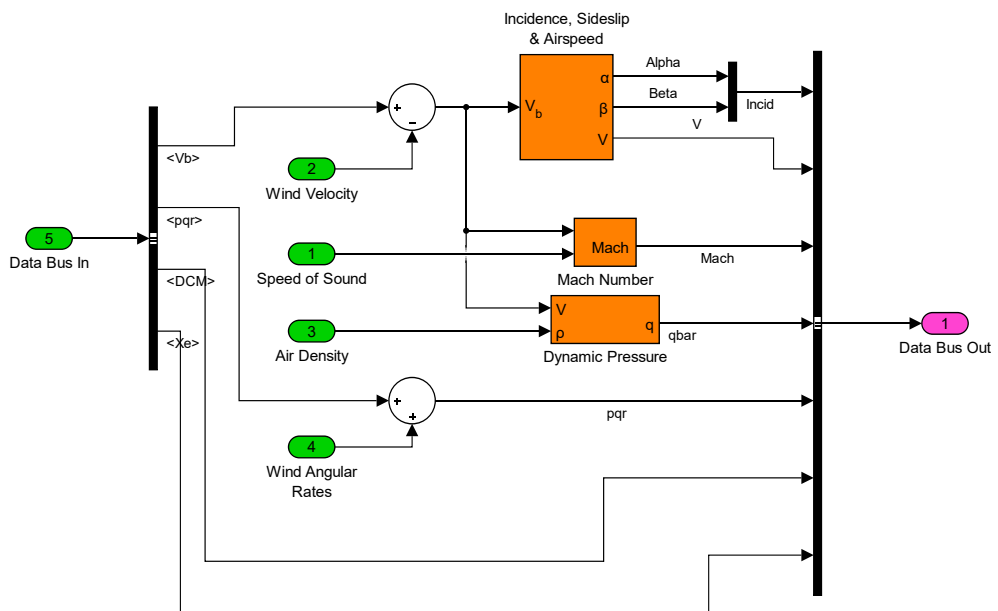


Figure 5-14: Alpha, Beta, Mach subsystem

5.4 Model Validation

As with every model the reality can not be described exactly, but that is not required anyway as simplifications speed up the modeling process while the results may still yield usable results. But for serious employment the models precision and accuracy must be in specified scopes. To show compliance with these requirements and to check the accuracy the model is validated against real flight recordings and another rocket flight simulation program, OpenRocket¹. On a level deeper studies point out MDATCOMs coefficient results compared with wind tunnel tests [11]–[13]. Findings of [12] show that normal forces correlate well to wind tunnel tests, the same holds for pitch moment coefficients. Bigger discrepancies in the magnitude of 12% regarding axial force occur, underestimating drag for most configurations.

5.4.1 Comparison to Real Flight Recordings

Existing MDATCOM geometry files for GRMs predecessors xm1 and xm2 were used within the simulation framework. The results were compared with real flight recordings. Unfortunately not every information needed was available, like QNH or start device orientation at the starting site. Nevertheless they were reasonable assumed or researched at online weather service platforms. Other data like wind speed in different heights can not be provided and may differ by a large amount from the environmental assumptions, a constant wind speed and direction for every height.

Figure 5-15 (Height simulation comparison) shows the simulated height above ground versus a recorded flight of the xm2 missile. The green line is the recorded flight while the other two dashed lines correspond to the recorded flight height $\pm 15\%$. Like stated before the simulation underestimates the drag and therefore overestimates the apogee. The discrepancies between simulation and recorded flight after 15 s rise due to the non-existing parachute model. In real the parachute was deployed at the apogee. When comparing the vertical speed the values of the Simulink model are not that off. Another possibility for the differences may be wind during the real flight recordings. Depending on the wind direction it pitches the missile up- or downwards and with that the flight trajectory changes drastically. For appliances in this context, safety related, an overestimation is not crucial and thus not that of a problem.

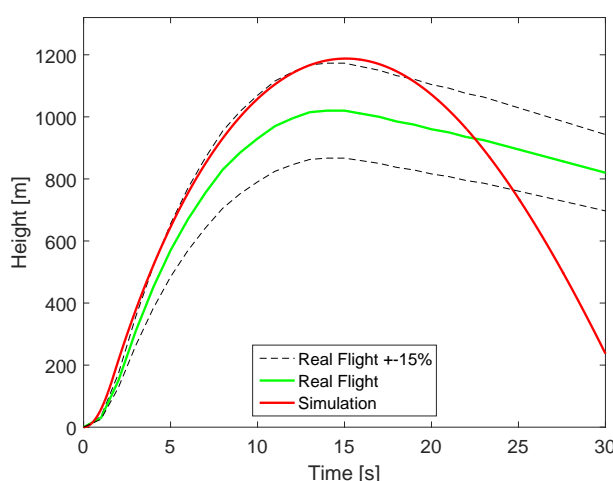


Figure 5-15: Height for the Matlab/Simulink model and real flight recordings $\pm 15\%$

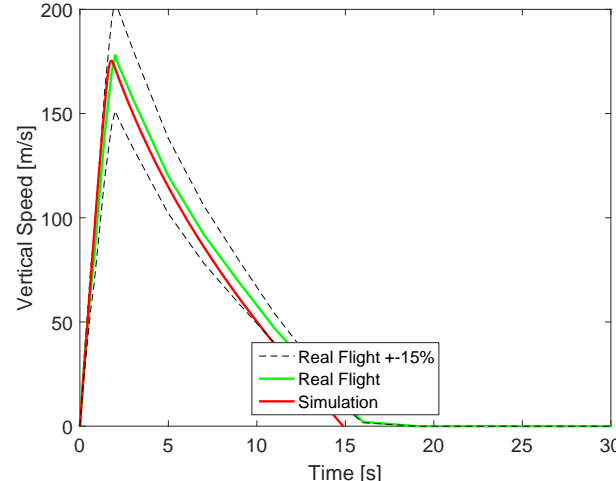


Figure 5-16: Vertical speed for the Matlab/Simulink model and real flight recordings $\pm 15\%$

¹<http://openrocket.sourceforge.net/>

5.4.2 Comparison to OpenRocket

Another Tool used for preliminary missile design is OpenRocket. It features an easy to use GUI and many advanced options but is still usable by non-experts. The simulation is six DoF as well and results can be exported and plotted. Since both MDATCOM and OpenRocket files are already available for the xm2 missile it is used in this comparison instead of the GRM. Simulations reveal that OpenRocket used the same method for the engine mass flow rate and hence the mass over time behavior is the same for both Matlab/Simulink and OpenRocket. As a consequence the CoG position is the same too. The biggest deviations occur if the drag forces respectively the axial forces are compared. As a result the trajectories differ by a greater amount as shown in Figure 5-17 and Figure 5-18. The maximums of the absolute values airspeed, apogee and range are listed in Table 5-2 with the respective deviation in percent. Maximum absolute airspeed is with 2.57% deviation close to the OpenRocket simulation, the same is true for the apogee with -4.6%. Only the range differs by approximately 117 m or 14.3%. Nevertheless these magnitudes are still in an acceptable scope.

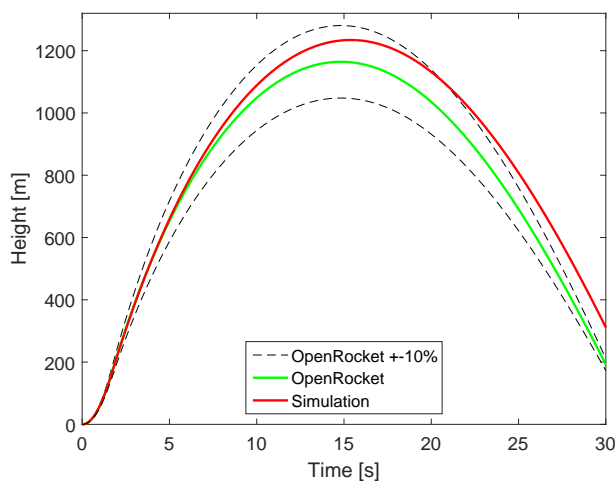


Figure 5-17: Height for the Matlab/Simulink model and the OpenRocket simulation $\pm 10\%$

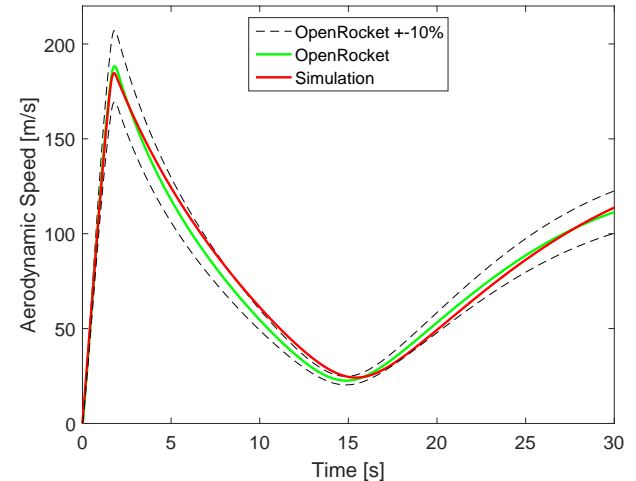


Figure 5-18: Absolute velocity for the Matlab/Simulink model and the OpenRocket simulation $\pm 10\%$

Variable	Matlab/Simulink	OpenRocket	Deviation
Maximum absolute airspeed	183.55 m s^{-1}	188.26 m s^{-1}	2.57%
Apogee	1220.43 m	1164.3 m	-4.6%
Range	816.71 m	699.85 m	-14.3%

Table 5-2: Deviation between Matlab/Simulink model and OpenRocket for different variables

6 Sensitivity Analysis

The reason for any sensitivity analysis is the same, the influential parameters have to be divided into crucial and non-crucial parameters. In this case the question to answer is the following, which parameters change the GRMs range and impact position and thus pose a danger to humans and equipments. The procedure is the same for every parameter, from the nominal value small deviations are introduced in the model and the responses are measured against this small deviations. For a better overview the six resulting figures are the same for every sensitivity analysis even if they are not that helpful in every case. The top-left figure (referred to as Plot 1) shows the sensitivity itself, that means the change of range with respect to the parameter. In a mathematically way a sensitivity can be expressed as $\partial Range / \partial Parameter$. Next to that the aerodynamic velocity in body-x direction over time shows influences of the parameter to that and the flight time (Plot 2). The two plots in the middle display the flight path from a top-down view and the impact position, that means the end of the flight path. The lower-left graph shows the flight path from a sideways point of view, hence the height over position in x-direction. Last but not least a 3D trajectory plot enhances the flight path understanding for more complex patterns.

The ranges over which the parameters are varied are chosen bigger than in the later conducted Monte Carlo simulations. With realistic deviations it is possible to estimate the change of range and impact position. Finally the main reason for the sensitivity analysis is to keep the simulation effort in a feasible region as mentioned in chapter 4 and to gain more insights in the model behavior. Parameters with a small influence are left out or a fixed worst case value is used for simulation. The ranges respectively fixed values used in the MCS and GA optimizations can be found in the corresponding sections. The probability distribution is set to uniformly distributed in every case, this way it is more likely that greater deviations are chosen while a maximum deviation exists unlike with a normal distribution.

6.1 Nominal Flight

For comparison a flight with nominal parameters and no environmental influences is shown. The temperature are 288.15 K and the QNH are 101 325 Pa. The start azimuth angle is 80 deg wide.

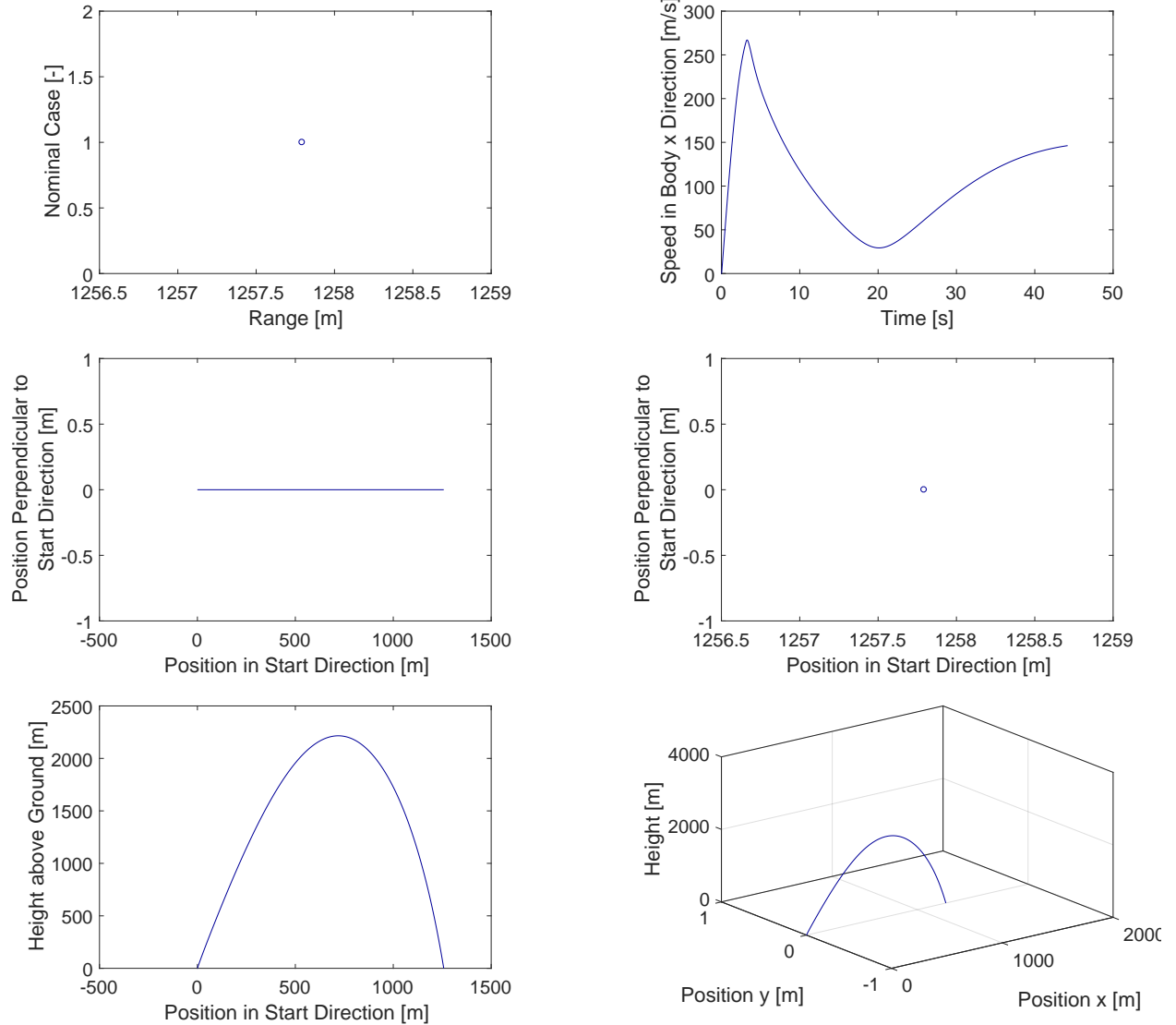


Figure 6-1: Nominal case trajectories and flight data

6.2 Azimuth Deviations

The azimuth angle is varied between 10 deg and 85 deg. Plot 1 shows that the range increases with rising angle and reaches a maximum of approximately 3372 m at around 45 deg. With further increased angle the range decreases again and approaches 0 m at an angle of 90 deg. The influence on the range is thus dependent on the start angle, a shift from 70 deg to 80 deg changes the range more than from 40 deg to 50 deg. Since the nominal angle is 80 deg this parameter has to be considered in the subsequent Monte Carlo simulation and Pareto front optimization. The value range for MCS and GA optimization is uniformly distributed between 77 deg to 83 deg.

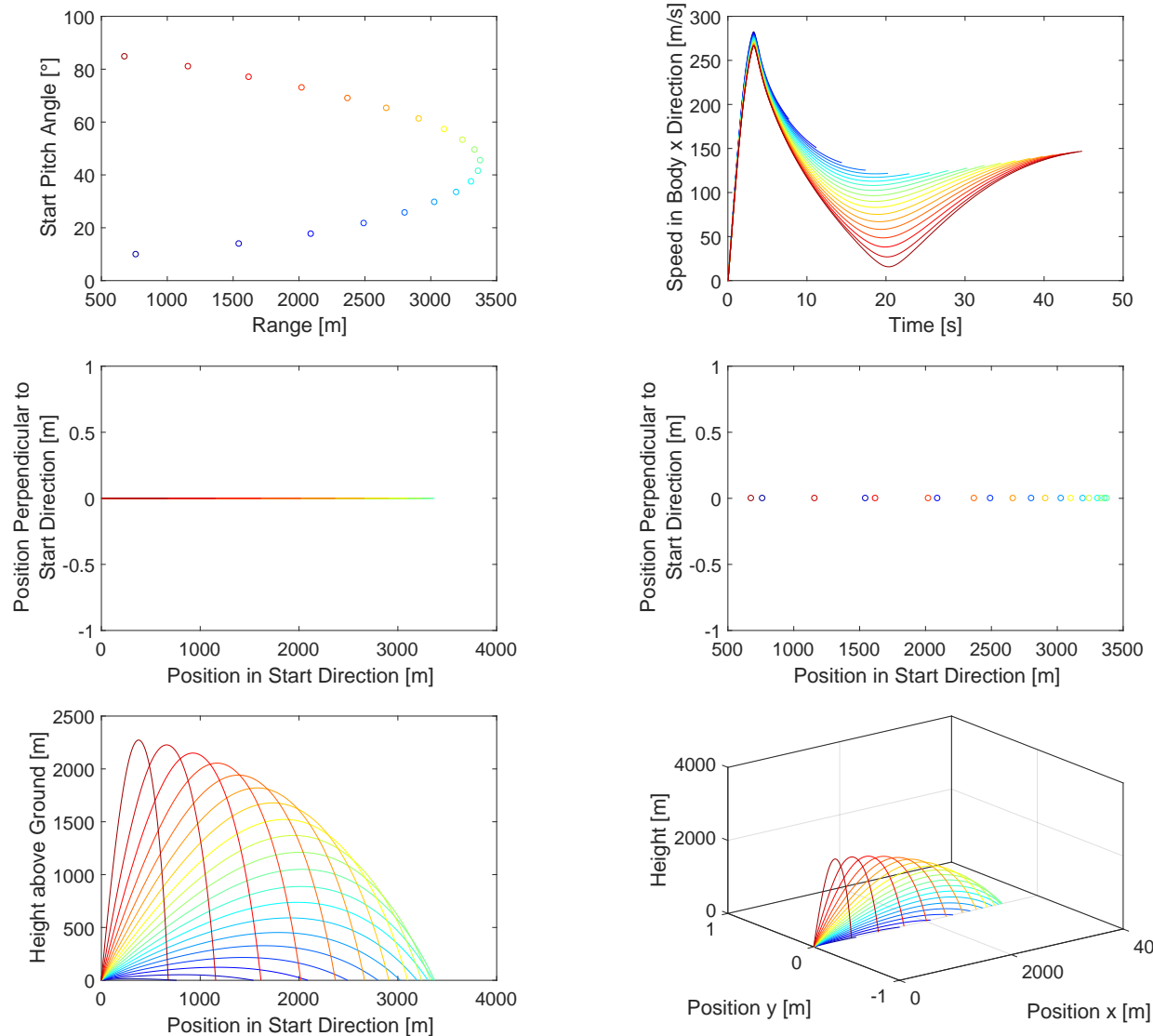


Figure 6-2: Start pitch angle sensitivity trajectories and flight data

6.3 CoG Deviation

The CoG position in body x-direction only plays a minor role regarding the range. A realistic deviation of 1 cm forward and backward is not crucial for the missiles impact position. Nevertheless the static stability changes but as long as the CoG stays in front of the aerodynamic center the missile is regarded stable. The values range from -0.518 m to -0.522 m .

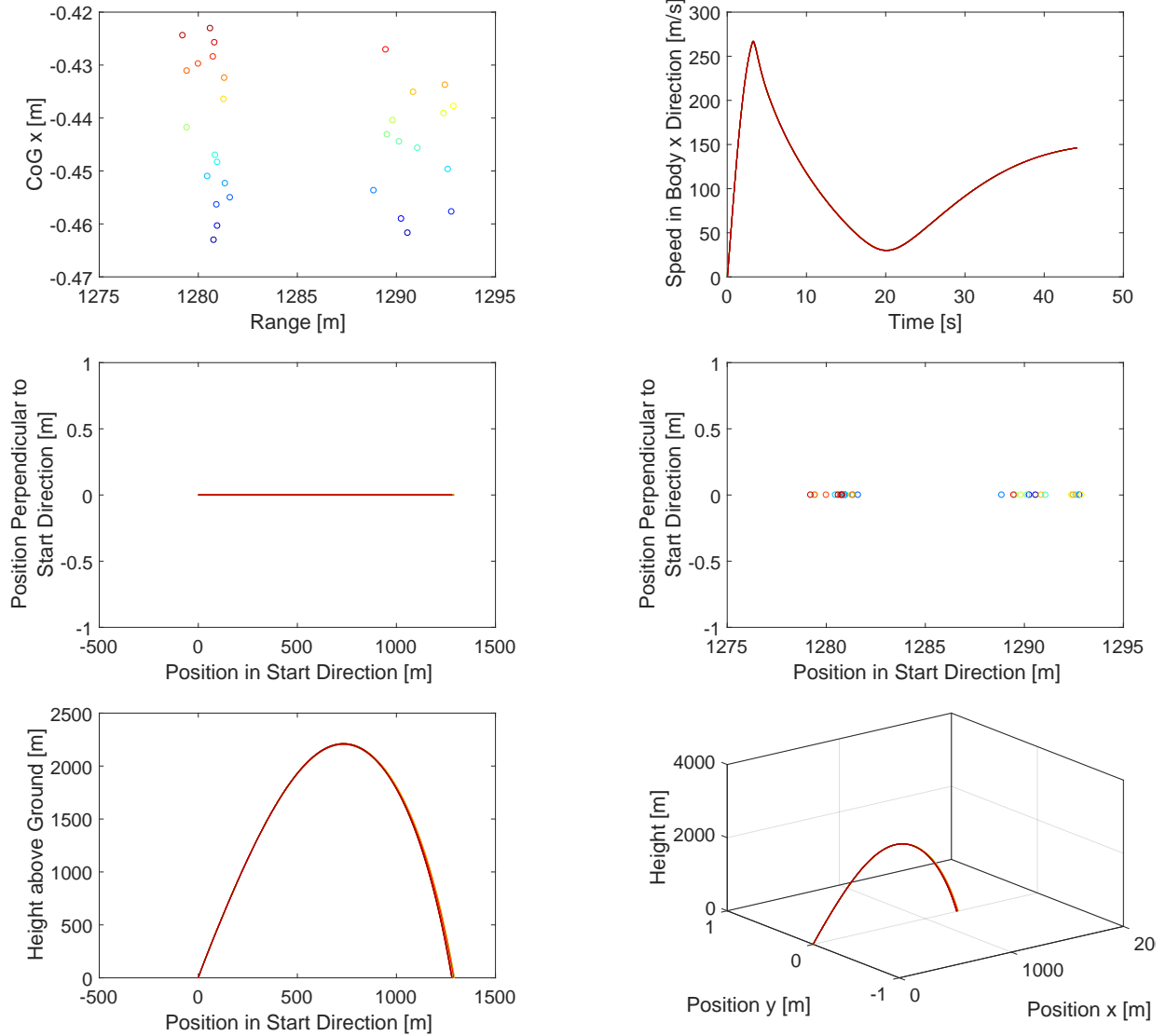


Figure 6-3: CoG in x-direction sensitivity trajectories and flight data

In body y-direction the impact of even small deviations as like 5 mm change the flight path drastically sideways the start direction. The range increases about 230 m and the impact position drifts 900 m aside. Other parameters like velocity and apogee remain almost constant. The location is in a range of -0.002 m to 0.002 m.

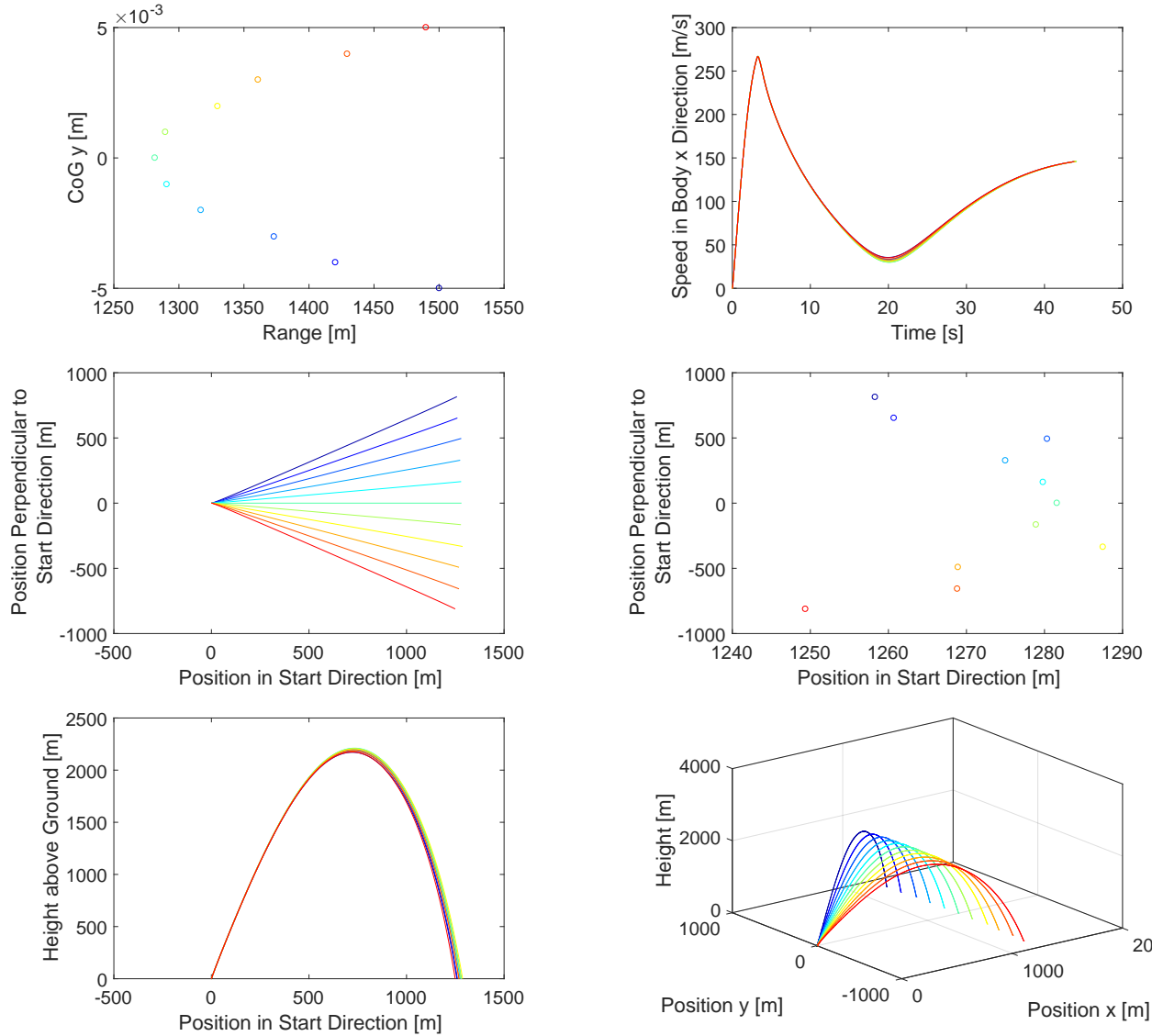


Figure 6-4: CoG in y-direction sensitivity trajectories and flight data

As in y-direction the body z-position of the CoG is sensitive, a 5 mm change increases the range of about 800 m. The effect is the same as a changed start azimuth but this variable can be controlled more precisely. Thus the exact alignment of calculated and real CoG in z-position is of high importance for later flights. As with the CoG y-position the range is from -0.002 m to 0.002 m .

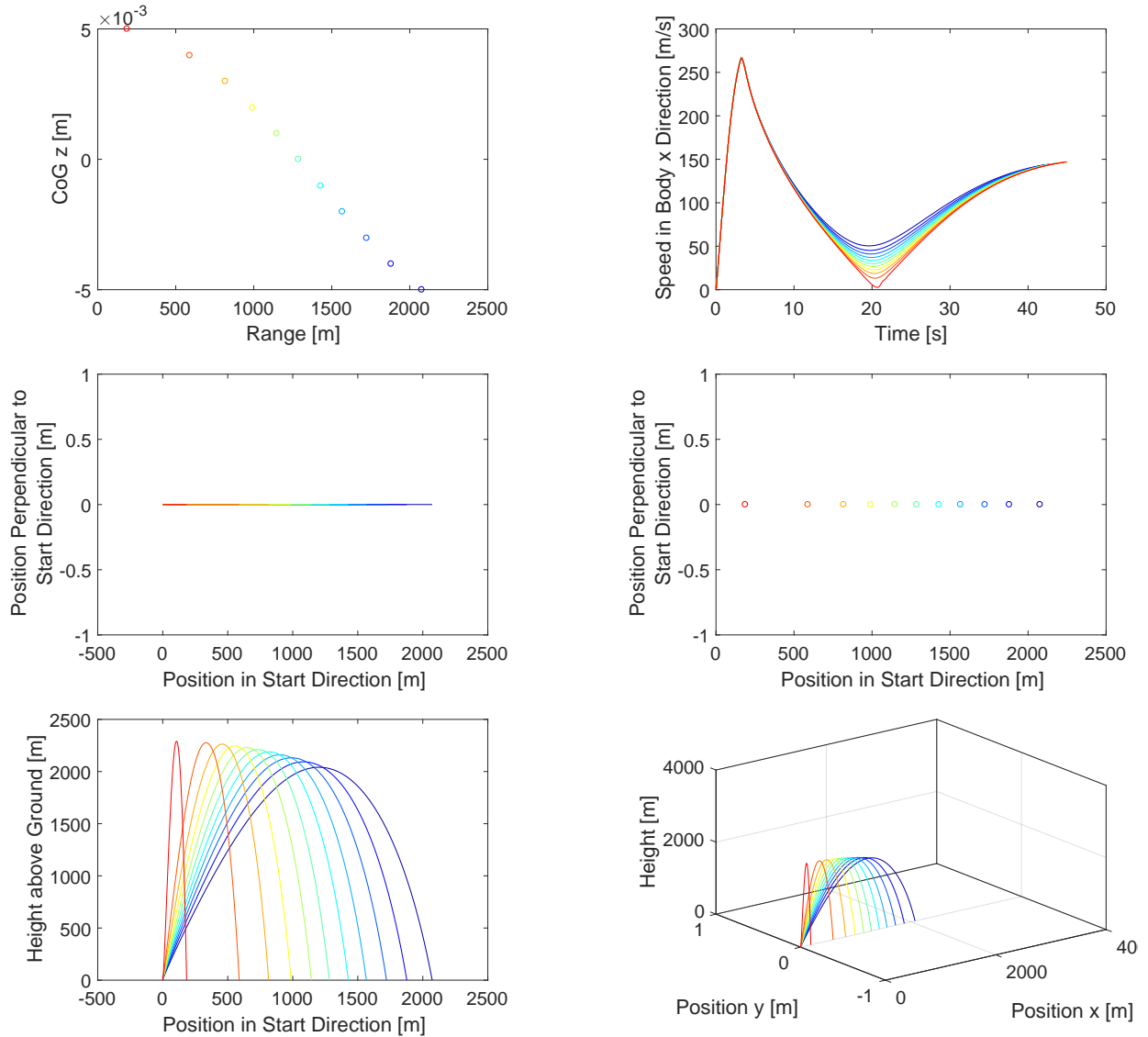


Figure 6-5: CoG in z-direction sensitivity trajectories and flight data

6.4 Mass and Inertia Deviation

As with the CoG in body x-direction the ZFW is less significant and in reality can be controlled with a weight scale very precisely. With realistic assumptions in mind, $\pm 10\text{ g}$, the importance can be more or less neglected but was still employed in the MCS, that means ZFW reaches from 3.592 kg to 3.612 kg.

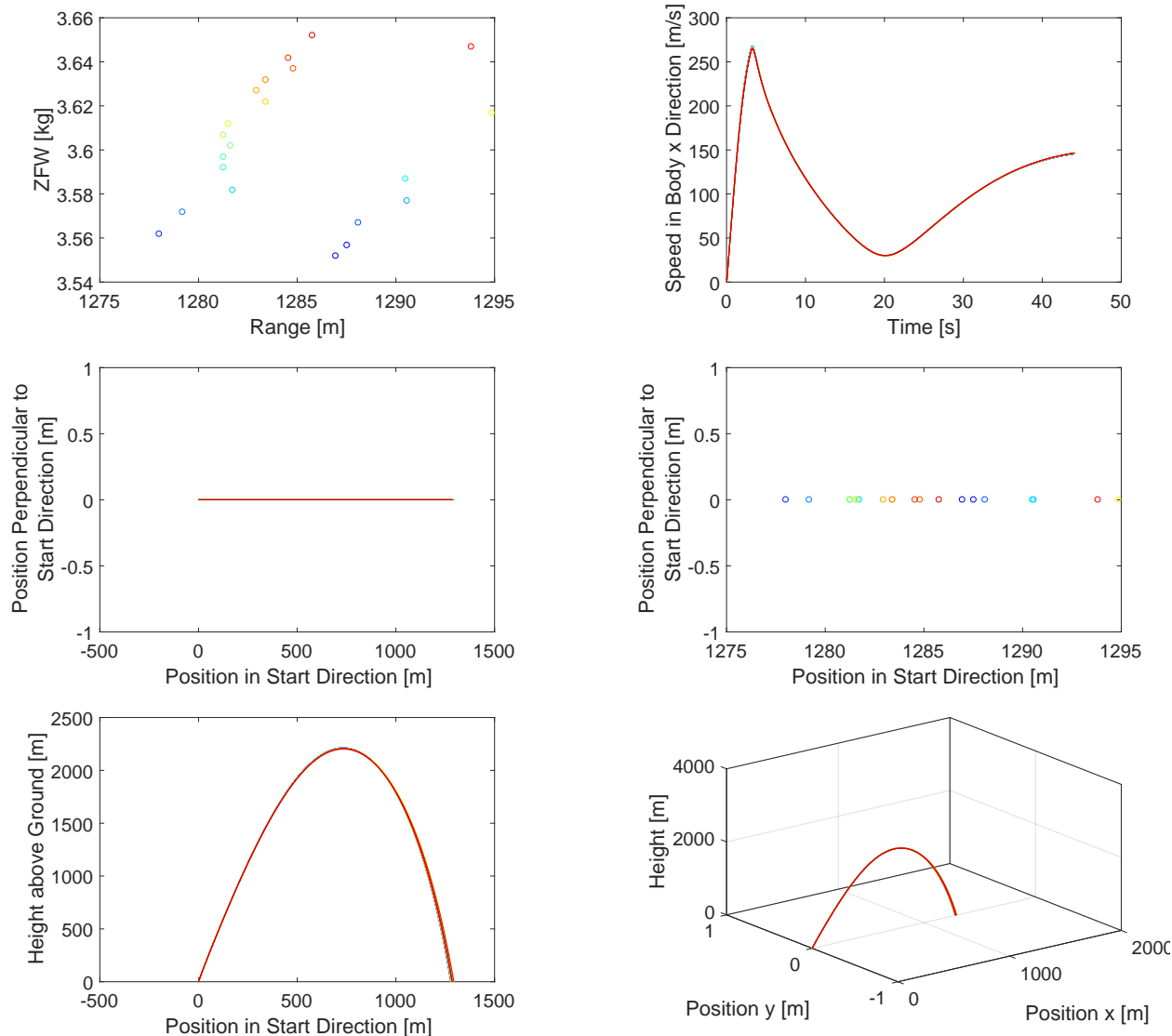


Figure 6-6: ZFW sensitivity trajectories and flight data

Every entry of the moment of inertia tensor was changed in its own sensitivity analysis. To enhance the magnitude of effects the initial rotation around the body-x axis (ρ) was set to 10 revolutions per second. Without that measure the influence would be almost zero. With realistic rotational speeds smaller than 10 rps and Mol deviations the sensitivity becomes almost diminishing small. Nevertheless the value gain varies from 0.95 to 1.05 for I_{xx} , I_{yy} and I_{zz} . Figures for I_{xy} , I_{xz} and I_{yz} are left out because their order is magnitudes smaller than the main diagonal elements of the Mol tensor. The sensitivities themselves are also diminishing small, hence their gain is set to 1 for every simulation.

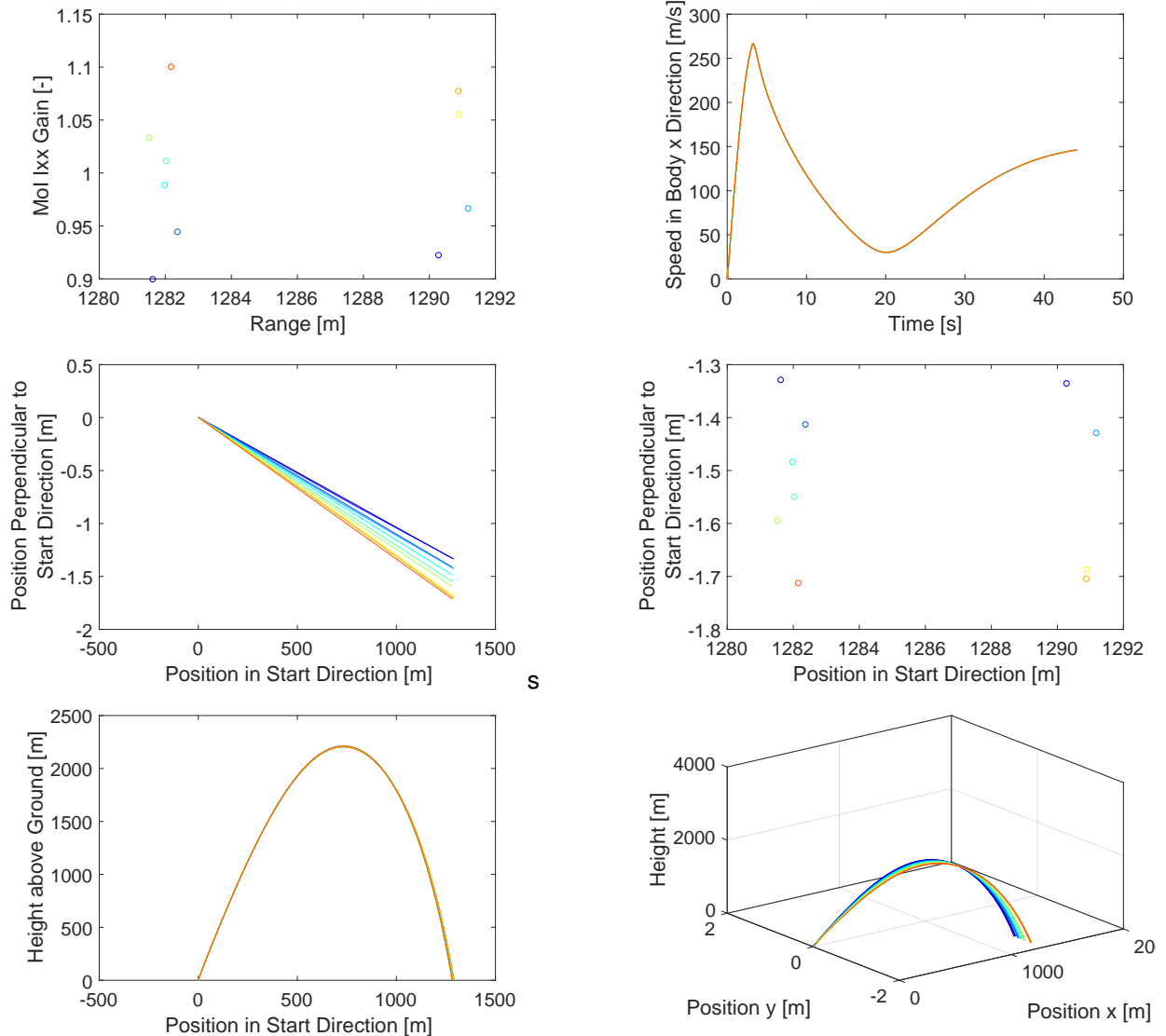


Figure 6-7: Mol Ixx gain sensitivity trajectories and flight data

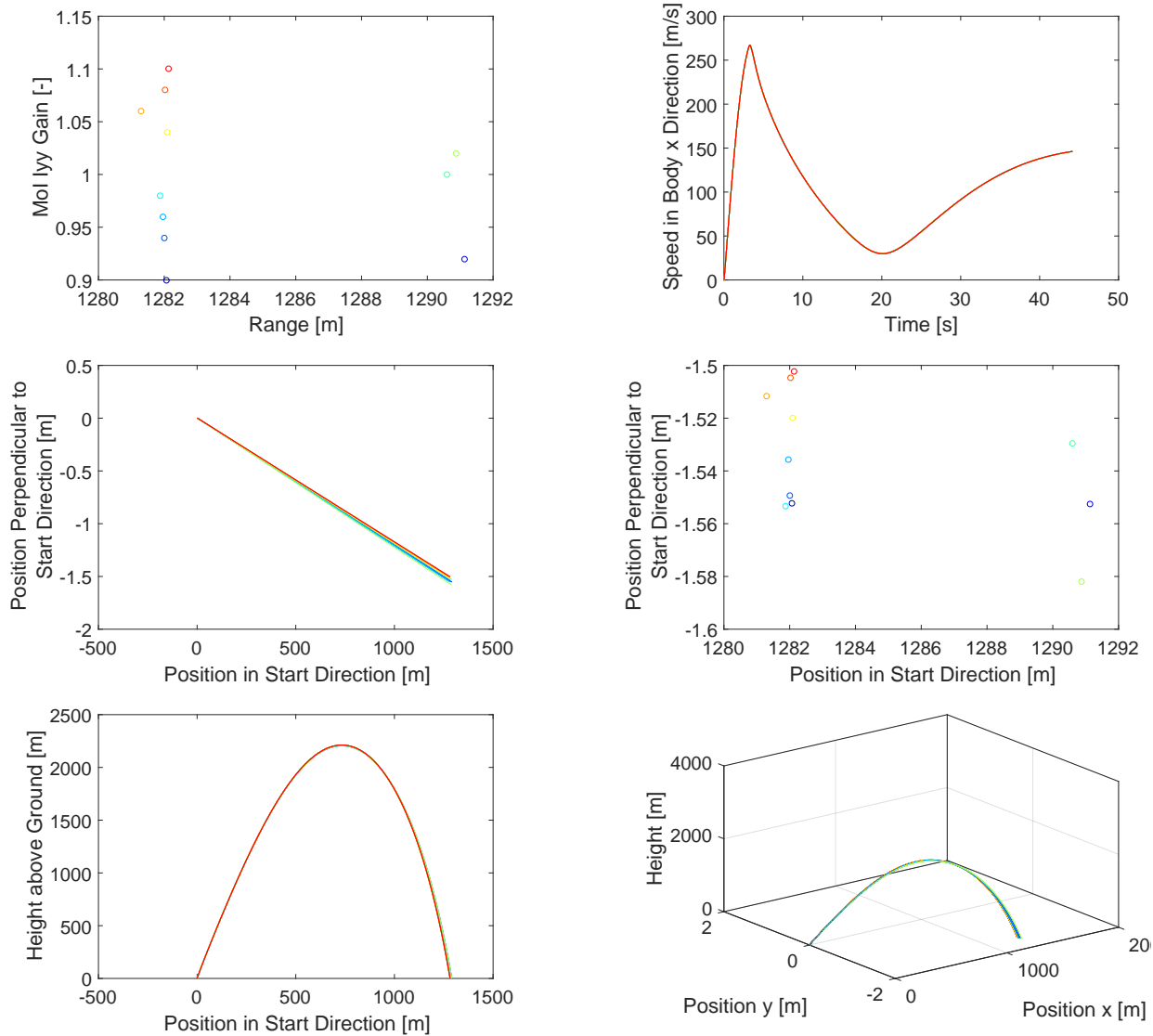
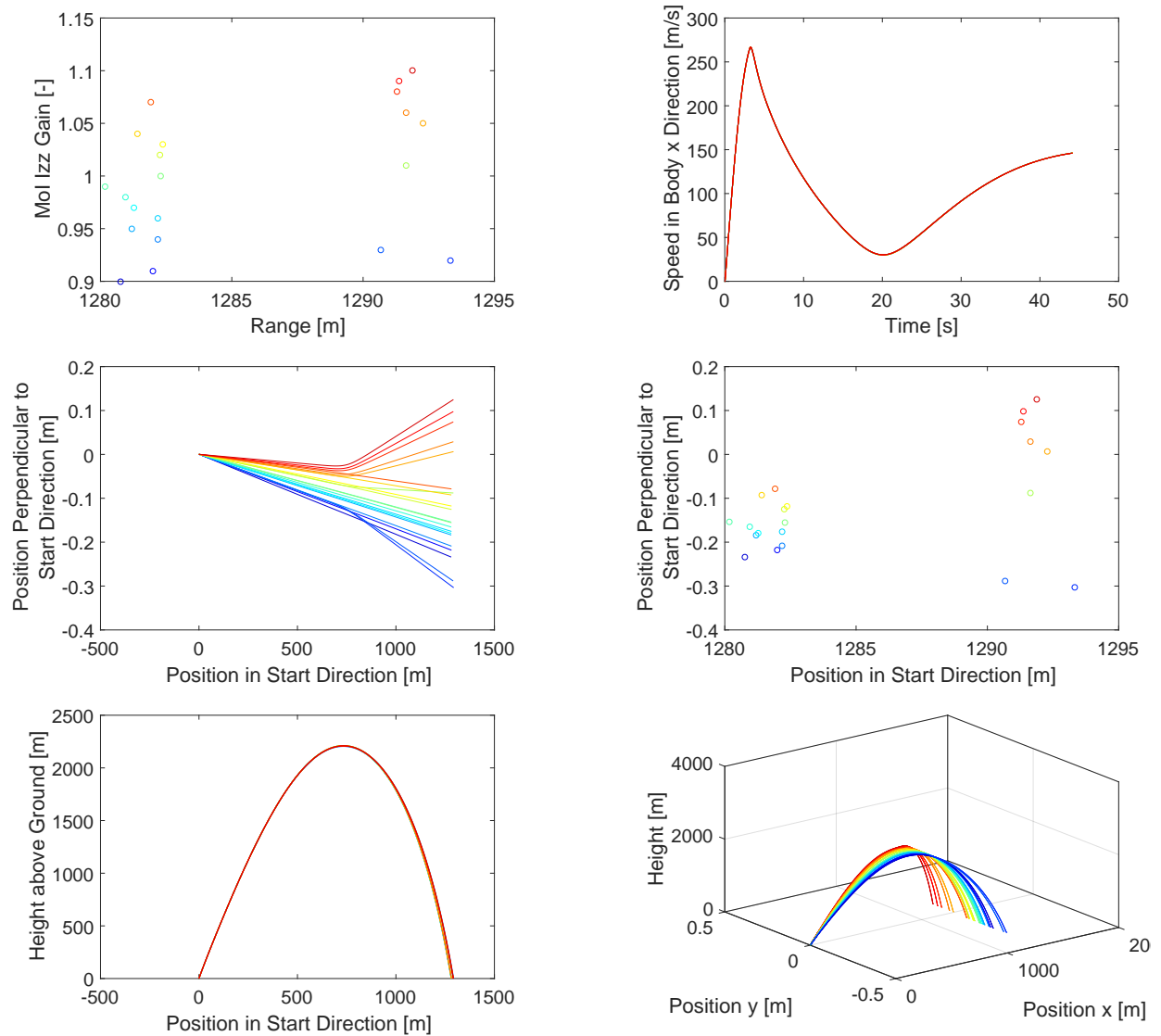


Figure 6-8: Mol Iyy gain sensitivity trajectories and flight data

**Figure 6-9: Mol Izz gain sensitivity trajectories and flight data**

6.5 Trust Deviation

With more engine trust the missiles range increases for the nominal start azimuth angle of 80 deg. But in interaction with wind speed and other variations the range could decrease with more trust. For that reason the trust gain factor was not set to 1 but varies between 0.95 to 1.05.

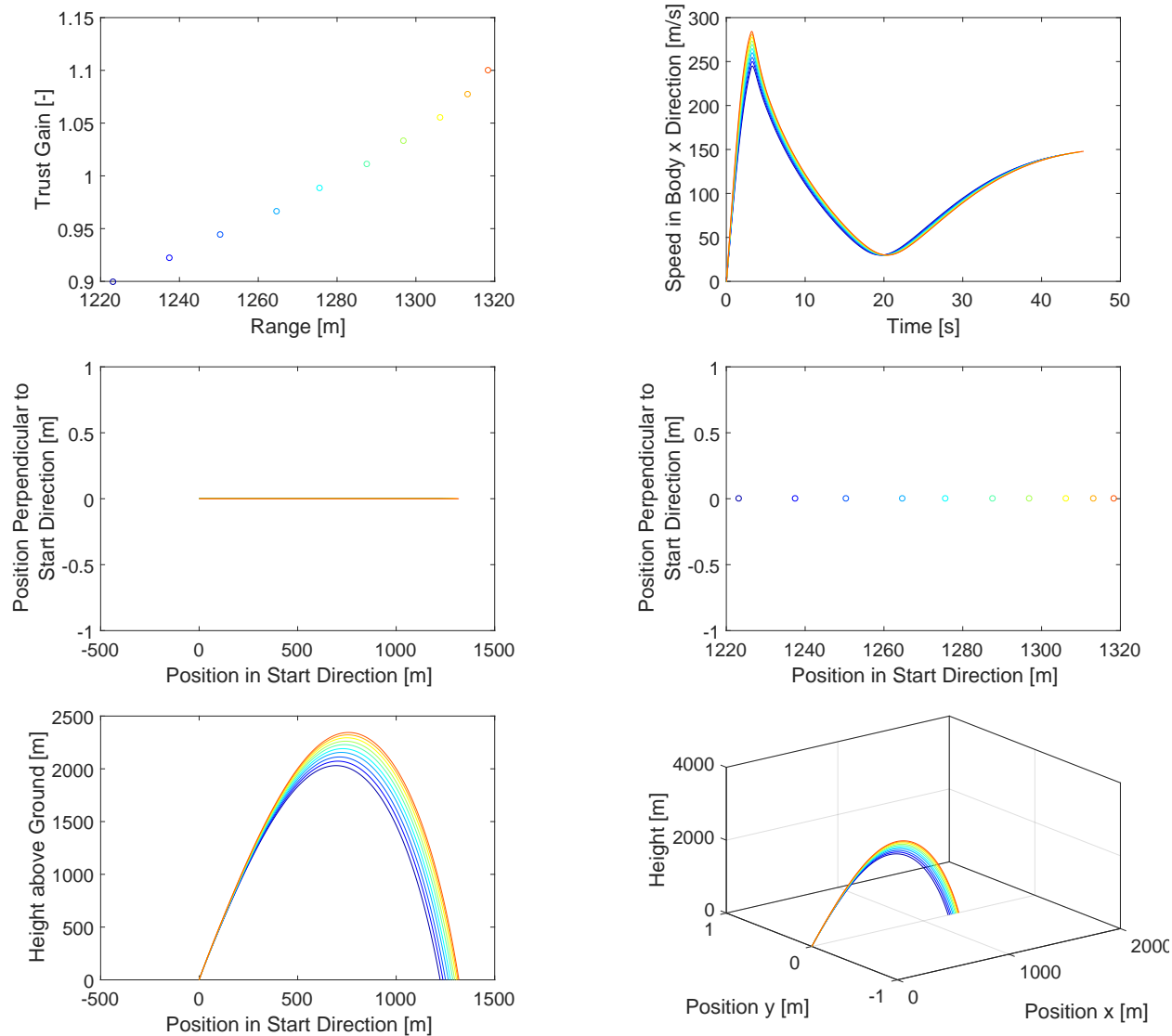


Figure 6-10: Trust gain sensitivity trajectories and flight data

The exhaust gas direction and with this the trust direction depends on an exact assembly of the engine and the rest of the GRM. Small deviations in the magnitude of -0.1 deg to 0.1 deg may occur. As with the CoG in body y and z-direction the sensitivity is large and varies the range between approximately 1282 m and 1295 m. The biggest influence on the impact position appears at the sideways impact position, that means due to the unaligned assembly the missile flies aside the designated target point. For the simulations the trust sideways angle takes values between -0.1 deg to 0.1 deg.

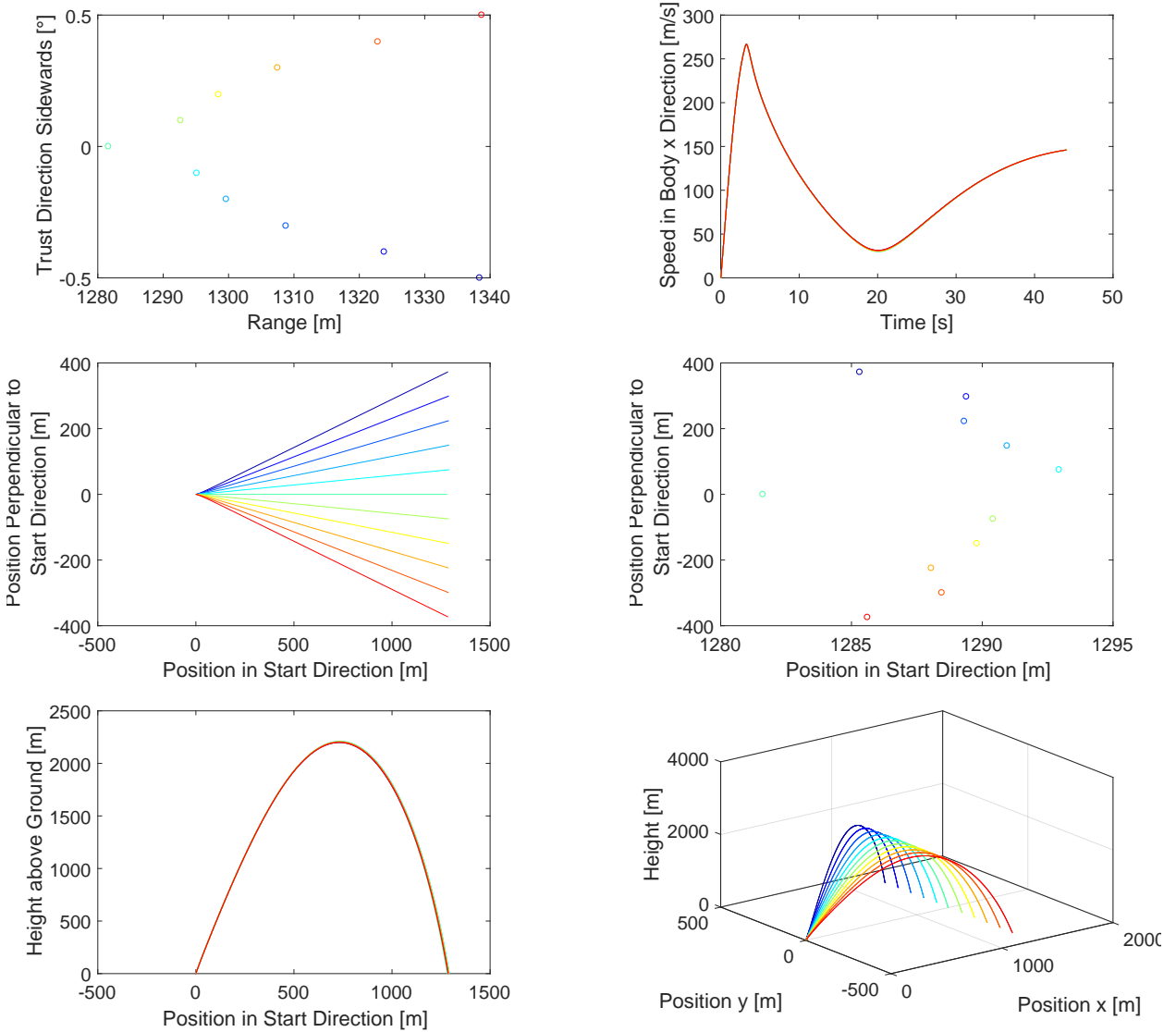


Figure 6-11: Trust direction sideways sensitivity trajectories and flight data

The trust direction pitch angle, thus the rotation of the trust direction around the body y-axis, influences the range similar to the start azimuth angle and CoG position in body z-direction. For the Monte Carlo simulation the trust pitch angles value is in the range from -0.1 deg to 0.1 deg resulting in a range sensitivity of around 70 m.

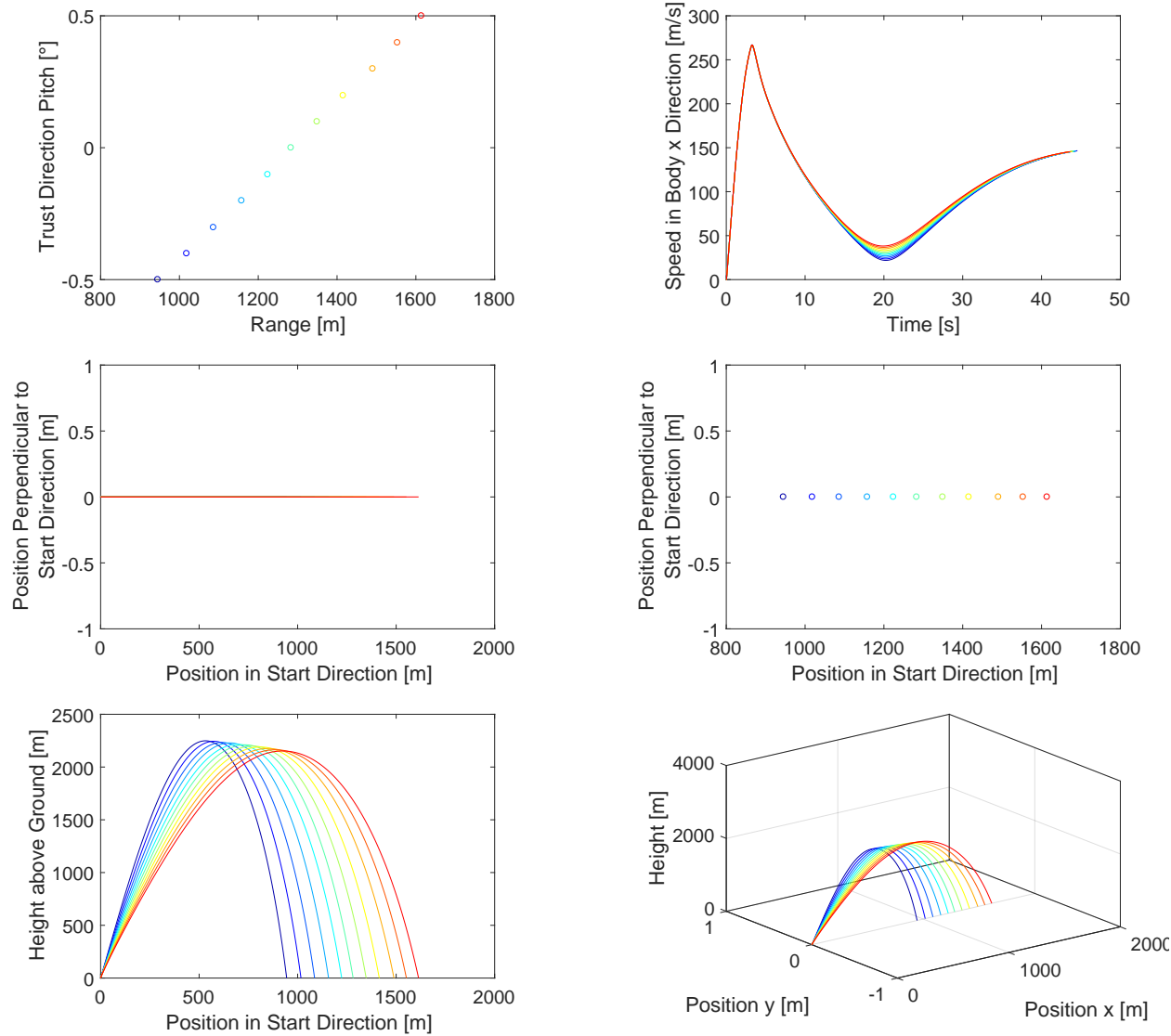


Figure 6-12: Trust direction pitch sensitivity trajectories and flight data

6.6 Control Surface Deflections

As with every servo the commanded angle and the real angle differ in a real world application. The design goal for the GRM is to reach an accuracy of ± 0.1 deg, so if the commanded angle is 0 deg the real angle is between -0.1 deg to 0.1 deg. For safety reasons and thus in the MCS a range of -0.25 deg to 0.25 deg is chosen. Another decision has to be made regarding the independent control of every fin. In reality every servo and with that fin can be controlled independently and thus 4 parameters have to be considered in the MCS and GA optimization. To simplify that circumstance and reduce the complexity fins lying opposite the GRM are assumed dependent. That means two fins act like an elevator and the other two fins act as rudder. Two MCS show the differences between independent and dependent control. For both cases the impact area is of similar size while the impact distribution is more uniform for latter case. For safety considerations nothing speaks against choosing the second approach with coupled fin angles.

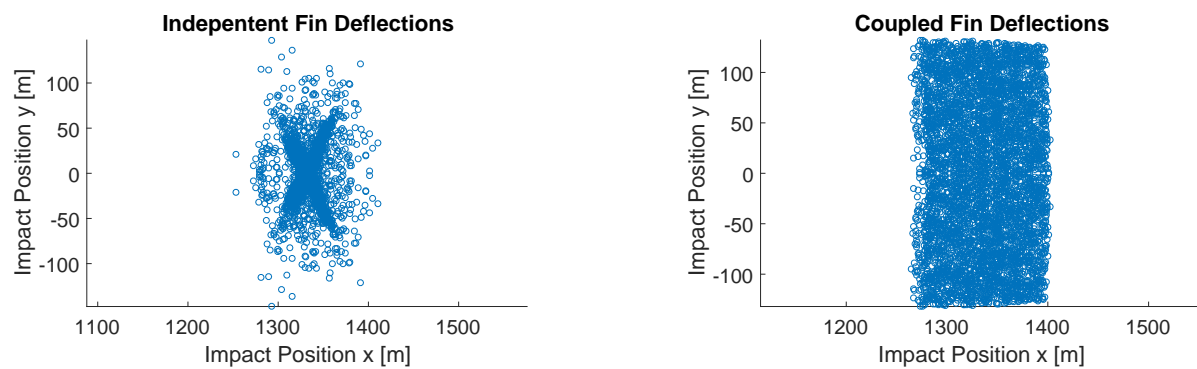


Figure 6-13: Fin deflection sensitivity impact positions

As required by the WTD 91 range and behavior in the case of rudder failure has to be determined. For this scenario one respectively two fins were deflected randomly within an uniformly distributed probability distribution ranging from -10 deg to 10 deg. The fins use NACA 0008 airfoils that stall around 10 deg of local AoA, thus these values were chosen. For the first case with only one fin deflected the upper fin was chosen, for the later case the upper and left fin (view from the back). Figure 6-14 shows the results for both cases. For the first variant the range does not change drastically, the missile drifts aside. For two deflected fins the impact position and with that the range differs greatly. Nevertheless all impact positions lie within the safety area that is computed in the next chapters. For both cases a MCS with 2500 runs was carried out.

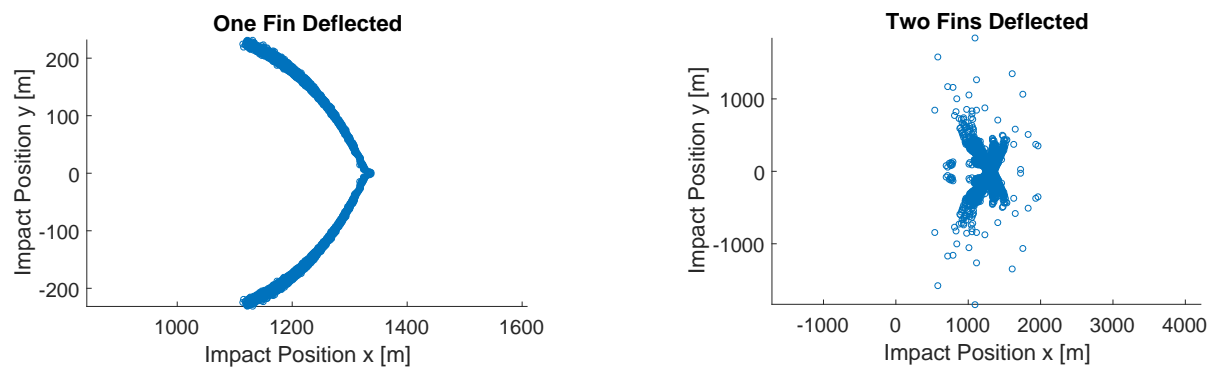


Figure 6-14: Maximum fin deflection impact positions

6.7 Shape Deviations

As stated in chapter 4 real dimensions, in our case the missile diameter and fin shapes, vary due to normal manufacturing processes. For the first parameter, the missile diameter, the sensitivity is not that small and is considered relevant for MCS and GA simulation. A feasible manufacturing precision for the diameter is ± 0.2 mm.

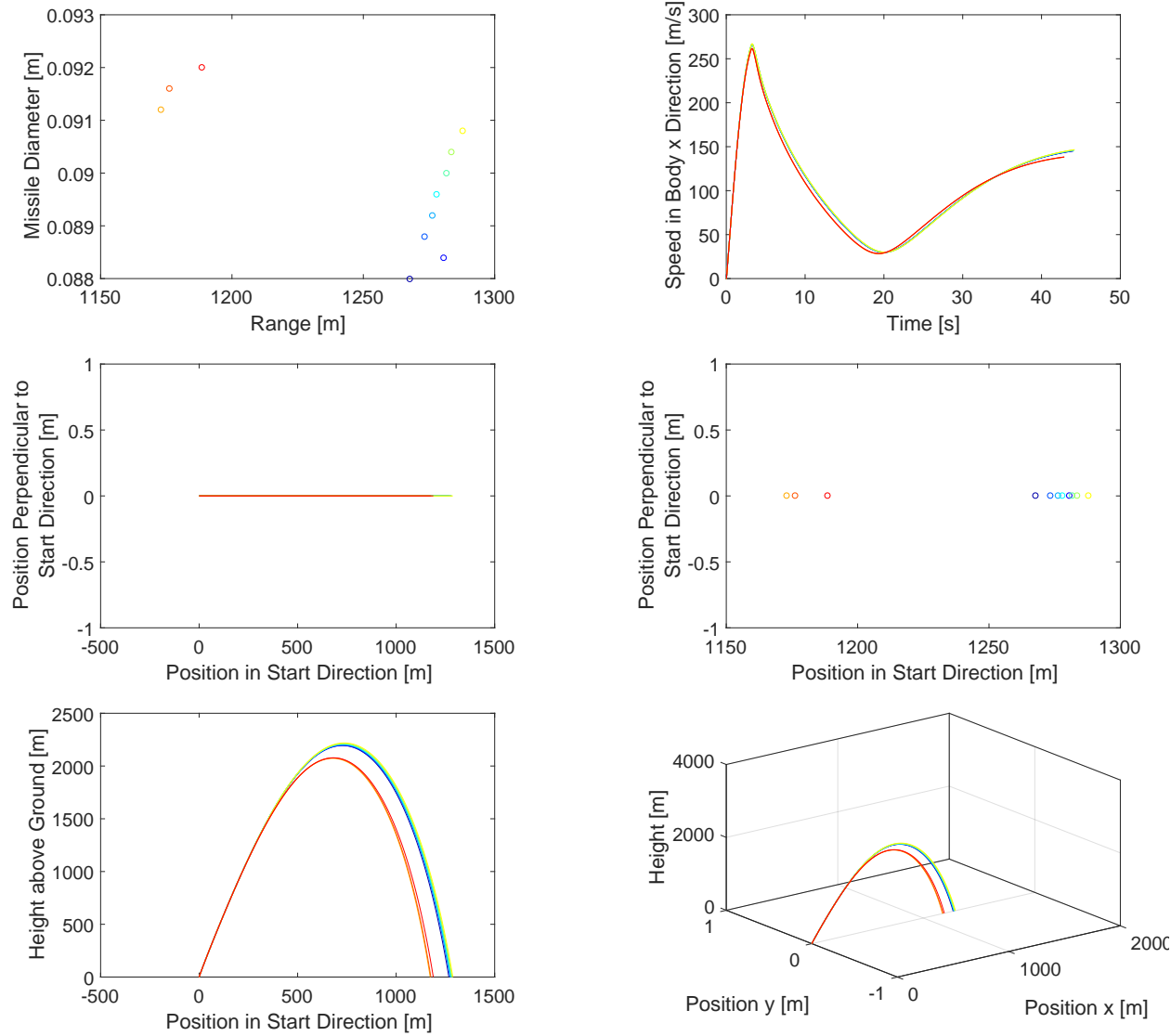


Figure 6-15: Missile diameter sensitivity trajectories and flight data

The second dimension that varies is the fin chord length with a nominal value of 70 mm. The maximum discrepancy from real to nominal length is ± 1 mm and with those values influence the MCS and GA optimization.

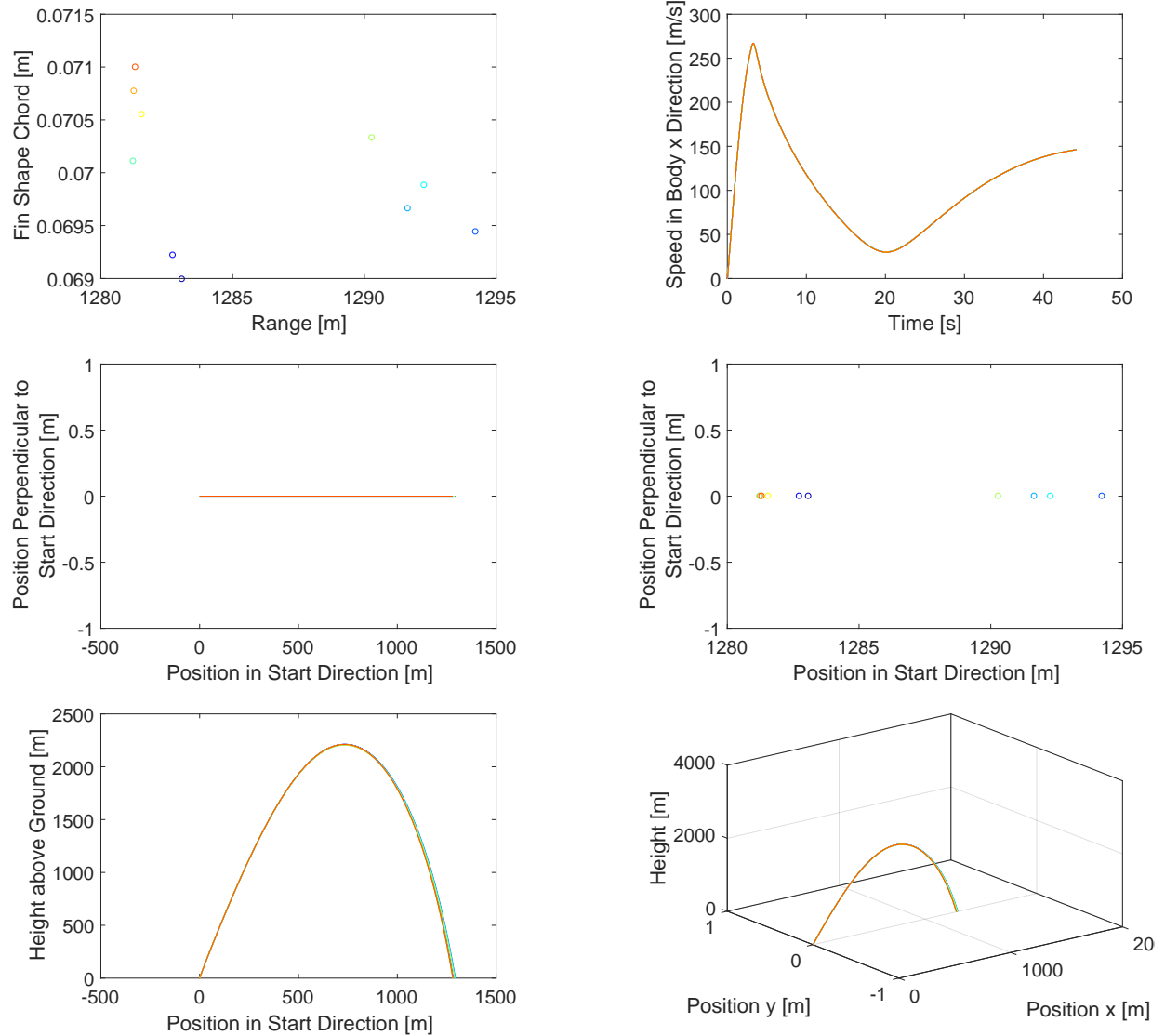


Figure 6-16: Fin shape chord sensitivity trajectories and flight data

The last dimension considered in this section is the fin span length with a nominal value of 140.5 mm. As with the fin chord length the values for MCS and GA optimization lie between the nominal value ± 1 mm.

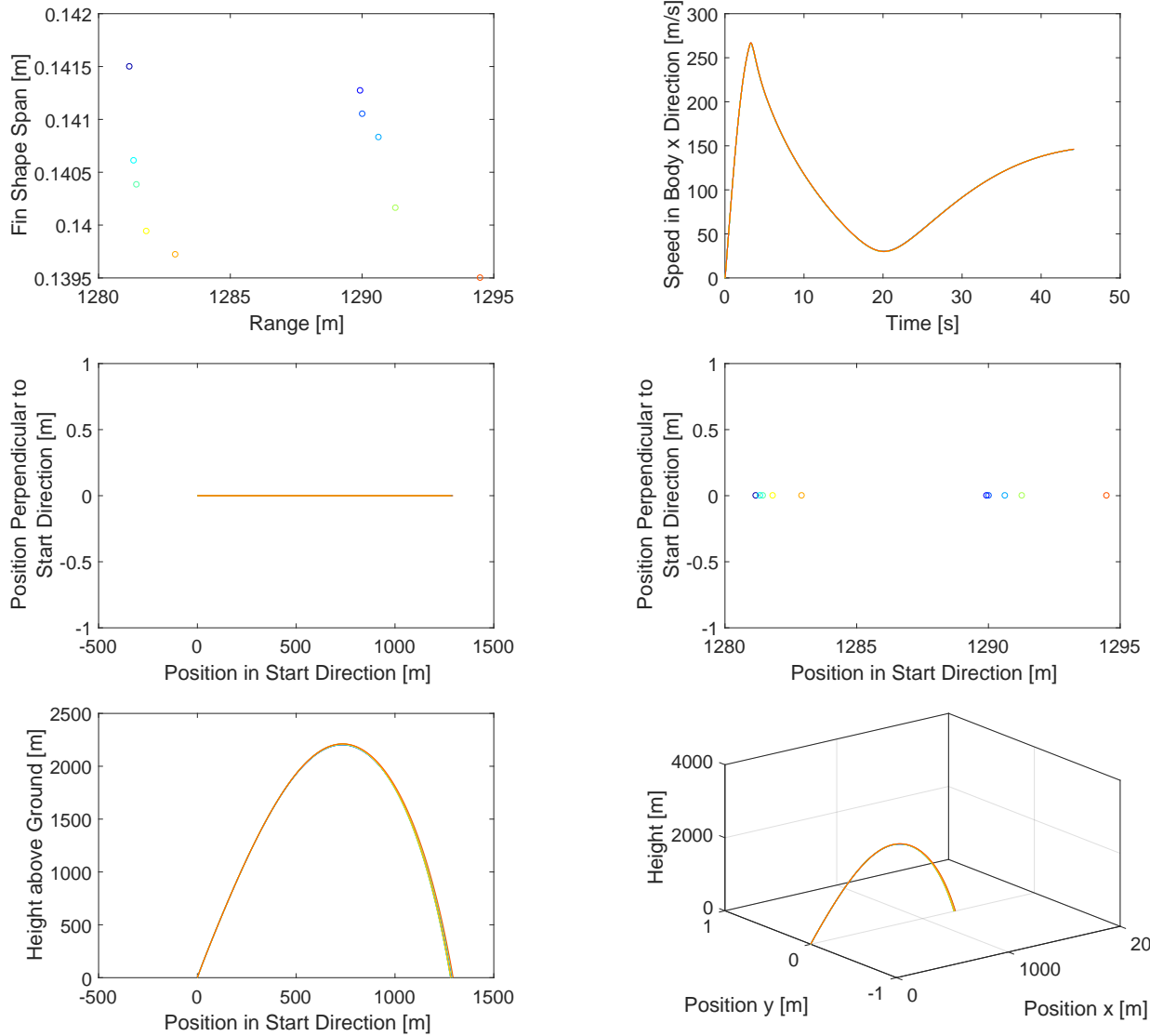


Figure 6-17: Fin shape span sensitivity trajectories and flight data

6.8 Model Uncertainty Deviation

While Missile DATCOM is a tool preferably used for preliminary design due to its fast computation speed and acceptable precision and accuracy the results do not calculate every aerodynamic coefficient in an exact way (see chapter 5). A multiplication of all aerodynamic coefficients with a gain factor yields the following figures. With decreasing gain the range increases as the drag reduces. As the GRM is a ballistic missile the generated lift does not contribute that large and hence the drag effect dominates. But for simplifications the gain is fixed to 1 as [12] states that MDATCOM already underestimates the range significantly in most cases. Instead a safety margin can be added to the final results.

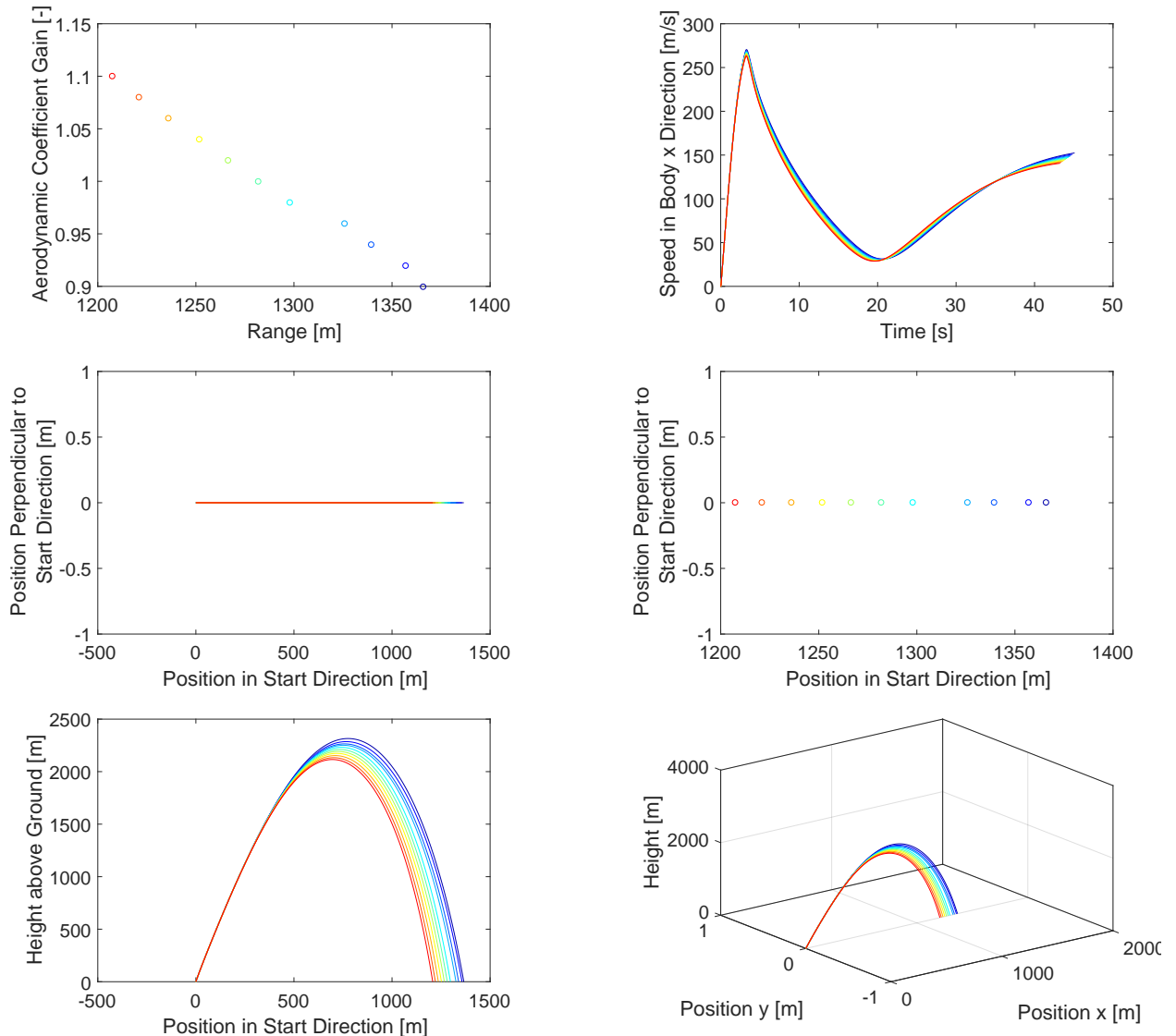


Figure 6-18: Aerodynamic coefficient gain sensitivity trajectories and flight data

6.9 Temperature and QNH Deviation

The aerodynamic coefficients are dimensionless parameters and need to be multiplied with the static pressure, a reference area and for moment coefficients with a reference length. The air density in Equation 5-12 changes with QNH, that is the air pressure at the launch sites ground, and temperature. The sensitivities are as follows: With rising temperature the air density decreases and thus the drag. For a higher temperature the range increases therefore. With QNH it is vice versa, a lower QNH increases the drag at same temperature. Conditions with low QNH and high temperature are also called hot and high conditions [14]. The extreme values for this sensitivity analysis were weather records in Germany [15]. For the MCS and GA optimization pessimistic and fixed values were taken, a QNH of 100 000 Pa and a temperature of 30 °C.

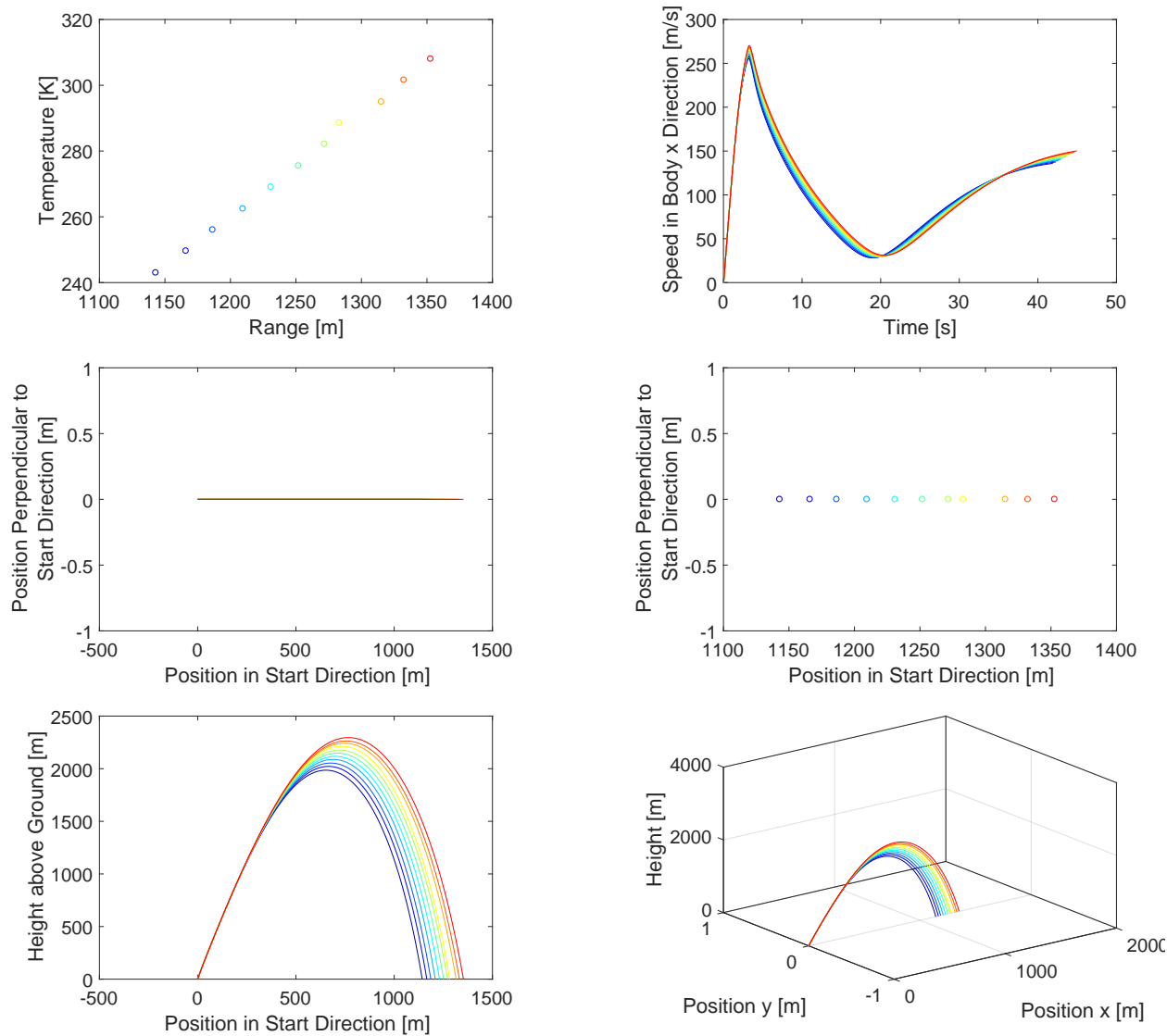


Figure 6-19: Temperature sensitivity trajectories and flight data

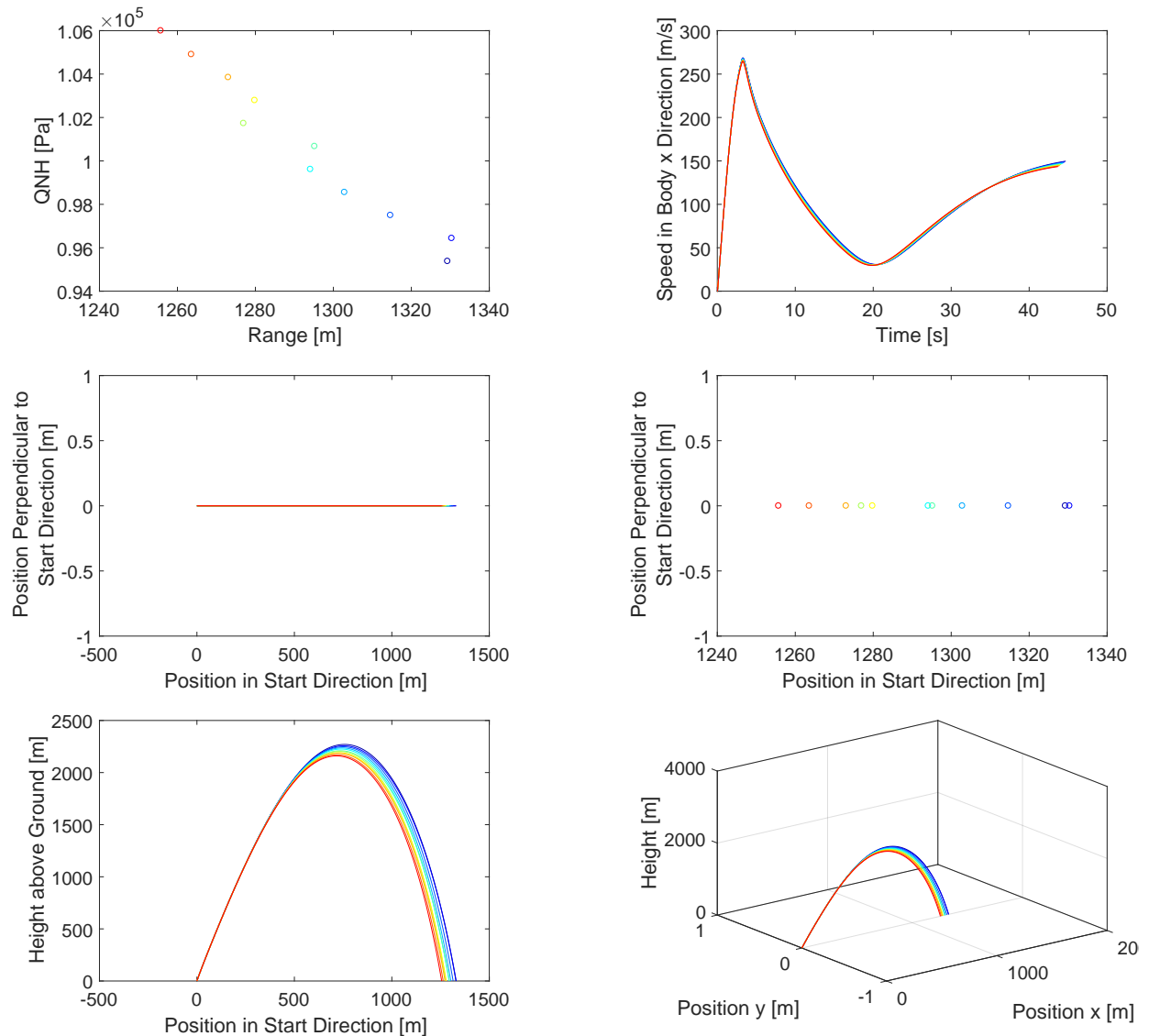


Figure 6-20: QNH sensitivity trajectories and flight data

6.10 Wind

The biggest impact on the flight path and impact position is the wind speed and direction. The wind direction differs from pure up wind to pure back wind. The speed has its limits at 13.9 m/sec corresponding to a 6 on the Beaufort-scale. At such speeds, strong branches of trees are moving and umbrellas are only hard to hold [16]. Figure 6-21 shows how a decrease of wind from 13.9 m/sec (up wind) to -13.9 m/sec (back wind) influences the flight path. The main effect of wind is a pitch moment in wind direction. The black path corresponds to the windless case. As wind appears from the front it pushes the fins backwards and thus the GRM pitch decreases during the first flight phase. After a certain wind speed is reached, the range decreases again as the wind pushes the missile back, it drifts backwards. The same effect is true for back wind. At moderate wind speed the wind pitches the GRM upwards, decreasing the range. Increased back wind results in impact position behind the start point. And with maximum wind speeds again the impact points drift forward. In Figure 6-22 the wind speed and simultaneously the wind direction are changed from front to side wind to up wind and to the maximum of 13.9 m/sec. The impact position depends heavily on both parameters, in fact it has the biggest influence on the point of touchdown. For the MCS and GA optimization the wind speed varies between 0 m s^{-1} to 13.9 m s^{-1} and the wind direction from 0 deg to 180 deg. To obtain a stable simulation the start ramp length was increased to 6 m for higher wind speeds, standard are 3 m.

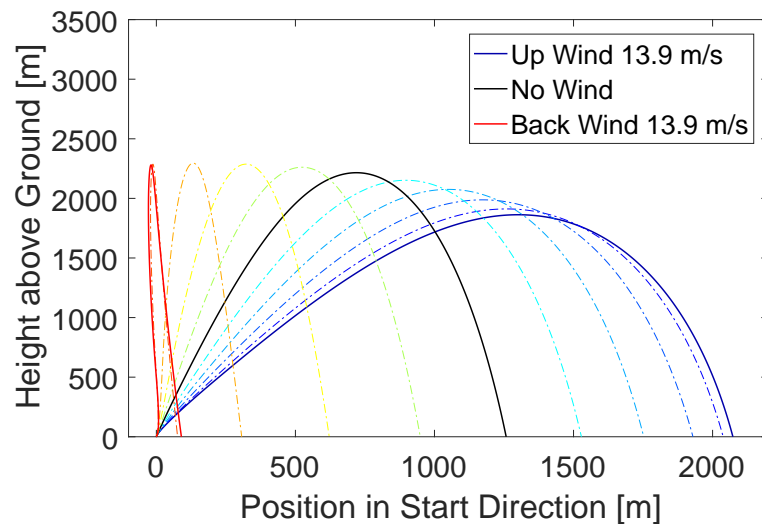


Figure 6-21: Wind speed influence

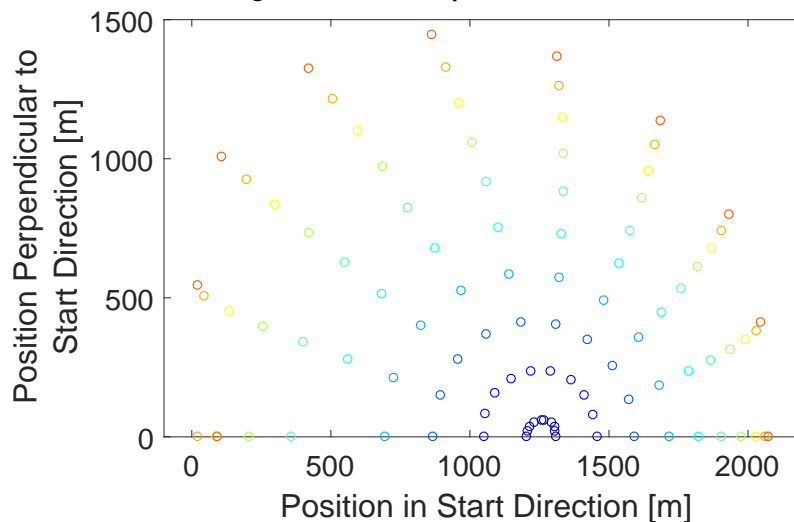


Figure 6-22: Wind speed and direction influence

7 Safety Assessment

After the identification of the biggest and thus crucial sensitivities the required safety calculations can be started. For this thesis a hybrid approach was used to handle two different basic needs of the requirement. First of all the impact possibilities are of high interest, that means where does the GRM impact with what probability. Second part of the safety assessment is the maximum safety zone (danger zone), that is defined by the area where the possibility that the missile impacts is nonzero. These two requirements are not that different but for an optimal computational efficiency the impact probability is approximated with Monte Carlo simulation and the safety zone with a genetic algorithm. In contrast to MCS later focuses on the edges of the possible impact positions but gives no information on the impact probability distribution. Additional hazard arises if the missile explodes on ground. That scenario is handled with simple formulas instead of simulations in the last part of this chapter.

7.1 Monte Carlo Simulation

For a variety of problems Monte Carlo simulations are more efficient than deterministic algorithms. In some cases MCS is the only feasible way to gather results yet for a problem [17]. The MCS relies on two fundamental laws of mathematics, the *law of large numbers* and the *central limit theorem* [17, p.21]. These two theorems guarantee that this approximation converges towards the true probability distribution with rising number of simulations. A simple example taken from [18, p.31] should illustrate the simplicity and ease of this method by approximating the value of π .

A random vector $X = (x_1, x_2)$ that is uniformly distributed over $[0, 1]^2$ is generated by a computer algorithm. If the expression $x_1^2 + x_2^2 \leq 1$ is true than the generated random point lies within the unit circle and a variable t is incremented by 1. After N such random simulations π is approximately $\pi = \frac{t}{N} * 4$. This basic idea transferred to our missile safety considerations is as follows. All parameters that determine (or at least influence it in a nonneglectable way) the impact position are stochastic variables and only the range and type of distribution (uniform, normal distributed etc.) are known. This probability distributions could be transferred in the equations of motion leading to a system of stochastic differential equations. Solving these equations leads to the desired impact probability distribution. Unfortunately this approach is hard to solve and unnecessarily complex for this case. Instead it can be approximated with MCS and following procedure. The underlying parameter PDF is the same as for the analytic stochastic differential equation system, see Table 4-1. In the next step a random number generator chooses one random value for each parameter. With that set of parameters a simulation is started and the impact position is saved. This steps are repeated many thousand times and afterwards a histogram can be computed that represents the impact probability distribution.

7.2 Genetic Algorithms and Pareto Optimization

The second approach in this thesis is the use of multi objective optimization incorporated in safety area computation. Most of the principles and terms originated in economics e.g. Pareto optimality named after Vilfredo Pareto. Nonetheless they can be applied to technical applications as well. To clear things up an introduction to multi objective optimization and genetic algorithms follows now.

7.2.1 Multi Objective Optimization

The next examples and definitions are taken from [19] and the Matlab documentation. An optimization problem OP is defined as

$$\text{OP} \left\{ \begin{array}{l} \min_x f(x) \\ \text{w.r.t constraints} \\ \text{w.r.t boundary conditions} \end{array} \right. \quad (7-1)$$

Where $f(x)$ is the so called utility function (sometimes also called fitness or objective function) and x is the design variable vector. Constraints and boundary conditions impose further complexity such as non-negative design variables and (in-) equality constraints. A simple example is $f = x^2 + y^2$ with x and y as design variables and no boundary conditions and constraints¹. In this case the minimum can be computed analytically or with sophisticated optimization algorithms like gradient based search procedures. The optimum is at $x = y = 0$. In many cases not only one utility function but many have to be considered, such that

$$\text{OP} \begin{cases} \min_x f_1(x), f_2(x), \dots f_i(x) \\ \text{w.r.t constraints} \\ \text{w.r.t boundary conditions} \end{cases} \quad (7-2)$$

With real functions it may look like 7-3 which is visualized in Figure 7-1. The two functions could represent the weight of an airplane in development and its prospective manufacturing costs.

$$\text{OP} \left\{ \min_x f_1(x) = (x + 2)^2 - 10, f_2(x) = (x - 2)^2 + 20 \right. \quad (7-3)$$

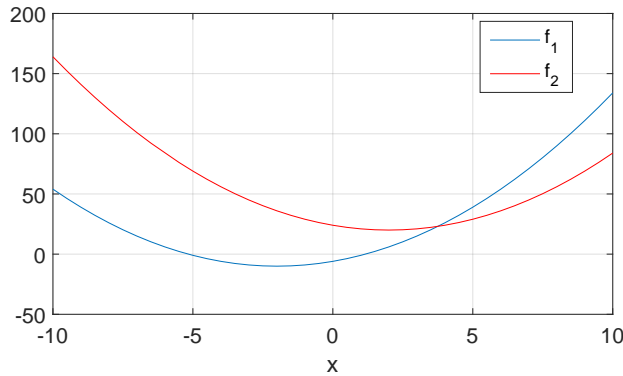


Figure 7-1: Multiobjective optimization, a concrete example with two utility functions.

It is evident that there exists no x such that both utility functions take their minimum value. In cases like these a person has to make preferences if f_1 is more important than f_2 and how much. In this example if it prefers a lightweight expensive aircraft over a heavier and less expensive. A simple approach is to multiply both functions with weights that sum up to 1 such that the multi objective optimization problem becomes a scalar optimization problem displayed in 7-4. The next step is to minimize this new optimization problem for every weight w . The results for f_1 and f_2 can be plotted against each other and result in the so called Pareto front, Figure 7-2. Every point in this figure corresponds to a different weight w and a corresponding design variable x . Altogether this makes it easier for decision makers to trade off between different utility functions.

$$\text{OP} \left\{ \min_x f(x) = w * ((x + 2)^2 - 10) + (w - 1) * ((x - 2)^2 + 20) \quad (7-4) \right. \\ \left. w \in [0, 1] \right.$$

Our safety area problem can also be stated as a multi objective optimization problem. The utility functions are the impact position vector entries, thus the impact positions in x and y direction. Without any further handling the GA would now try to generate the Pareto front that is in the first quadrant (only positive x and y values). To generate the Pareto front in the second quadrant negative x values are considered as a third utility function. Hence the Pareto front is now a surface in the 3-dimensional space. In the program code the negative x -axis regime is handled by an if-statement, so finally we arrive at Equation 7-5.

¹A boundary condition could be $x > 5$ and a constraint like $x + y = 4$

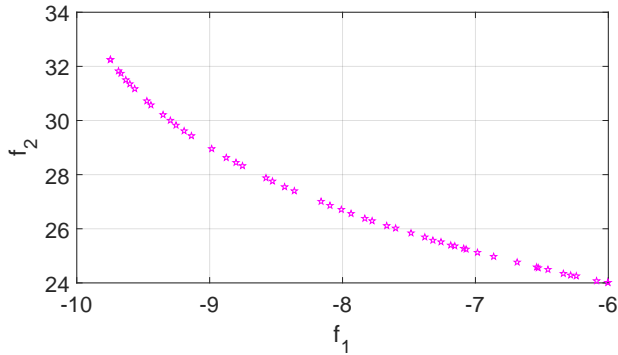


Figure 7-2: Pareto front for the example problem

$$\text{OP} = \min_x \begin{cases} f_1(x) = -\text{impact position } x, f_2(x) = -\text{impact position } y, f_3(x) = 0 & \text{if impact position } x > 0 \\ f_1(x) = 0, f_2(x) = -\text{impact position } y, f_3(x) = \text{impact position } x & \text{if impact position } x < 0 \\ x \in \text{Table 4 - 1} \end{cases} \quad (7-5)$$

The negative sign in front of f_1 , f_2 and f_3 transforms the maximization problem into a minimization, $\max_x f(x) = \min_x -f(x)$, because we want to obtain the maximum distance in every direction instead of the minimum safety area and most optimization algorithms are programmed to minimize functions. With the stated problem the only step left is to solve it using appropriate algorithms discussed next.

7.2.2 Genetic Algorithms

Genetic Algorithms are like MCS stochastic algorithms and mix them with the simple but effective idea of evolution. The basic principle is the survival of the fittest, the more outside a simulated flight impacts the higher its fitness. The flights with the highest fitness are then chosen for the next round (generation) and slightly modified via mutation and recombination. Matlab uses a variant of the NSGA-II algorithm for normal and multi objective problems². This algorithm can compute the Pareto front within only one run, there is no need to solve the optimization problem for different weights w . The procedure is as following.

- At first a chosen number (the so called population size) of simulations of the missile flight are run with randomly distributed parameters from Table 4-1. This step is the same as with MCS and results in the initial population. Every simulation is now ranked by its utility which is computed with the concept of dominance. Figure 7-3 shows the Pareto front for an example where a lower utility function is regarded better. The green individuals (simulations) are dominating the yellow ones since the values for f_1 and f_2 are for every dominating individual and case smaller than the remaining dominated individuals. As a consequence the green individuals have the utility function value 1 and are left out from now on. For the remaining individuals the dominance is checked again and the new dominating individuals have an utility function value of 2. This step is repeated until there are no individuals left.
- Now come the steps that are obligatory for genetic algorithms, *tournament selection*, *recombination* and *mutation*. These methods generate a new offspring generation from the preceding one.
 - Tournament selection lets a specified number of randomly chosen individuals "fight" against each other and the one with lowest utility function survives the tournament and is saved [20]. After some tournaments, less than the population size, a new set of individuals made up of the winners enters the next round of recombination. This set has a lower average utility function as the initial population.

²See Matlab Documentation gamultiobj

- During recombination the individuals of the winner set are mixed up randomly pairwise in hope to achieve better ones, like in nature. The number of newly generated individuals is such that the total number of winner set individuals and newly generated individuals sum up to the population size.
 - The last step mutation is to generate more diverse individuals than only with recombination. During mutation properties of a few individuals are changed randomly. With this last step the new generation is completely generated.
3. The newly generated population is simulated and their utility functions is determined. Now the algorithm continues with step 1. but with the new and better generation.

A few additional techniques like elitism and crowding distance sorting enhance the quality of solutions even further. Elitism ensures that the best individuals of the last generation are kept for the new one. With that approach it is ensured that the solution does not get any worse. Crowding distance sorting selects individuals that are well distributed among the Pareto front.

As for safety area computation the consequences are clear. Instead of simulating thousands of missile flights that do not contribute to the Pareto front the GA focuses on the more critical flights. A drawback is that no impact probability density function can be approximated at the same time and only convex solutions are obtained.

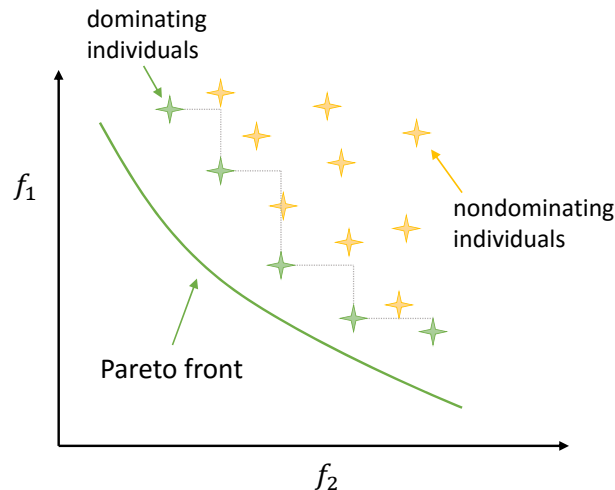


Figure 7-3: Dominating and nondominating individuals are the main concept of multi objective optimization.

7.3 MCS and GA Results

During the next pages the results for MCS and GA are shown and compared regarding their quality and utility. On the left side GA optimization is shown and on the right side the MCS. The number of flight path simulations is the same for MCS and GA optimization. The number of generations was 20, so for the first example with a population size of 50 the number of simulation runs was 1050 (The initial population does not count as generation). Hence the number of MC simulations was also bounded to 1050 simulations.

7.3.1 1050 Simulation Runs

The Pareto front in Figure 7-4 is clearly visible. The color corresponds to the generation, blue points are members of the initial population and red points belong to the last one. It is clear to see that the GA focuses more and more on the edges, converging towards the Pareto front. This can be also seen in the impact histogram in Figure 7-6, the density of impacts on the edges is clearly higher than in the middle.

On the right hand side the normal MCS already enables to identify the region of high impact probabilities located at approximately 1500 m in x direction and 0 m in y direction. The density of points at the edges is drastically lower than with GA, the safety area is badly defined. But in any case the number of simulations is not enough for qualitative and reliable results. For further comparison the convex hull is drawn for the MCS and GA results, see Figure 7-8. The number of points this hull is made up is 19 for the MCS and 43 for the GA approach. The shape is almost identical but the GA hull is better defined. On a computer with Intel Core i5-4670K @3.4GHz Processor and 8GB RAM under Windows 10/Matlab R1015b the total time for computation is around 11 min or 1.6 s per simulation with a rapid accelerated simulation setting.

7.3.2 2100 Simulation Runs

With increased population size of 100 individuals the Pareto front is more dense than with only 50. The outer shape is better defined and the individuals along the front are more uniformly distributed. As before the MCS already gives a good impression of the impact probability distribution but still lacks the outer regions. Nevertheless the histogram is quite noisy and more simulations are needed. Both convex hulls are defined through more points than with only 50 individuals, MCS hull is made up of 25 points and the GA hull out of 53. The shapes are more distinct than in the previous example and the convex hull of GA optimization is more outwards the start point except for the left edge where the MCS hull is more distant.

7.3.3 6300 Simulation Runs

While the convex hull obtained by GA optimization is already of good quality the MCS computed probability density distribution lacks detail. A further increase of the population size to 300 individuals and a corresponding MCS with 6300 simulations finally enables sufficient results for both Pareto front and impact histogram. The convex hull computed with GA is now even more increased and the discrepancy on the left edge is reduced. In total the safety area obtained by GA is significantly larger than with MCS and the gap between defining points, 31 with MCS and 61 with GA, increases even more.

7.3.4 MCS with 70000 Simulation Runs

To improve the impact probability histogram quality further the number of MCS runs was increased to 70000 simulations. The results were mirrored against the x-axis to obtain a complete picture of the impact probability and further reduce the noise. The results do not need to be improved further for this case. But regarding the Pareto front the GA computed hull (300 individuals) is still better defined and overall greater, while only a 1/10 of simulations were needed. To mention is the number of convex hull defining points, from 6300 simulations to 70000 no additional point was added to the hull.

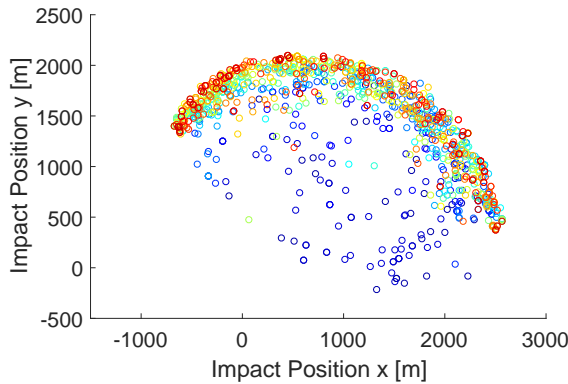


Figure 7-4: Pareto front after 20 generations and a population Size of 50

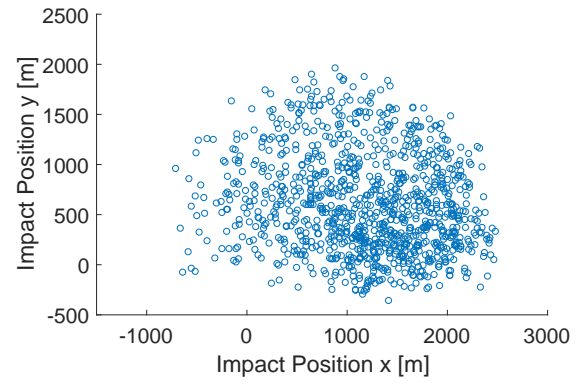


Figure 7-5: MC Simulation with 1050 simulations, same amount as with GA

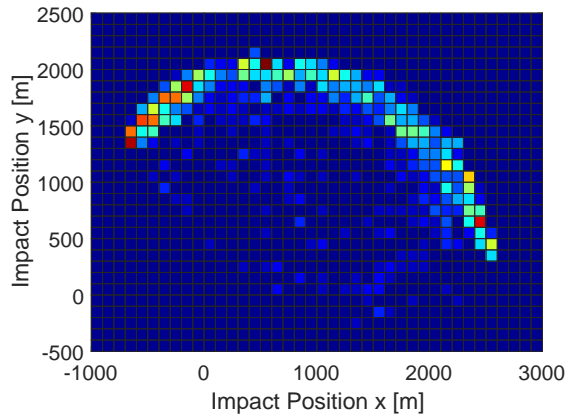


Figure 7-6: Pareto front histogram after 20 generations and a population size of 50

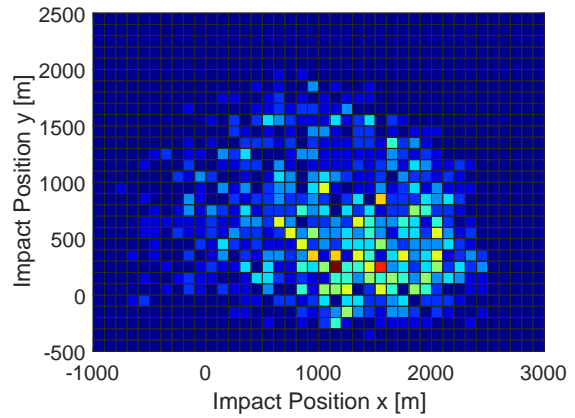


Figure 7-7: MC Simulation histogram with 1050 simulations, same amount as with GA

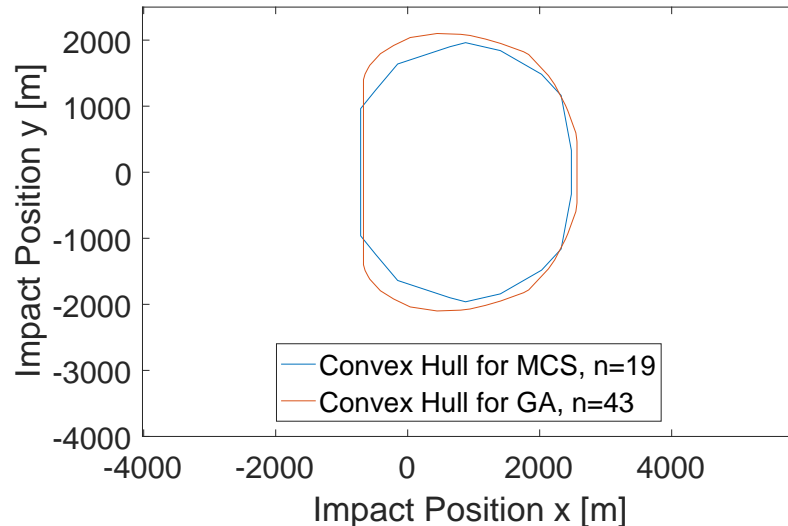


Figure 7-8: Convex hull for GA optimization with 50 individuals per generation and 1050 MC simulations.

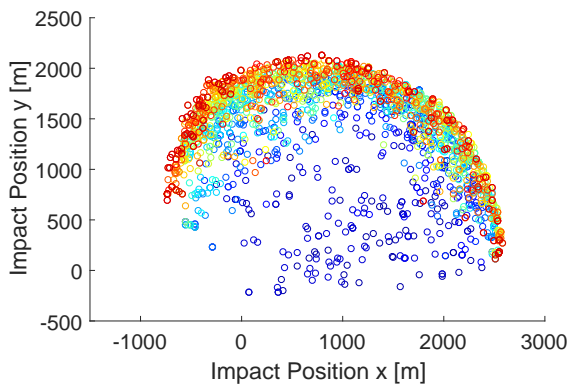


Figure 7-9: Pareto front after 20 generations and a population size of 100

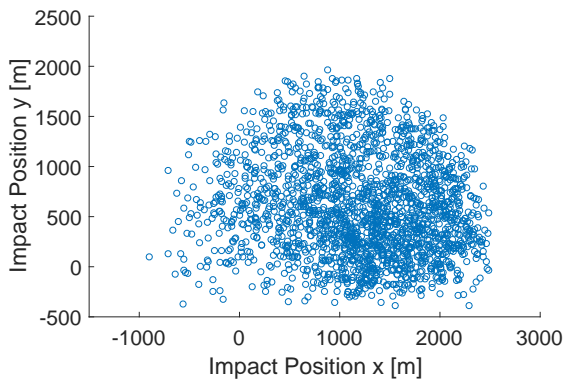


Figure 7-10: MC Simulation with 2100 simulations, same amount as with GA

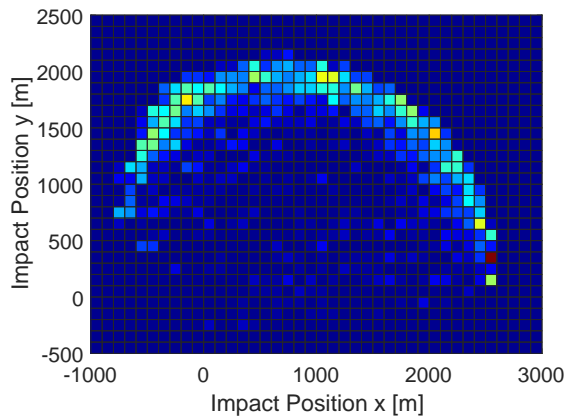


Figure 7-11: Pareto front histogram after 20 generations and a population size of 100

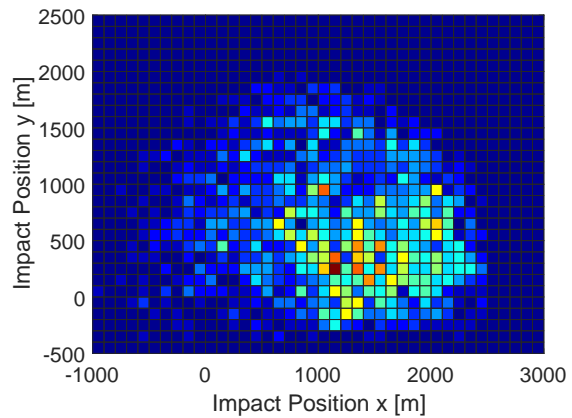


Figure 7-12: MC Simulation with 2100 simulations, same amount as with GA

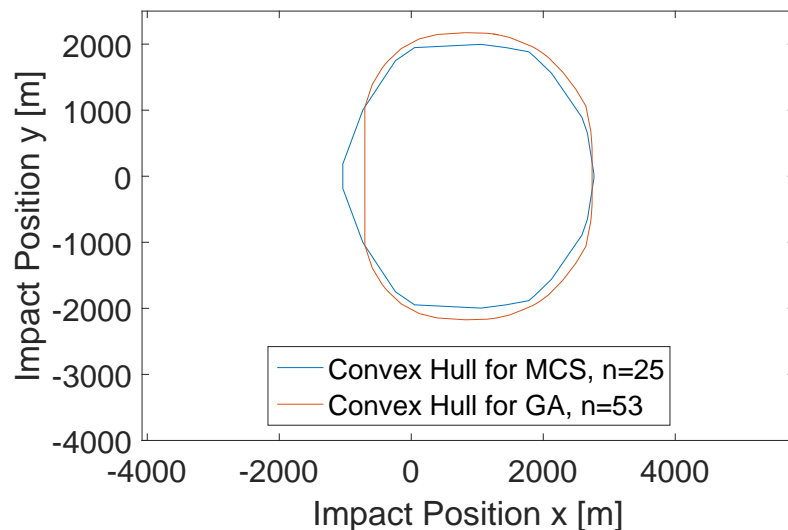


Figure 7-13: Convex hull for GA optimization with 100 individuals per generation and 2100 MC simulations.

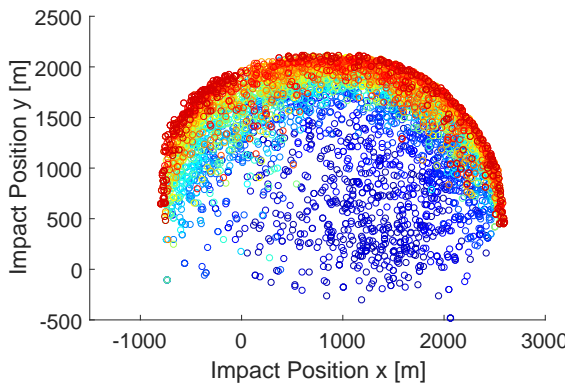


Figure 7-14: Pareto front after 20 generations and a population size of 300

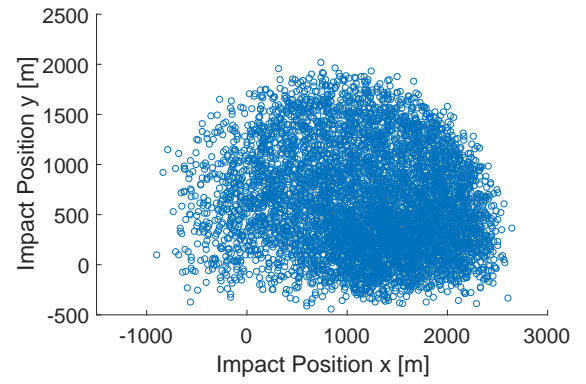


Figure 7-15: MC Simulation with 6300 simulations, same amount as with GA

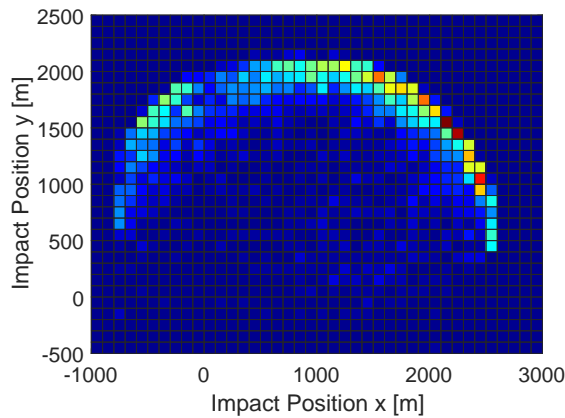


Figure 7-16: Pareto front histogram after 20 generations and a population size of 300

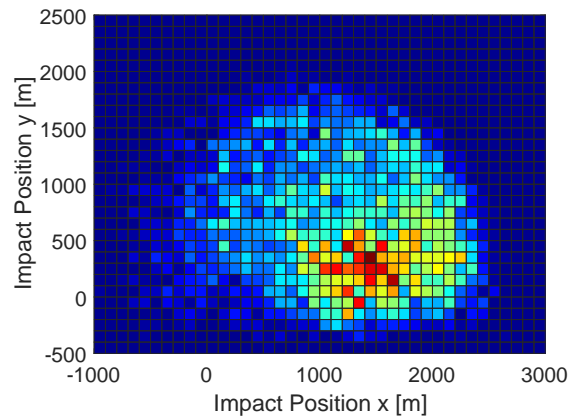


Figure 7-17: MC Simulation with 6300 simulations, same amount as with GA

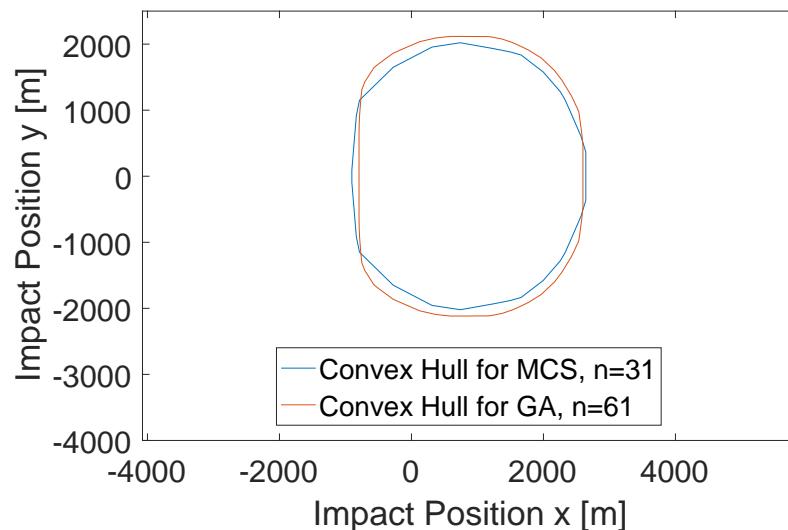


Figure 7-18: Convex hull for GA optimization with 300 individuals per generation and 6300 MC simulations.

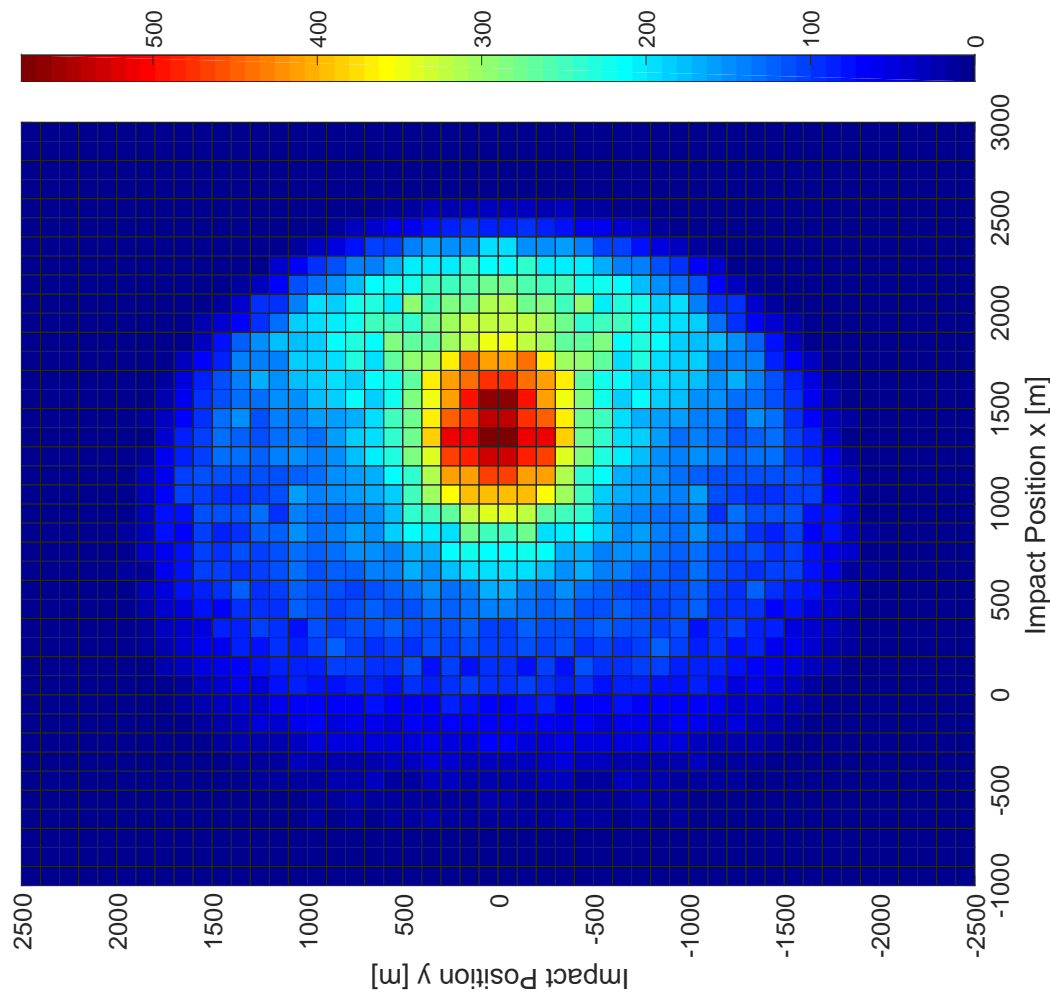


Figure 7-19: MCS with 70000 simulations, the number in the legend corresponds to impacts per square

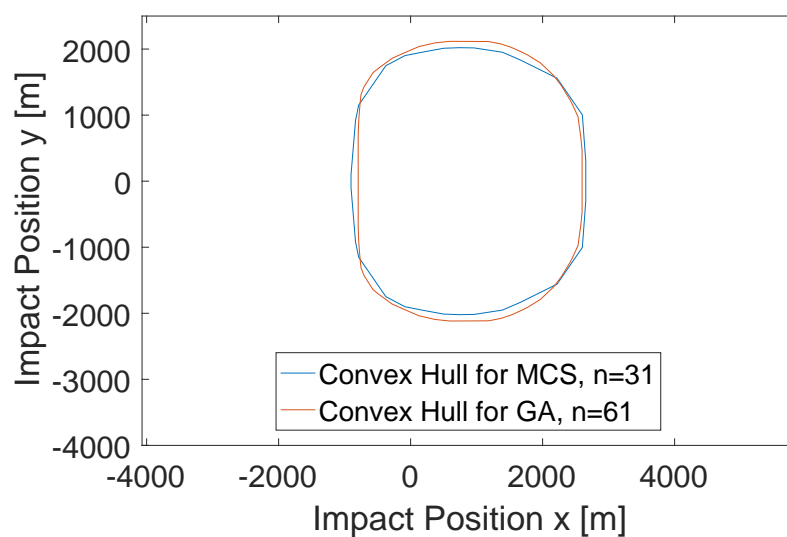


Figure 7-20: Convex hull for GA optimization with 300 individuals per generation and 70000 MC Simulations.

7.4 Explosion on Ground

A truly different safety threat even before the missile flight comes from the fact that the engine is made up of explosives. The chance of such an explosion is, when the engine is operated by the right personnel, diminishing small. But the severity and consequences are in worst case lethal for people standing within the proximity of the starting point. Not only debris and splinter endanger humans and equipment, due to the explosion a shock wave with enormous sound level pressures accrues. Very high sound pressure peak levels lead to hearing loss and injuries, for that this section deals with both aspects of an explosion on ground. An institution dealing with danger zones that emerge from weapons and explosives is the US Army, they published a manual on safety ranges and danger zones for every weapon used by them. For bare explosive charges they provide simple tables and formulas [21].

Debris Hazard Referring to Table 15-2 in [21, p. 201] the safe distance for personnel near bare charges is a minimum of 300 m. Additional starting point preparations for charges of less than 2.27 kg reduce this distance to at least 50 m. These include that the ground is pebble and stone free sand that was loosed and raked. The second preparation includes a barricade of minimum 1 m height constructed of sandbags or similar within a radius between 1 m and 2 m measured from the missile. For a more detailed information see [21, para 15-1f(2)(a)]. For this safety assessment the designated danger zone is 300 m.

Shock Wave Hazard The second endangerment for humans is the shock wave. The threshold of pain varies between $130 \text{ dB}_{\text{SPL}}$ and $140 \text{ dB}_{\text{SPL}}$ ³ [23]. Table 15-3 in [21, p. 201] gives a distance of 275 m (interpolated value for an explosives mass of 0.792 kg) for the $140 \text{ dB}_{\text{SPL}}$ contour. When compared to debris hazard it is clear that the resulting danger zone radius is the maximum of these two, hence 300 m at least.

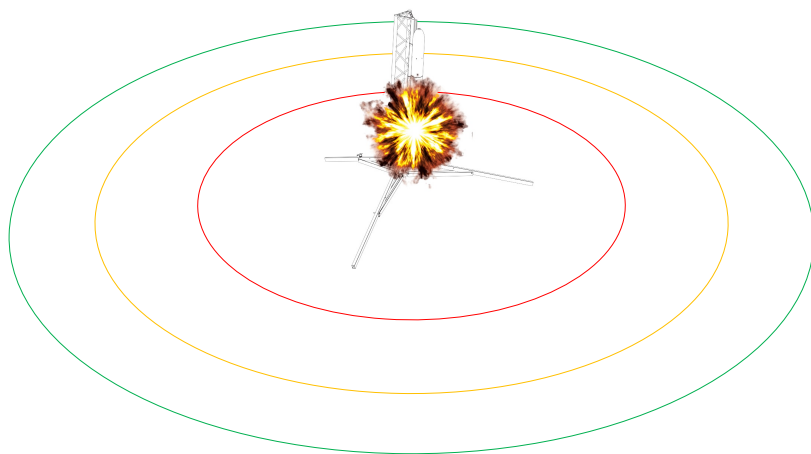


Figure 7-21: Danger zones explosion on ground. Red circle with radius 50m is reduced danger zone. Yellow circle with radius 275m corresponds to 140 dB contour. Green circle is the border of the danger zone with radius 300m.

³As an example, vuvuzelas reach $120 \text{ dB}_{\text{SPL}}$ at 1 m distance [22]

8 Results and Conclusion

The various flight simulations done during the MCS and GA optimizations answer the required research questions as stated in chapter 3. The missile flight poses no risk at all if the subsequent results are taken into account. With further self-imposed restrictions the danger zone could be reduced and alternative shooting ranges could be used.

8.1 Stable Flight under Various Conditions

Due to the inherent aerodynamic stability as shown in chapter 2 and additionally shown with the simulations the missile is under any condition considered stable. Environmental influences and mass properties like CoG and Mol deviations do not impose the chance of an unstable behavior under the taken assumptions.

8.2 Wind Influenced Range

The wind influenced range is calculated in section 6.10 for the maximum wind speed of 13.9 m s^{-1} or Beaufort 6, see Figure 6-22. The range depends on the specific wind speed and direction, an increase or decrease is possible. While up wind at first increases the range for higher wind speed it decreases again. For the back wind case the contrary holds, moderate wind speeds decrease the range, under the right conditions the missile might impact near the start point or even behind it. Side wind lets the missile drift aside up to 1500 m and increases the range in every case. For the subsequent missile operation the wind speed can be restricted to smaller values since Beaufort 6 is very pessimistic. With lower wind speeds the range and danger zone decreases.

8.3 Range and Behavior in the Case of Rudder Failure

Already discussed in section 6.6 a rudder failure, in our case modeled by one or two deflected fins, does not impose a safety threat. One unwanted fin deflection increases the range by a small amount. Two fin deflections alter the impact position drastically, but the impact positions does not exceed the danger zone computed in the next section in any case. Small deviations of the fin positions result in a similar impact position influence, the drift aside and in flight direction is 120 m at maximum.

8.4 Danger Zone Estimation

For the danger zones size and shape the GA optimization results with a population size of 300 are used primarily. The outline is better defined and more outward as the MCS results in most directions except the one against start direction. In total the danger zone is made up of both convex hulls, whichever is more outwards. The final danger zone is shown in Figure 8-1 and Figure 8-2 displays the area as an overlay on Area WTD 91. The probability of impact outside this area can be treated as nonexisting under the taken assumptions. For shooting ranges higher elevated or for hotter days than the 30°C assumed, the assessment has to be repeated. The self imposed maximum danger zone as in Figure 3-1 is not exceeded.

8.5 Next Steps and Suggestions

Since the final design of the GRM is still in development only projected values are used in this thesis. The next step would be to simulate the safety area computation again after the design is finalized and data like CoG, Mol etc. are known. Additional wind tunnel tests can replace the MDATCOM data and thus remove one of the biggest uncertainties. As mentioned the operational boundary conditions like wind speed, temperature etc. can be altered which requires the calculations to be redone. For the control algorithm development the model has to be expanded with controllable fin deflections and a sensor model.

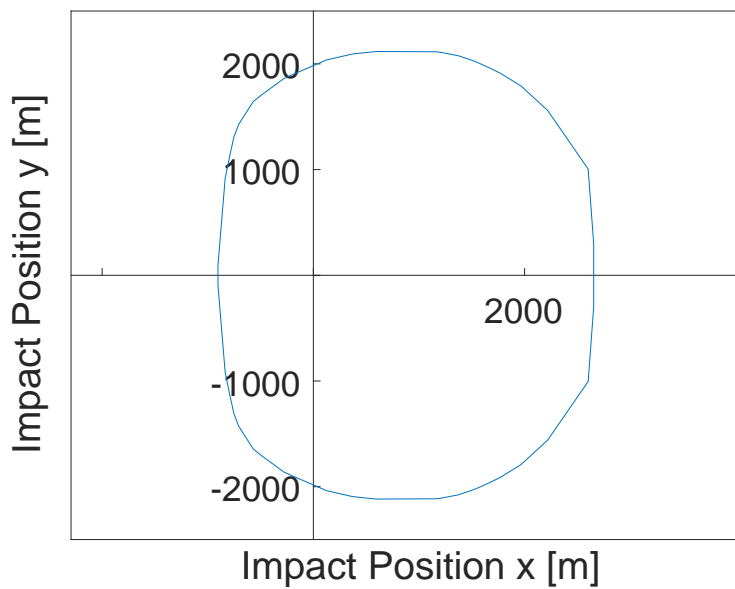


Figure 8-1: The final danger zone

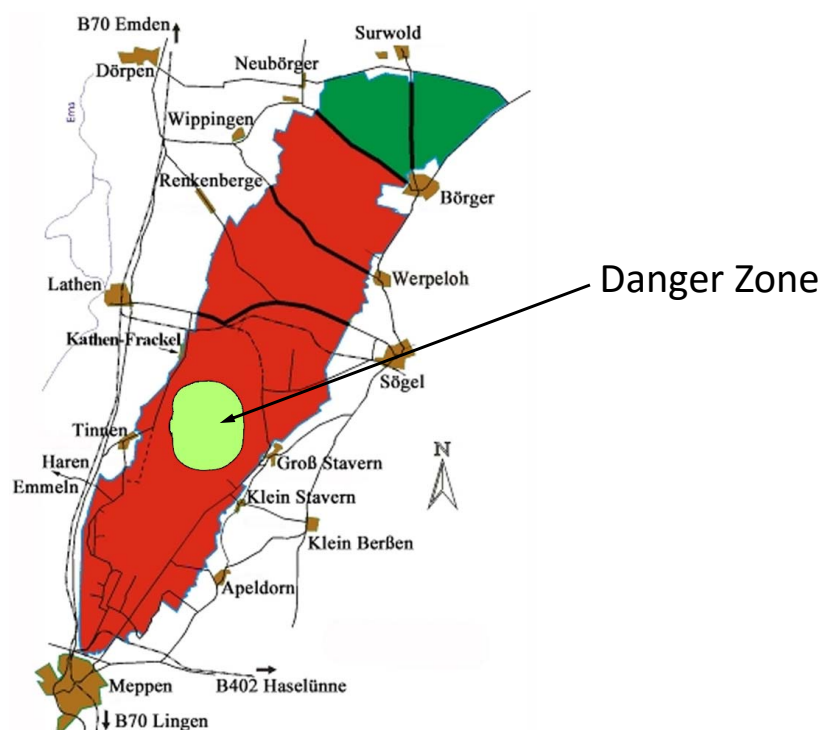


Figure 8-2: Danger zone in comparison to area WTD 91

References

- [1] M. V. Cook, "Flight dynamics principles (third edition)", in, M. V. Cook, Ed., Third Edition, Butterworth-Heinemann, 2013, pp. 1 –11, ISBN: 978-0-08-098242-7. DOI: <http://dx.doi.org/10.1016/B978-0-08-098242-7.00001-8>. [Online]. Available: <http://www.sciencedirect.com/science/article/pii/B9780080982427000018>.
- [2] P. Petit, "Guided research missile (grm) tu münchen", 2015.
- [3] NASA, *Fault tree handbook with aerospace applications*, 2002.
- [4] William J. Hughes Technical Center, "Global positioning system (gps) standard positioning service (spss) performance analysis report", Tech. Rep., 2014.
- [5] G. P. Sutton and O. Biblarz, *Rocket propulsion elements*. John Wiley & Sons, 2011.
- [6] D. J. Martin, "Summary of flutter experiences as a guide to the preliminary design of lifting surfaces on missiles", Tech. Rep., 1958.
- [7] K. Sato, "Vertical wind disturbances in the troposphere and lower stratosphere observed by the mu radar", *Journal of the Atmospheric Sciences*, vol. 47, no. 23, pp. 2803–2817, 1990.
- [8] R. V. Rhode, *Some effects of rainfall on flight of airplanes and on instrument indications*, 1941.
- [9] C. Rosema, J. Doyle, L. Auman, M. Underwood, and W. B. Blake, "Missile datcom user's manual-2011 revision", DTIC Document, Tech. Rep., 2011.
- [10] P. A. Barnard, "Graphical techniques for aircraft dynamic model development", in *AIAA Modeling and Simulation Technologies Conference and Exhibit*, 2004, p. 4808.
- [11] J. Sturm, "Aerodynamische untersuchungen an experimentalflugkörpern der xm-serie", Semester Thesis, Technical University Munich, 2012.
- [12] T. J. Sooy and R. Z. Schmidt, "Aerodynamic predictions, comparisons, and validations using missile datcom (97) and aeroprediction 98 (ap98)", *Journal of spacecraft and rockets*, vol. 42, no. 2, pp. 257–265, 2005.
- [13] E. J. Abney and M. A. McDaniel, "High angle of attack aerodynamic predictions using missile datcom", *AIAA*, vol. 5086, p. 2005, 2005.
- [14] J. Reynolds, "Hot, high and heavy . the deadly cocktail of density altitude", *NOAA's National Weather Service*, 2012.
- [15] Deutscher Wetterdienst, "Wetterrekorde in deutschland und weltweit", 2015.
- [16] Deutscher Wetterdienst, Wetterlexikon, "Beaufort-skala", in, 2016.
- [17] W. L. Dunn and J. K. Shultis, *Exploring Monte Carlo Methods*. Elsevier, 2011.
- [18] K. R. Thomas Müller-Gronbach Erich Novak, *Monte Carlo-Algorithmen*, First Edition. Springer-Verlag Berlin Heidelberg, 2012, ISBN: 978-3-540-89140-6. DOI: 10.1007/978-3-540-89141-3. [Online]. Available: <http://www.springer.com/de/book/9783540891406>.
- [19] P. W. Christensen and A. Klarbring, *An introduction to structural optimization*. Springer Science & Business Media, 2008, vol. 153.
- [20] B. L. Miller and D. E. Goldberg, "Genetic algorithms, tournament selection, and the effects of noise", *Complex Systems*, vol. 9, no. 3, pp. 193–212, 1995.
- [21] Department of the Army, *Pamphlet 385–63 - safety - range safety*, 2014.
- [22] D. W. Swanepoel, J. W. Hall III, and D. Koekemoer, "Vuvuzela: Good for your team, bad for your ears", *SAMJ: South African Medical Journal*, vol. 100, no. 2, pp. 99–100, 2010.
- [23] J. R. Franks, C. Merry, et al., *Preventing occupational hearing loss: A practical guide*, 96-110. US Dept. of Health et al., 1996.

A 1

Component	Description	Further Details
Dimensions	Length Caliber Mass	1000 mm 90 mm 5 kg
Aerodynamic Control	4 Fins in the aft section and therefore stable No additional roll moments due to vortex separation No Wings	
Control System	Beagle Bone Black	1 GHz Cortex-A8 SoC 2x200 MHz real time capable CPUs 4 UART, 8 PWM, 2 SPI, 2 I2C Linux based RTOS
Sensors	Position and orientation Fin position sensor Air-Data GPS	6 DoF INS or IMU RM08 non-contact rotary encoder Aeroprobe Air Data System with P-C06H06S-SX-S-203 Air-Data Probe commercial off the shelf GPS receiver
Electronics and Actuators	4x Savöx SB-2261 mg Servos Amber Ultra Long Range Telemetry module	57 g 6 V 1 N m 0.076 s/60° 869 MHz radio frequency
Engine	Cesaroni Pro54 1635K445-17A	See Table A-2
Performance	Max. longitudinal acceleration Max. lateral acceleration Max. speed Flight Duration	14 g 9 g 250 m s ⁻¹ 10 s

Table A-1: GRM technical data overview

Single-Use/Reload/Hybrid	Reloadable
Loaded Weight	1398 g
Propellant Weight	792 g
Burnout Weight	572 g
Motor Dimensions	54 mm × 404 mm
Total Impulse	1636.3 N s
Maximum Thrust	664.83 N
Avg Thrust	445 N
Burntime	3.67 s

Table A-2: Pro54 1635K445-17A data

(Source: <http://www.pro38.com/products/pro54/motor/MotorData.php?prodid=1635K445-17A>)

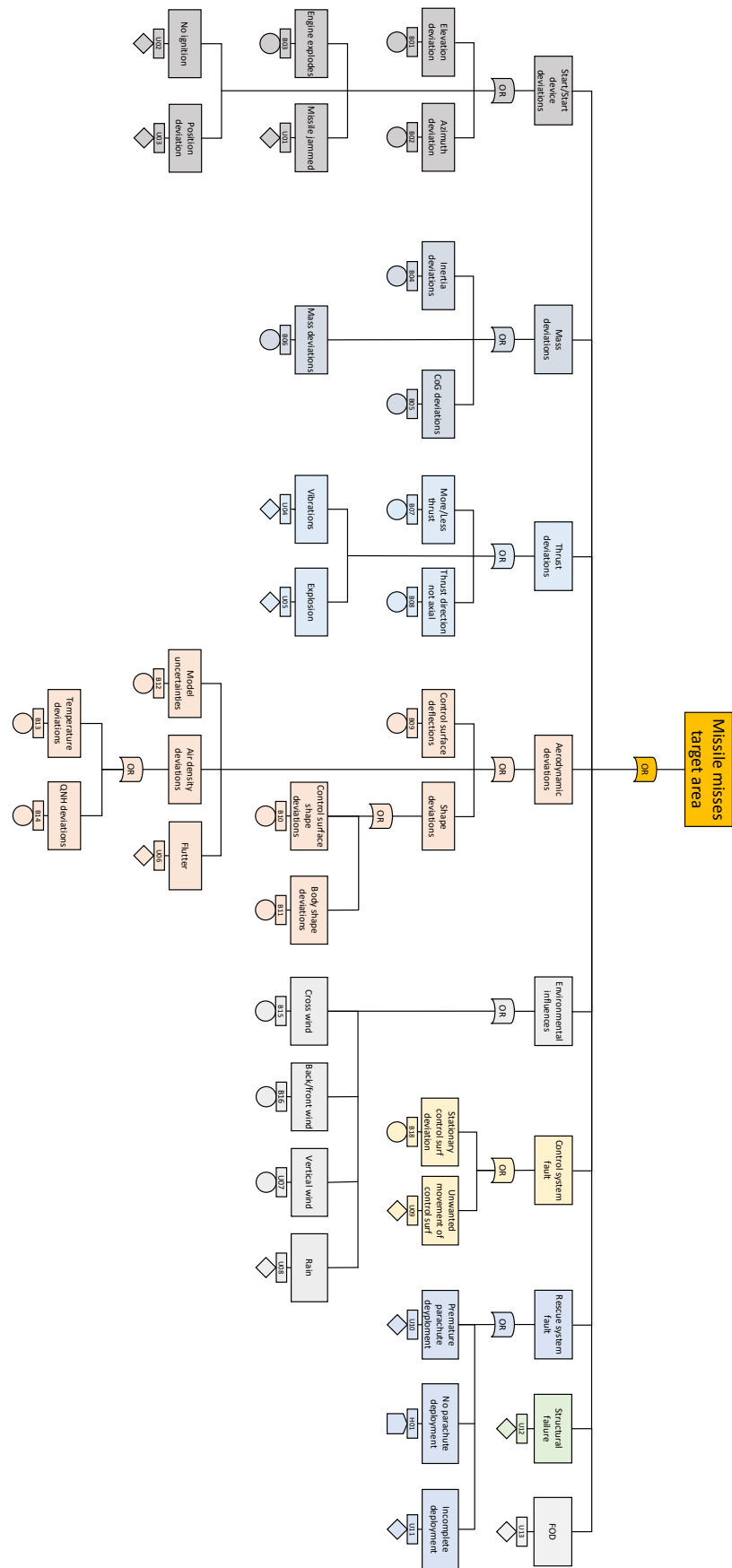


Figure A-1: The final Fault Tree for the top event missile impact outside safety zone.

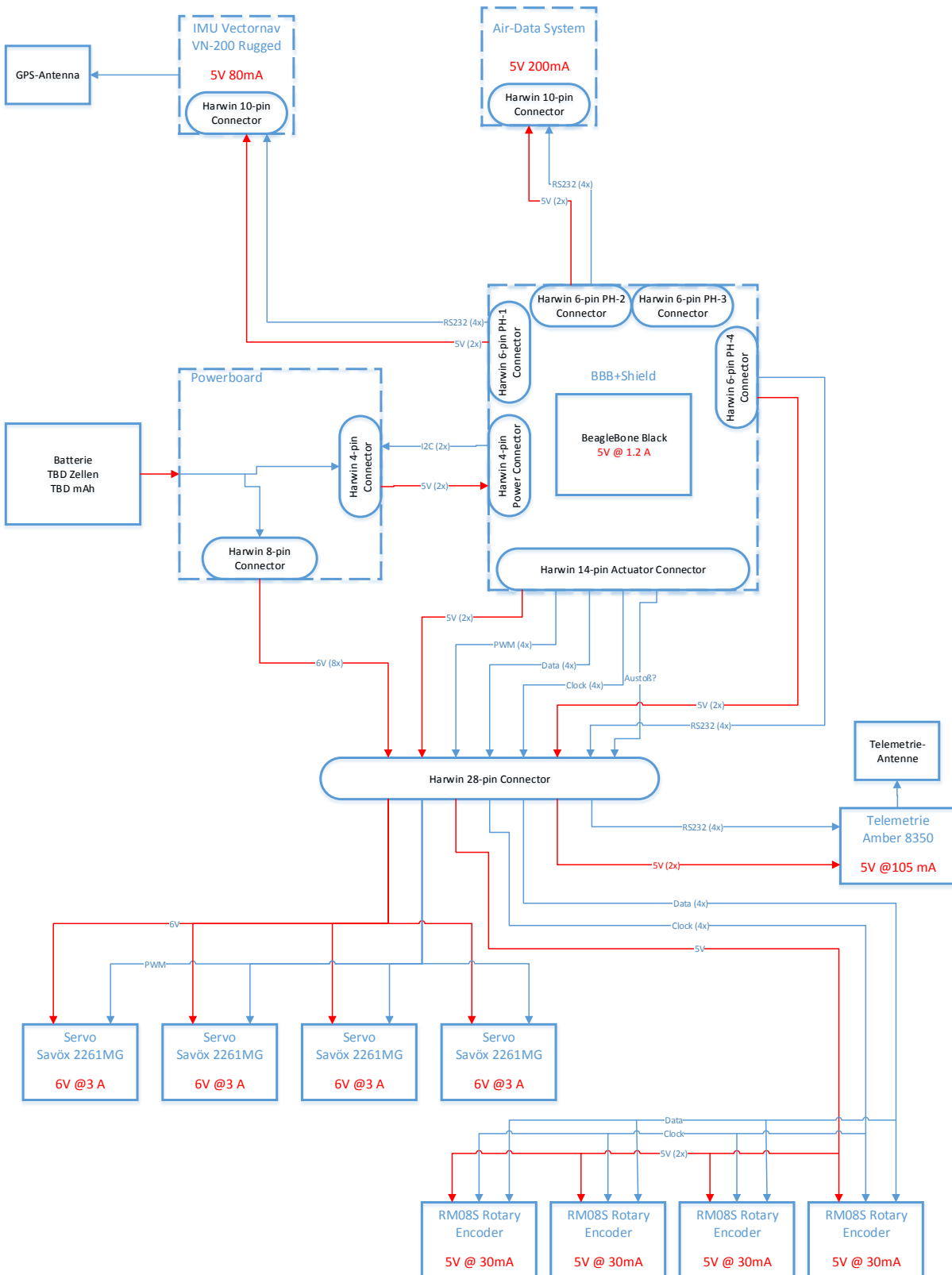


Figure A-2: Electronic architecture with Beagle Bone Black as flight control computer and centerpiece

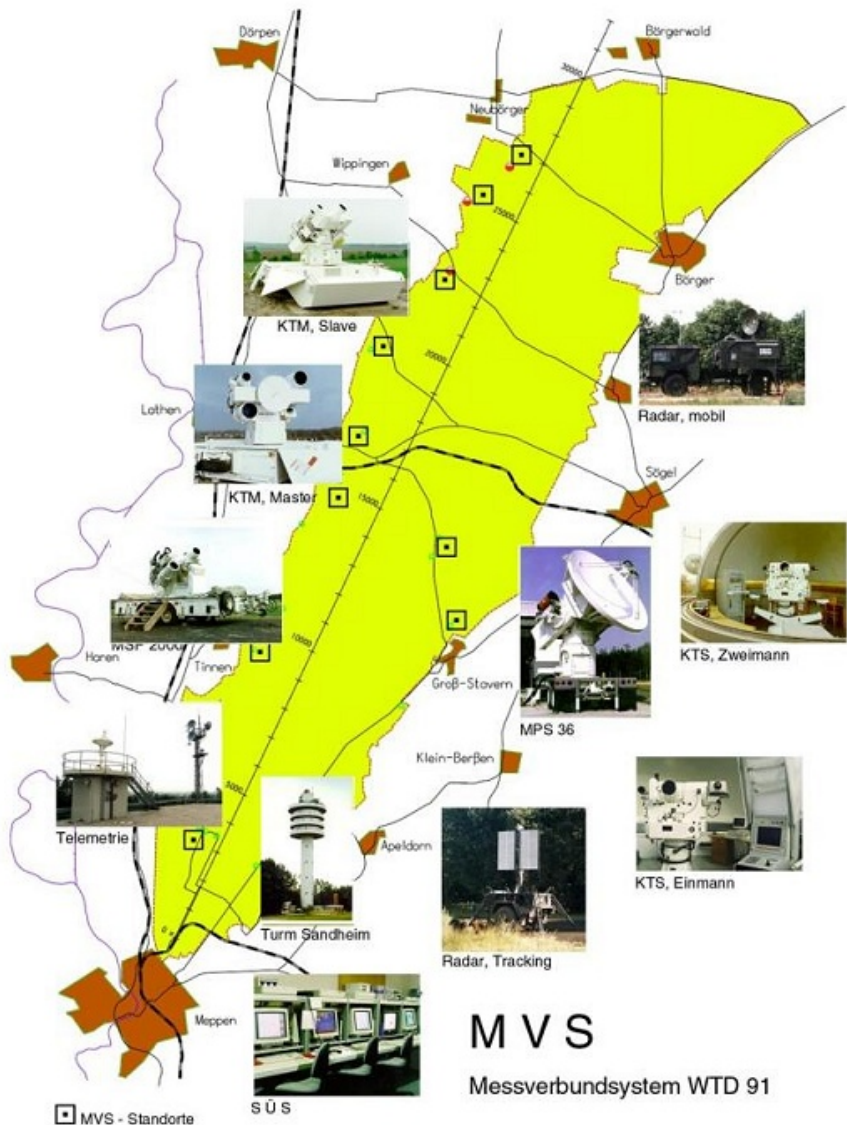


Figure A-3: WTD 91 Test Area (Source: Bundeswehr / WTD 91)

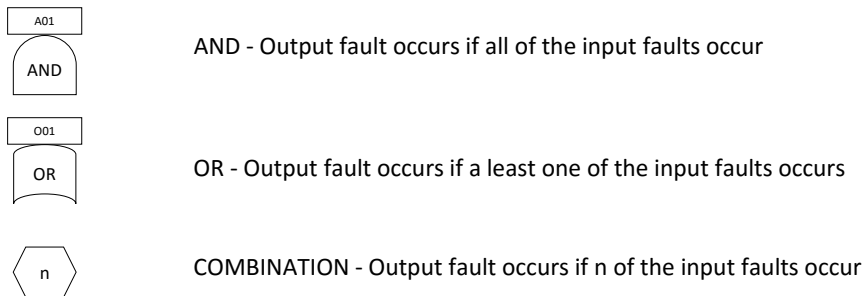


Figure A-4: Different types of links are possible, taken from [3]

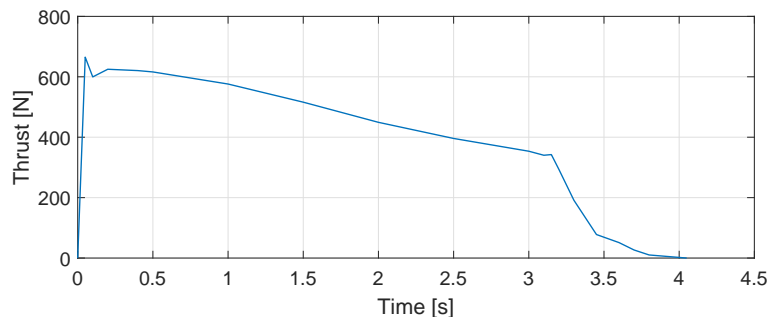


Figure A-5: The measured thrust over time for the used engine.



Figure A-6: The GRM is launched with a start device as shown in this picture.

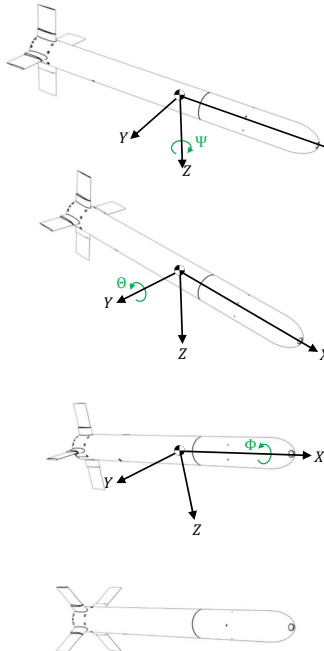


Figure A-7: The rotation is done subsequently around the z,y and x axis.

Abbreviation	Description
CN	Normal Force Coefficient
CM	Pitching Moment Coefficient
CA	Axial Force Coefficient
CA0B	Axial Force Coefficient with no base drag included
CAF0B	Axial Force Coefficient with full base drag included
CY	Side-Force Coefficient
CLN	Yawing Moment Coefficient
CLL	Rolling Moment Coefficient
CL	Lift Force Coefficient
CD	Drag Force Coefficient
CL/CD	Lift-to-Drag Ratio
X-C.P.	Distance from nose to Center of Pressure
CNA	Normal Force Coefficient change wrt Angle of Attack
CMA	Pitching Moment Coefficient change wrt Angle of Attack
CYB	Side-force Coefficient change wrt Sideslip Angle
CLNB	Yawing Moment Coefficient change wrt Sideslip Angle
CLLB	Rolling Moment Coefficient change wrt Sideslip Angle
CNQ	Normal Force Coefficient change wrt Pitch Rate
CMQ	Pitching Moment Coefficient change wrt Pitch Rate
CAQ	Axial Force Coefficient change wrt Pitch Rate
CNAQ	Normal Force Coefficient change wrt Angle of Attack change Rate
CMAD	Pitching Moment Coefficient change wrt Angle of Attack change Rate
CYQ	Side-force Coefficient change wrt Pitch Rate
CLNQ	Yawing Moment Coefficient change wrt Pitch Rate
CLLQ	Rolling Moment Coefficient change wrt Pitch Rate
CYR	Side-force Coefficient change wrt Yaw Rate
CLNR	Yawing Moment Coefficient change wrt Yaw Rate
CLLR	Rolling Moment Coefficient change wrt Yaw Rate
CYP	Side-force Coefficient change wrt Roll Rate
CLNP	Yawing Moment Coefficient change wrt Roll Rate

Table A-3: Aerodynamic coefficients and other variables provided by MDATCOM
(Source:[9])

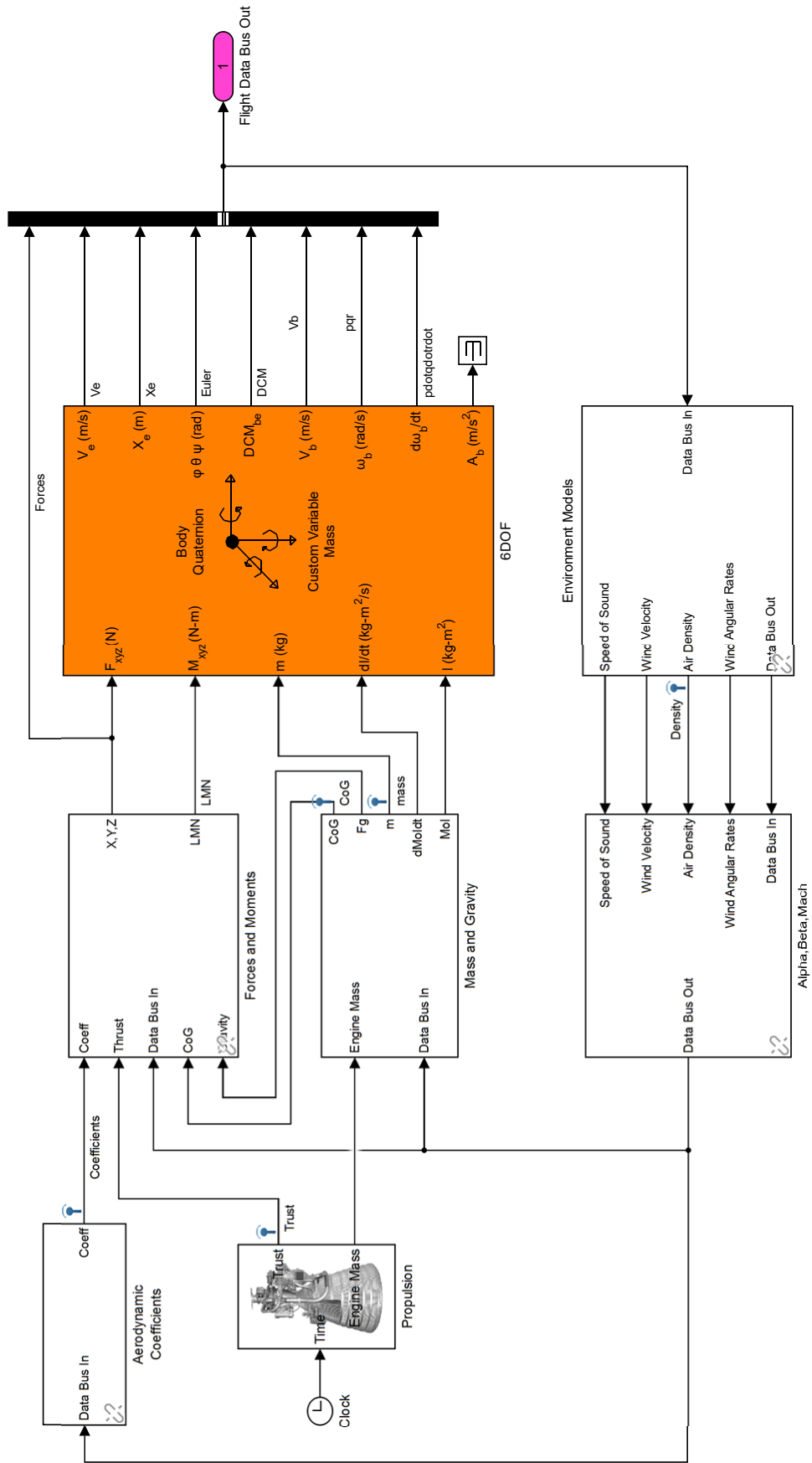


Figure A-8: GRM Simulink model and its submodels as an overview.